

MACROCYCLIC COMPLEXES AS MODELS FOR NONPORPHINE METALLOPROTEINS

VICKIE McKEE

Chemistry Department, The Queen's University of Belfast, Belfast BT9 5AG,
Northern Ireland

- I. Scope
- II. Introduction
- III. Mononuclear Systems
 - A. Hydrolytic Zinc Enzymes
 - B. Type 1 Copper
 - C. Nickel Enzymes
- IV. Dinuclear Sites
 - A. Di-zinc Enzymes
 - B. Urease
 - C. Superoxide Dismutase
 - D. Dinuclear Copper Sites
 - E. Mixed-Valence Di-copper
 - F. Oxo-Bridged Diiron
 - G. Oxo-Bridged Dimanganese
- V. Polynuclear Active Sites
 - A. Trinuclear Copper
 - B. Manganese in Photosystem II
 - C. [4Fe-4S] Clusters
- VI. Conclusion
- References

I. Scope

In 1979 Godeken reviewed comprehensively the use of macrocyclic complexes to model bioinorganic active sites (1). Growth in the area has been such that this is no longer a reasonable target and some selectivity is now required. In this chapter only metalloprotein active sites are considered and those for which the role of the metal ion is largely structural are neglected, as are the processes of metal ion transport and storage. Porphyrins, chlorophylls, corrins, and other por-

phine systems define the coordination environment of complexed metal ions quite closely. The problems of modeling these sites are different, in kind as well as in degree, from those of modeling nonporphine sites, and only the latter will be considered here.

Some information concerning the structures and functions of the metalloprotein active sites is required for any discussion of model complexes. Brief descriptions of the natural sites are therefore included and more detailed accounts may be found in the references. Where possible, references concerned with the metalloproteins themselves include recent reviews.

No attempt has been made to be comprehensive, partly because the determination of what constitutes a model complex is both subjective and dependent on the current state of knowledge about the metalloprotein in question.

II. Introduction

A close relationship has existed between the field of bioinorganic chemistry and that of macrocyclic or macropolycyclic chemistry for the last 20 years. In part, this is due to direct overlap relating to the existence of the natural macrocyclic antibiotics and porphyrins. However, a long and fruitful association also exists in a third area: the use of macrocyclic or cryptate complexes to model metalloprotein active sites or to mimic their chemistry (1-3).

The metalloproteins that have attracted most attention are those whose properties are most obviously different from those observed in the normal "classical" aqueous coordination chemistry of the metal ions. The challenge is to account for (initially) unique spectral or chemical properties in terms of the coordination chemistry of the metalloprotein active site, as moderated by the protein environment. With increasing frequency, as in the case of type 1 copper (Section IIIB), crystallography reveals the active site structure with sufficient clarity to provide strong clues as to the origin of the unusual spectroscopy. However, an important test of the structural and spectroscopic analyses is to reproduce the same effects in a model complex. On other occasions, as with the [4Fe-4S] proteins (Section VC), many questions remained even after the structures were known. In spite of the very impressive achievements of protein crystallography, there remain many metalloproteins for which structural data are either not available or inconclusive.

The aim of synthetic model studies is to reproduce the spectroscopic features, and ultimately the function, of the active site in a low-molecular-weight complex of known structure (4–6). This is generally a cyclic process, as illustrated in Fig. 1, and the potential for refinement has not yet been exhausted for any single metalloprotein. Negative results are often valuable in modifying the model, especially in earlier stages of the process and are in any case useful in expanding the underlying coordination chemistry. The problems addressed by bioinorganic chemistry lie principally in coordination chemistry and spectroscopy. It is arguable that the design and synthesis of model complexes for metalloprotein active sites have contributed as much (or more) to the development of these areas as they have to biochemistry.

As understanding of a particular metalloprotein develops, so the questions to be addressed by models change and “last year’s model” can become dated very rapidly. To use the terms introduced by Hill (5) and expanded by Fenton (6), the normal progression is from speculative models through corroborative ones to fully functional synthetic analogs. The aims of this process are twofold, to understand the structure

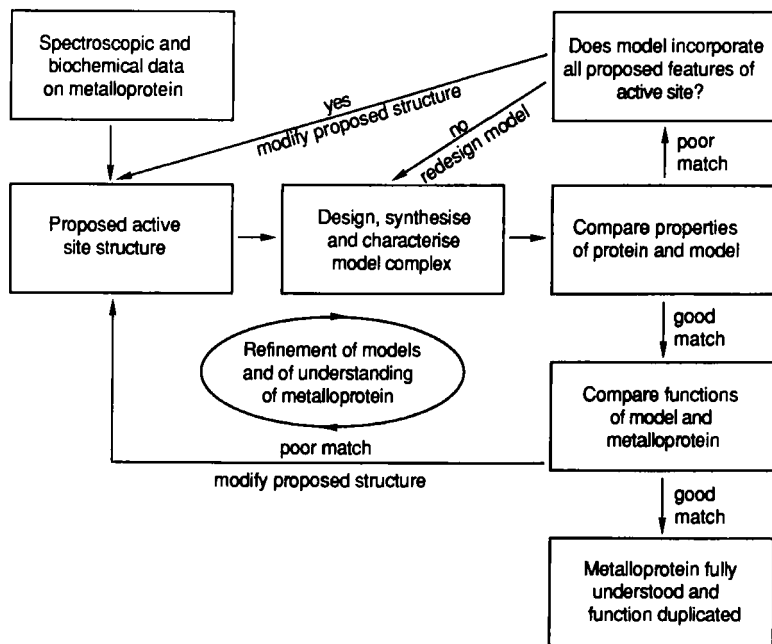


FIG. 1. Steps in the development of models for a metalloprotein active site.

and function of the metalloprotein and, ultimately, to duplicate its function. There is a distinction to be made between mimicking the structure and spectroscopic properties of a metalloprotein active site and reproducing its function in a synthetic complex. Both objectives require a good understanding of the factors that control the properties of the natural site, but a functional model need not necessarily mimic the structure very accurately.

Some metal ions in metalloproteins retain a "normal" metal environment, behave as classical coordination complexes, and are less studied because they appear to be understood (although perhaps this is a smaller class than it once appeared). The particular properties of other sites can often be traced back to unusual geometry or ligation at the active site; these systems have generally been more studied because they are more intriguing.

Many of these unusual properties can also be induced in macrocyclic systems and can be ascribed to many of the same factors. Control of the structures and geometries in macrocyclic complexes generally lies somewhere between two extreme positions. On the one hand, the metal ion may impose its preferred geometry on the macrocyclic ligand. On the other, the macrocycle may impose some particular geometry or environment on the metal. In the first case, the complex is likely to have classical properties, but the second introduces the possibility of unusual properties of some sort. In most cases some degree of compromise is reached between the preferred geometry of macrocycle and that of metal. Some of the more important means by which the properties of a metal ion can be modified are outlined below.

1. Unusual Donor Sets

A metal ion in a protein will bind to donors it would not normally favor if the donor is part of the imposed coordination environment and if there is no alternative ligand available. The metal ion must accept or reject the site as a whole and, provided there are sufficient donors to which the metal binds strongly, the complex will be stable. The protein may be considered a host presenting a converging and fixed donor set to the metal ion guest (7). The fixed relative positions of the donors prevent side reactions, such as oxidation of thiolate ligands to disulfides, which would occur if the ligands were independently labile. Macrocyclic or macropolycyclic ligands may also present a set of donors, one or more of which may not normally bind strongly to the metal in question. Binding is promoted by the presence of strongly binding donors that maintain the less-favored donor within the coordination

sphere. The stability of the complexes is enhanced by the high kinetic stability of most macrocyclic complexes.

2. *Unusual Geometry*

The concept of the protein (or macrocycle) as a host with a prearranged donor geometry is also relevant here. The situation is related to Cram's concept of a preorganized ligand in which a very stable complex may be formed between a metal ion guest and a host preorganized so that the binding of the metal does not result in any significant change in geometry (7). The difference in metalloproteins is that the preorganized geometry of the host is often not that usually favored by the metal ion guest. The purpose of the preorganization is to disrupt the preferred geometry of the metal and thus to modify its properties. This is not to imply that the geometry of metalloprotein active sites is totally controlled by the protein structure; there are many cases in which binding a metal ion alters the geometry of the host protein, and this is important to the function of the metal site. Even when this is the case, however, constraints of protein structure may still impose unusual metal geometry. Factors such as coordinative unsaturation or metal-metal interactions can also be controlled by suitable design of the host cavity.

3. *Environment*

If the local site geometry and metal ion spectroscopy appear to have been reproduced accurately, then any effects not accounted for are (conveniently) ascribed to the protein environment; this is perhaps the equivalent of "packing effects" in crystallography. Factors such as access to the site, polarity, and a protic or nonprotic environment in the vicinity of the metal are controlled by the amino-acid residues in that region of the protein and by the extent of exposure of the site to external solvent. Although it is probably true that "design and mimicry in truly inorganic models is stretched beyond its limits by the presence of folded proteins" (8), modeling these subtle effects can be tackled in a number of ways, from use of nonprotic solvents to the construction of large macrocyclic ligands that wrap around the metal site (Section VC).

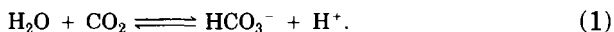
III. Mononuclear Systems

In modeling mononuclear metalloproteins, the aim is to mimic the ligation, geometry, and possible environment of the active site in ques-

tion. If this is achieved, the spectroscopic and other properties of the metalloprotein should also be reproduced. The relative importance of each of the above factors varies from case to case, as does the relative importance of matching particular properties.

A. HYDROLYTIC ZINC ENZYMES

Carbonic anhydrase catalyzes the hydration (and dehydration) of carbon dioxide:



Silverman and Lindskog (9) suggest that the rate-determining step in this process is deprotonation of the water molecule. The active site of carbonic anhydrase (10, 11) is shown in Fig. 2. The zinc atom is bound to three histidine residues and approximate tetrahedral coordination is thought to be completed by a coordinated water molecule. The $\text{p}K_a$ of the bound water molecule is about 7 (9, 12, 13). This value is so much below the range observed for classical aqueous zinc complexes ($\text{p}K_a$ values of 8–9) that doubt has been cast on the identity of the species for which this value was measured (13–15). It is now generally accepted as referring to coordinated water and such a conclusion is supported by recent theoretical calculations (16). A requirement for a $\text{p}K_a$ of this magnitude is implicit in the “Zn—OH mechanism” for carbonic anhydrase. In the scheme proposed (9, 16, 17) Zn^{II} —OH acts as a nucleophile, attacking the substrate carbon atom. Such a mechanism requires significant formation of the deprotonated species under biological conditions, i.e., at pH 7.4–7.6. The reverse reaction requires significant amounts of Zn^{II} —OH₂ in the same pH range. Thus, the function of carbonic anhydrase requires the bound water to have a $\text{p}K_a$ close to the pH of blood. There have been suggestions that the deprotonation of the bound water molecule is assisted by neighboring amino-acid

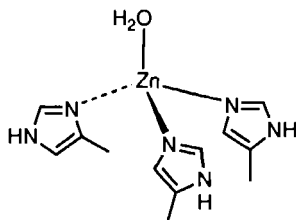


FIG. 2. The active site of carbonic anhydrase.

residues (16), and by the hydrophobic environment of the active site. A similar mechanism is proposed for carboxypeptidase A (13, 18). In this enzyme the bound water molecule has an even lower pK_a (ca. 6), and it has been suggested that such a value can be achieved only by assistance from a glutamate residue (19).

Few zinc-containing model systems for carbonic anhydrase have been reported (although cobalt and copper model complexes have been widely used (20–22)). In part, this is because of the difficulties of establishing the structures of labile zinc complexes in solution. However, a second serious problem arises in trying to reproduce pH-sensitive chemistry when the pK_a of the model system is grossly different from that of the metalloprotein. One of the most useful zinc model systems involves the Schiff-base macrocycle L1 (Fig. 3). A complex containing $[Zn(L1)H_2O]^+$ was prepared by Woolley (23) and characterized by X-ray crystallography. The macrocyclic ligand provides sufficient stability for the solution species to be reliably identified. The approximately square pyramidal geometry of the complex bears little relation to that of carbonic anhydrase, and the pK_a of the coordinated water molecule (8.7) is much higher. Nonetheless this complex proved a valuable model for the enzyme; it will catalyze hydration of CO_2 , although it is much less effective than carbonic anhydrase. Significantly, both model and carbonic anhydrase also catalyze hydration of acetaldehyde in basic solution, which aqueous Zn^{2+} does not. The reduction of the pK_a to 8.7 was ascribed to the five-coordinate square pyramidal geometry about zinc and provided support for the $Zn-OH$ mechanism. Woolley suggested that a four-coordinate zinc ion might be expected to reduce the pK_a even further (23).

A remarkable dependence of pK_a values on macrocyclic ring size has been shown for a series of complexes of general formula $[Zn(L)(H_2O)]^{2+}$, where L represents a saturated tri- or tetraaza macrocycle (Fig. 4). Kimura *et al.* (24) reported that complexes of the 12-membered macrocycles [12]aneN₃ and iso[12]aneN₃ show a marked reduction in pK_a , to values almost identical to that observed for carbonic anhydrase

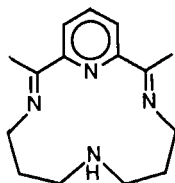


FIG. 3. The Schiff-base macrocycle L1.

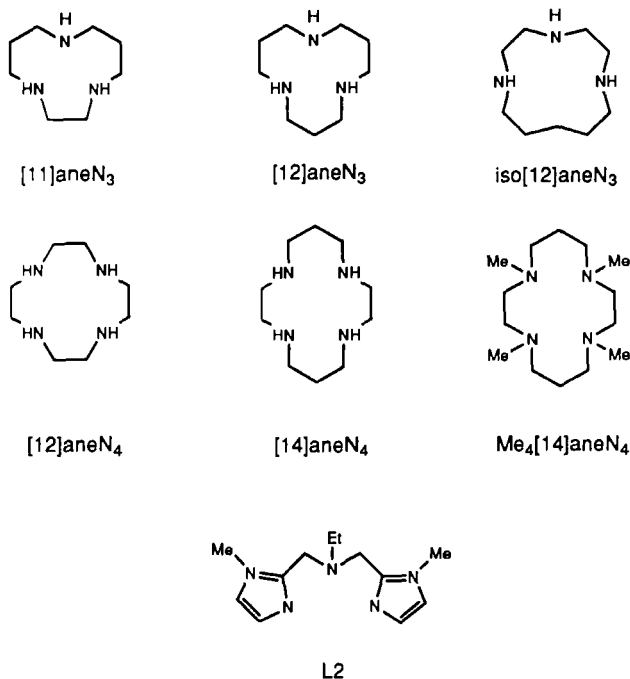


FIG. 4. Some ligands used to model hydrolytic zinc enzymes.

(Table I). These complexes also have high thermodynamic and kinetic stability in aqueous solutions so that complexation is complete at low pH. The macrocycle [12]aneN₃ forms tetrahedral zinc complexes in which monodentate ligands fill the apical site. The X-ray structure of [Zn([12]aneN₃)OH]₃(ClO₄)₃·HClO₄, which contains the almost tetrahedral [Zn([12]aneN₃)OH]⁺, is shown in Fig. 5. There is structural evidence for a strong Zn—OH interaction and the Zn—O and Zn—N(aver-

TABLE I

pK_a VALUES FOR [Zn(L)(H₂O)]²⁺

L	pK _a	L	pK _a
[11]aneN ₃	8.2	[11]aneN ₄	8.0
[12]aneN ₃	7.3	[14]aneN ₄	9.8
iso[12]aneN ₃	7.3	Me ₄ [12]aneN ₄	8.4
L1	8.7	L2	8.3

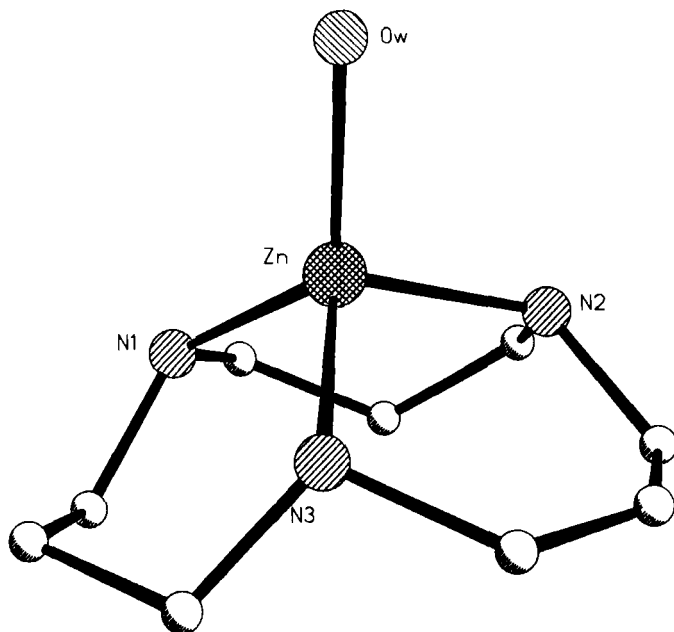


FIG. 5. The structure of $[\text{Zn}([12]\text{aneN}_3)\text{OH}]^+$.

age) distances (1.944(5) and 2.20 Å) are close to those predicted from AM1 calculations (16) for the Zn—OH metalloenzyme active site.

This complex has been shown to be an excellent structural and functional model for the zinc hydrolytic enzymes, particularly carbonic anhydrase but also carboxypeptidase and the zinc phosphate esterases (24–26). The same complex also catalyzes the hydration of acetaldehyde and hydrolysis of carboxylic esters. These reactions appear to progress via a mechanism similar to that proposed for carbonic anhydrase. The rates are slower for $[\text{Zn}([12]\text{aneN}_3)\text{OH}]^+$ than for the enzyme but an order of magnitude faster than for existing model systems such as $[(\text{NH}_3)_5\text{Co}(\text{OH})]^{2+}$ (26).

The order and magnitude of 1:1 anion binding constants for $[\text{Zn}([12]\text{aneN}_3)\text{OH}]^+$ with various anions are similar to those reported for carbonic anhydrase. Anions are thought (9, 27) to inhibit CO_2 hydration by carbonic anhydrase either by displacing the bound water or by increasing the coordination number. Hydroxide ion binds to $[\text{Zn}([12]\text{aneN}_3)]^{2+}$ with a log *K* of 6.4 (vs 6.5 for carbonic anhydrase). The strength of this binding explains why anionic inhibition effects disappear at high pH, where hydroxide ion concentrations are significant.

If an extra anion binds to form a five-coordinate complex, it should become more difficult to dissociate a proton from bound water, so raising the pK_a and decreasing the catalytic efficiency. This theory has been tested using the pendant arm ligand L3 (Fig. 6), which forms a five-coordinate zinc complex $[Zn(L3)(H_2O)]ClO_4$. An X-ray structure of the

Ligand	R	R'
[12]aneN ₃	H	H
L3	H	
L4		H
L5		H
L6		H
L5		H
L8	H	

FIG. 6. Ligands derived from [12]aneN₃.

latter (Fig. 7) shows approximately pentagonal pyramidal geometry about the zinc, with the water molecule axial and the deprotonated phenolate donor equatorial (28). The phenolate is strongly bound ($\text{Zn}-\text{O}$, 1.930 Å) and the water molecule is less strongly held than in the tetrahedral [12]aneN₃ complex ($\text{Zn}-\text{O}$, 2.219 and 1.944 Å, respectively). The pK_a of the phenol is correspondingly low (6.8) but that of the water is raised to 10.7. A similar structure may account for the observed (27) inhibition of carbonic anhydrase by phenol. Acetazolamide, a sulfonamide inhibitor of carbonic anhydrase, also bonds strongly to $[\text{Zn}(\text{L3})(\text{H}_2\text{O})]^{2+}$ via a deprotonated amide nitrogen atom. The tosylamidopropyl derivative of [12]aneN₃ (L4) binds in the same manner (29).

The ligand L3 was initially intended to provide enforced tetrahedral coordination at the metal. Moore and co-workers (30, 31) have successfully used the pendant arm macrocycle L5, also a derivative of [12]aneN₃, for the same purpose (although in view of the foregoing discussion, enforcing the geometry may not have been necessary). The three macrocyclic nitrogen donors form the base of a tetrahedron and the pendant amine fills the apical site. If the pendant arm is shorter,

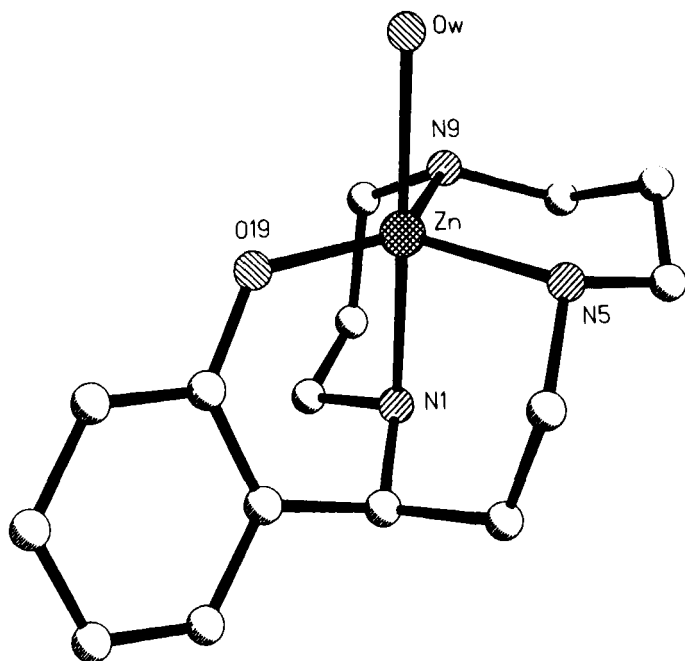


FIG. 7. The structure of $[\text{Zn}(\text{L3})(\text{H}_2\text{O})]^{2+}$.

as in the case of macrocycles L6 and L7, the amine group may still bind but is sterically prevented from reaching the apical position. The resulting space in the coordination sphere can be occupied by another ligand to give five-coordinate complexes.

It is interesting to note that the geometry and stability of the model complex are more important than the particular identity of the donors in modeling the hydrolytic zinc enzymes. Ligands such as L2 (32) appear to be closer mimics of the active site donors than the amine macrocycles but the water molecule in $[\text{Zn}(\text{L2})(\text{H}_2\text{O})]^{2+}$ has a $\text{p}K_a$ of 8.3.

B. TYPE 1 COPPER

The type I copper sites function as electron transfer centers in the blue copper proteins and in multicopper enzymes, particularly oxidases (33). They are characterized by their intense blue color, their unusually small A_{\parallel} values, and their very positive redox potentials (Table II). X-ray crystal structures of several blue copper proteins have been determined, notably plastocyanin (34), azurin (35), cucumber basic blue protein (36), and pseudoazurin (37). The active site structures show marked similarities but also distinct differences (Fig. 8).

The plastocyanin structure was the first to be determined and serves as the basic model; it has been very extensively studied, in both oxidation states and over a range of pH values. It is usually described as having distorted tetrahedral geometry with relatively normal bond lengths to two histidine residues and one cysteine and a long interaction with the thioether donor of a methionine group. The structure of azurin shows similar coordination with the addition of another long interaction to a glycine carbonyl oxygen donor. This geometry is best described as trigonal bipyramidal. Stellacyanin, for which no crystal structure

TABLE II
DATA FOR SOME TYPE 1 COPPER PROTEINS

Protein	E^0 (mV) (pH)	Blue band λ (nm) (ϵ ($M^{-1} \text{ cm}^{-1}$))	A_{\parallel} ($\times 10^4 \text{ cm}^{-1}$)	Reference
Plastocyanin	+ 370 (7.0)	597 (4500)	63	33
Azurins				
<i>A. denitrificans</i>	+ 276 (7.0)	619 (5100)	60	35
<i>P. Aeruginosa</i>	+ 308 (7.0)	631 (3800)	60	38
Stellacyanin	+ 184 (7.1)	609 (3400)	37	38
Cucumber basic	+ 317 (7.0)	597 (4500)	55	36

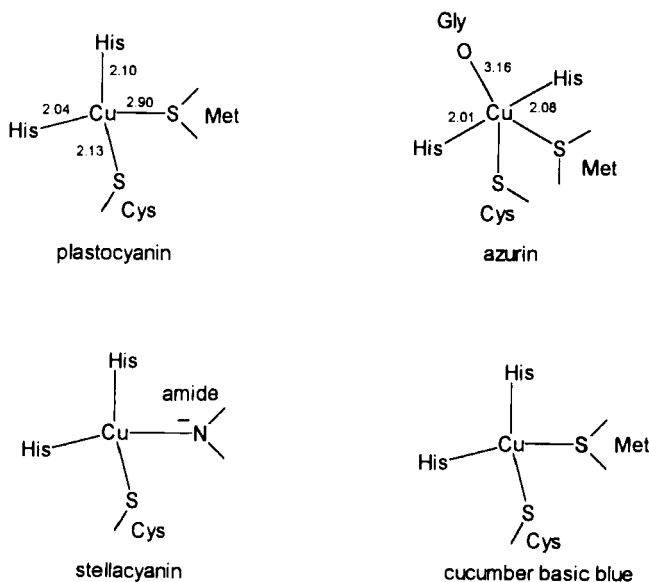


FIG. 8. Active sites of type 1 copper proteins.

has yet been obtained, must necessarily have a different coordination environment since the protein contains no methionine (38). Recent ENDOR results (39) suggest that the fourth donor is likely to be the nitrogen atom of a deprotonated amide donor, at least at high pH. Comparison of the structures of oxidized and reduced forms of plastocyanin and azurin shows that the geometrical changes on redox are very slight.

The combination of similar spectral properties with a rather dissimilar coordination environment has been explained by extensive spectroscopic analysis and molecular orbital calculations carried out largely by Solomon and co-workers (38, 40). The particular spectroscopic features of the site are essentially due to the Cu—S(Cys) interaction, which is common to all the type 1 sites.

In plastocyanin, the character of the Cu—S(Cys) bonding (essentially two π interactions and one σ interaction) is defined by the C—S—Cu bond angle of 107° , which forces the in-plane $3p$ S orbital to overlap with copper in a pseudo- σ configuration. This geometry is defined by the protein structure at the active site. The resulting strong π interaction orients the highest energy, half-occupied copper orbital $d_{x^2-y^2}$ so that it bisects the Cu—S(Cys) bond instead of lying along it. This geometry accounts for the very intense thiolate $\pi \rightarrow \text{Cu}$ transition that dominates

blue copper electronic spectra. These calculations also show the existence of a weak but significant bonding interaction between the copper and the methionine sulfur but, when applied to the azurin active site, reveal no net bonding between the copper and the carbonyl oxygen.

Given the above bonding scheme, the small A_{\parallel} value in the EPR spectrum arises not, as often suggested, from the distorted geometry of the site, but rather from delocalization of the unpaired electron onto the ligands. SCF-X α -SW calculations suggest the half-occupied orbital has only ca. 42% copper $d_{x^2-y^2}$ character and about 36% sulfur $p\pi$. The consequent delocalization reduces the interaction of the electron with the copper nuclear spin and generates the small A_{\parallel} . So, according to this model, the spectroscopic properties of the site are largely due to the particular constrained geometry of the Cu–thiolate bond.

The site described above is extremely difficult to mimic. The requirements include coordination of two sulfur donors, one only weakly but one strongly and with a particular strained configuration. In spectroscopic terms the most important factor is the geometry of the Cu–S(Cys) bond. The geometry about the copper center is irregular and difficult to duplicate with any degree of accuracy, but perhaps the most difficult requirement is that the geometry should not change on redox.

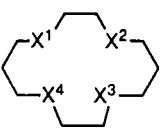
The redox behavior of the proteins is controlled by a combination of geometry and ligation. A rigid, constrained site, leading to minimal change in geometry on redox, is expected (41) to result in a low Franck–Condon barrier and rapid electron transfer kinetics. This will be the case whatever the actual geometry about the metal ion. The particular geometry adopted, and the donor atoms involved, will control the thermodynamics of electron transfer, i.e., the value of the reduction potential. If geometry and donors favor the lower oxidation state, the reduction potential will be raised and vice versa.

Macrocyclic ligands (42) provide a means of introducing constraints on the coordination geometry about a copper atom and also of encouraging binding of sulfur donors to copper(II), generally not a very favorable process. Extensive studies involving macrocyclic thioether and mixed N/S donor ligands have been undertaken to establish the effects of ligation and geometry on the properties of copper complexes. Much of this work has been reviewed (41, 43–46) and only selected data, illustrating the main results, will be summarized here.

Addison (47, 48) and Rorabacher (41, 49–51) have attempted to isolate and quantify the individual factors contributing to redox behavior. Actual half-wave-potential values are dependent on the experimental conditions but some general observations can be made. First, substitution of a thioether for an amine donor invariably leads to an increase

in $E_{1/2}$. These increases are approximately additive along a series such as the Cu(II) complexes of the [14]aneS_xN_(4-x) ligands (Fig. 9 and Table III). The changes in redox behavior are paralleled by a shift in the absorption spectrum to longer wavelengths and higher absorption coefficients as the number of sulfur donors is increased (49). Notably, the stability constants of the Cu(II) complexes decrease markedly as the number of sulfur donors increases, whereas those of the Cu(I) state remain approximately constant. Hence, the increase in $E_{1/2}$ can be attributed to destabilization of the Cu(II) state, due to the relatively weak interaction with thioethers rather than to any stabilization of the Cu(I) state by sulfur coordination (50). An interesting aside is that, for thioether systems, there is no discernable macrocyclic effect for the Cu(I) complexes, although one does exist for Cu(II) analogs (50). Several other similar ligand series have been investigated (43, 52–54).

The effects of structural constraints are more difficult to interpret. Certainly, irregular geometries are induced on coordination of Cu(I) or Cu(II) by thioether-containing macrocycles and these may affect reduction potentials or spectra but in no case are the constraints strong enough to prevent geometric rearrangement on redox. In fact, it is rare to find a Cu^{I/II} redox pair with the same donor set (55). In some cases the rearrangement on redox is slow, leading to observation of a "square scheme mechanism" in the electrochemistry (56–58). The scheme is



Ligand	X ¹	X ²	X ³	X ⁴
[14]aneS ₄	S	S	S	S
[14]aneNS ₃	NH	S	S	S
[14]aneN ₂ S ₂	NH	NH	S	S
[14]aneNSSN	NH	S	S	NH
[14]aneNSNS	NH	S	NH	S
[14]aneN ₃ S	NH	NH	NH	S
[14]aneN ₄	NH	NH	NH	NH

FIG. 9. The [14]aneS_xN_(4-x) ligands.

TABLE III

DATA FOR COPPER COMPLEXES OF [14]aneS_xN_(4-x) LIGANDS

L	$E_{1/2}^a$ (V vs NHE)	log K		λ_{\max} (nm) (ϵ ($M^{-1} \text{ cm}^{-1}$)) ^c
		Cu ^{II} L ^b	Cu ^I L ^b	
[14]aneS ₄	0.58	4.34	12	390 (8000), 570 (1900)
[14]aneNS ₃	0.38 (pH > 3.5)	9.25	13.6	365 (7700), 550 (1000)
[14]aneN ₂ S ₂	0.04 (pH > 5.0)	15.26	13.9	337 (7600), 530 (780)
[14]aneNSSN	-0.01 (pH > 5.0)	15.72	13.5	335 (7300), 530 (640)
[14]aneNSNS	—	15.15	—	356 (7800), 545 (780)
[14]aneN ₃ S	-0.24 ^d	ca. 20	13.7	315 (3900), 510 (330)
[14]aneN ₄	-0.66 ^d	27.2	13.8	255 (8200), 510 (90)

^a Half-wave potentials for Cu^{II}/L in aqueous solution (50).^b Thermodynamic stability constants; for details of calculation methods, see Rorabacher *et al.* (49, 50).^c For Cu^{II}L in aqueous solution.^d Estimated from values in methanol solution.

illustrated in Fig. 10. Reduction of the Cu(II) complex leads first to a metastable conformer of Cu(I), which then rearranges to the stable conformer. Oxidation of the Cu(I) complex also proceeds via a metastable Cu(II) configuration. This has some implications in modeling gated electron transfer in enzyme systems (59). Observation of the square scheme behavior, which is more pronounced at fast scan rates and low temperatures, implies that the rearrangements are slow—of the same order as the cyclic voltammetry scan. This suggests that a slightly higher barrier to reorganization could lock the geometry in place. One possible way to achieve this would be to reinforce the macrocyclic geometry by introducing unsaturation or steric restraints on flexibility;

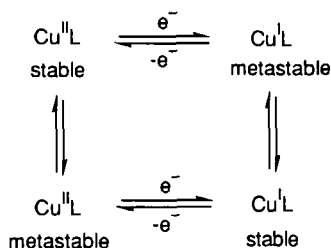


FIG. 10. The square scheme mechanism.

this has been attempted by Hancock (60), Wainwright (61–65), and others (66, 67). Some examples of macrocycles that might be expected to show restricted flexibility are illustrated in Fig. 11. Using ligands such as these, it is possible to synthesize Cu(I) complexes in highly distorted geometries reminiscent of the type 1 sites; an example is shown in Fig. 12. However, generation of such a geometry for the Cu(I) complex does not mean it will be retained on oxidation.

One of the rare examples of Cu(I) and Cu(II) complexes with identical donor sets and closely related geometries is illustrated in Fig. 13 (68, 69). At first sight the structures appear very similar; in each case the copper atom is coordinated to all five macrocyclic donors and the geometry lies somewhere between trigonal bipyramidal and square pyramidal. On closer inspection, however, some differences become apparent. In [Cu(L13)](ClO₄) the Cu(I) ion bonds most strongly to N9, S2, and S16, and the bonds to the imine nitrogen atoms are relatively

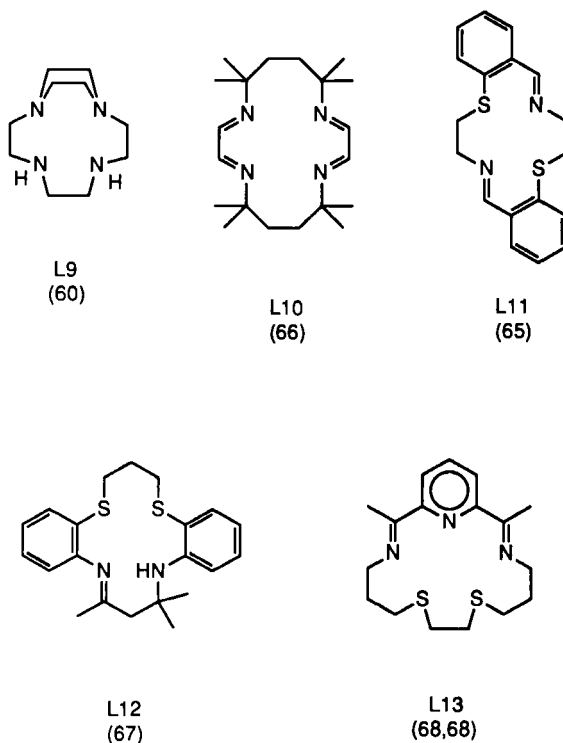
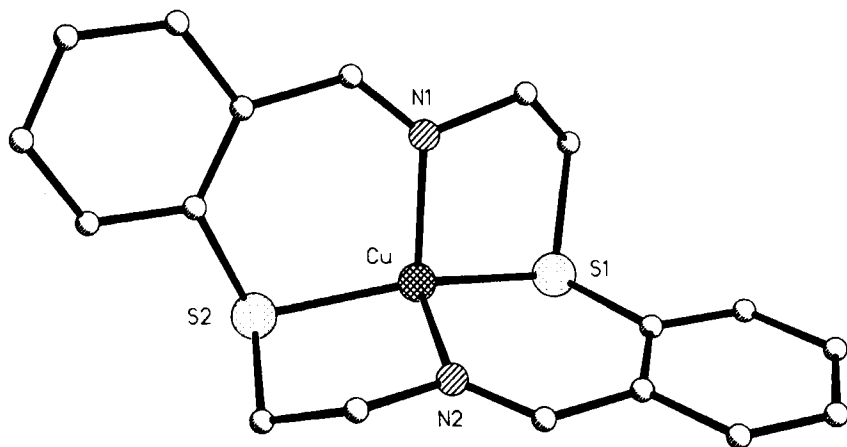


FIG. 11. Macrocycles with restricted flexibility.

FIG. 12. The structure of $[\text{Cu}(\text{L11})]^+$.

weak (2.52 and 2.28 Å to N6 and N12, respectively). There is an approximate twofold axis running along the Cu—N9 bond so that, overall, the geometry approximates trigonal bipyramidal (68). In the cupric complex $[\text{Cu}(\text{L13})(\text{ClO}_4)_2]$, the copper atom binds strongly to the three nitrogen donors. The N9—Cu—S16 angle is 149° (compared with 131° in the Cu(I) complex) and Cu—S2 is significantly longer than Cu—S16 (2.47 and 2.38 Å, respectively). The geometry of the complex is, therefore, better described as approximating square pyramidal, with S2 as the apical ligand (69). The redox chemistry of this system has not been reported but the Cu(I) complex is unreactive toward oxygen.

The structural data for $[\text{Cu}^{\text{I}}([\text{14}] \text{aneS}_4)]^+$ and $[\text{Cu}^{\text{II}}([\text{14}] \text{aneS}_4)(\text{ClO}_4)_2]$ are more typical of $\text{Cu}^{\text{I/II}}$ pairs (Fig. 14). The Cu(I) complex adopts an approximately tetrahedral geometry (in this case a polymeric arrangement is adopted), whereas the Cu(II) analog adopts tetragonal geometry and coordinates extra anionic ligands (51).

Possibly, achieving redox without geometrical change may require a rigid donor set defined by a three-dimensional cavity in a macropolycyclic or cryptand ligand. In this connection, it is interesting that a small dicopper(I) cryptate (70) may apparently be oxidized by one electron without change in geometry (Section IVD).

The work described above has led to a much deeper understanding of the factors controlling the redox properties and spectroscopy of copper ions in irregular coordination environments. It has contributed very significantly to understanding of the type 1 copper sites but, as yet, an accurate structural model has not been characterized.

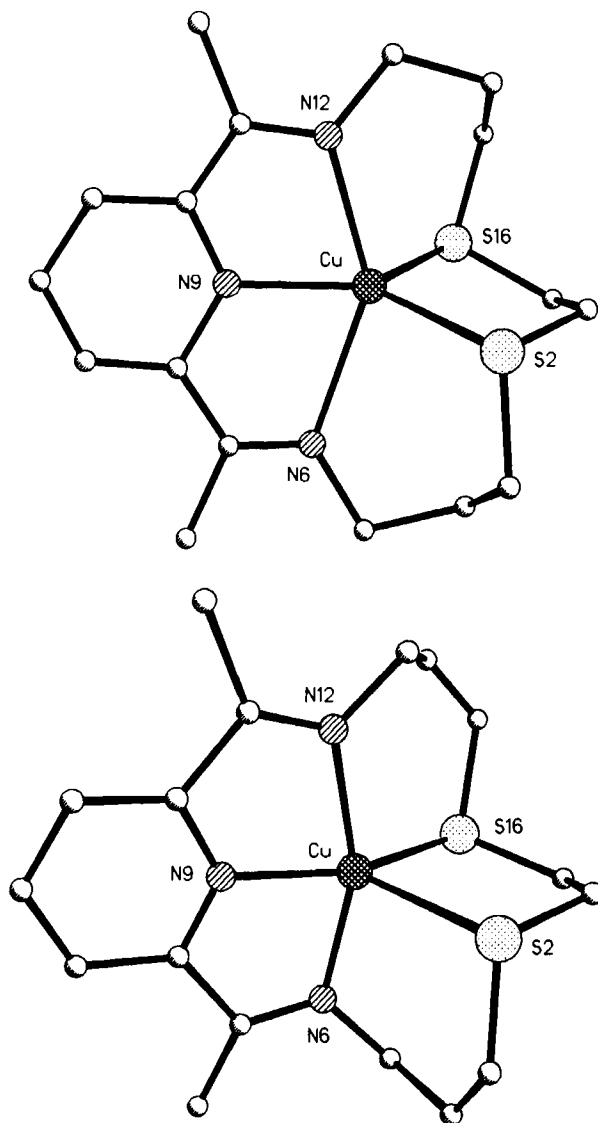


FIG. 13. The structures of $[\text{Cu}(\text{L13})]^+$ (top) and $[\text{Cu}(\text{L13})]^{2+}$ (bottom).

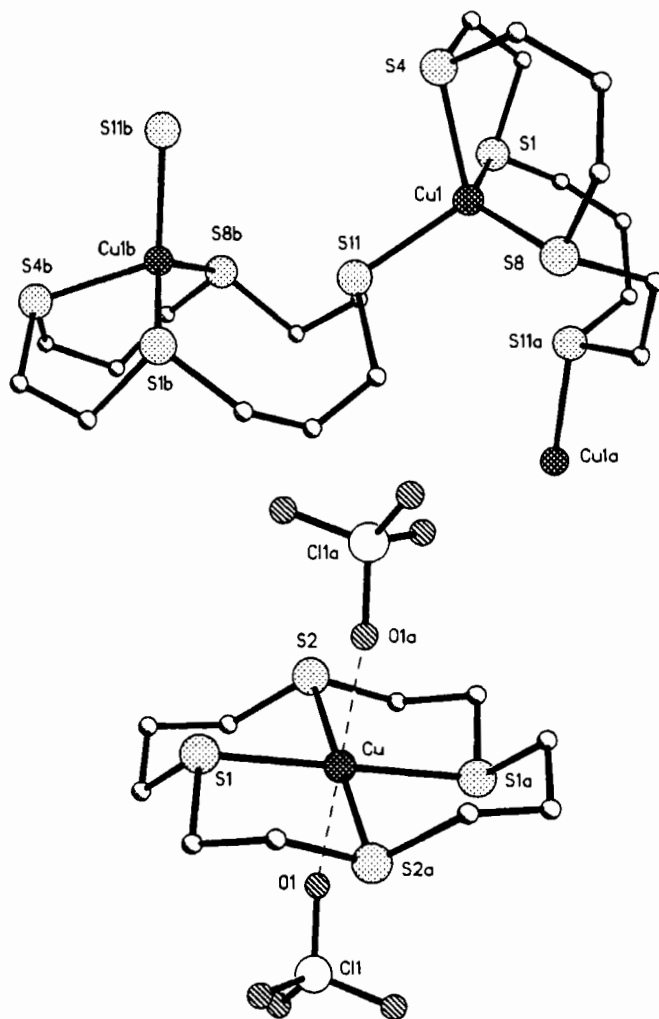


FIG. 14. The structures of $\{[\text{Cu}([\text{14}] \text{aneS}_4)]^+\}_n$ and $[\text{Cu}([\text{14}] \text{aneS}_4)(\text{ClO}_4)_2]$.

C. NICKEL ENZYMES

Since 1975 four classes of nickel metalloenzymes have been identified (71). The nickel hydrogenases and carbon monoxide dehydrogenases are considered here and the dinuclear active site of urease is described in Section IVB. The fourth class, methyl-S-coenzyme-M reductases,

contains nickel bound within a tetrahydro derivative of a porphinoïd prosthetic group (71, 72) and is outside the scope of this chapter.

Hydrogenases catalyze the production or consumption of hydrogen in several classes of bacteria and algae (71, 73):



They all contain iron-sulfur clusters and a subclass, the nickel hydrogenases, also contains functional nickel centers. Some nickel hydrogenases have recently been shown to contain a selenium donor (from a selenocysteine residue) coordinated to the nickel atom (74, 75). The most studied nickel hydrogenase is that from *Desulfovibrio gigas*, which contains one nickel ion, one [3Fe-4S] cluster, two [4Fe-4S] sites, and no selenium. The electronic spectra of the nickel centers are obscured by the more intense absorptions due to the iron-sulfur clusters. However, MCD spectra have been obtained for the oxidized forms of several examples for which the only paramagnetic component is Ni(III). Bands are observed in the ranges 300-460 nm and 530-670 nm and assigned to Ni(III) *d-d* and S → Ni charge transfer, respectively.

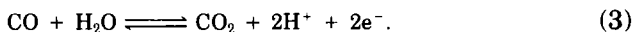
The inactive, oxidized form of the enzyme shows an EPR signal (labeled Ni-A) and frequently a second, minor component (labeled Ni-B). These are both assigned to low-spin Ni(III), probably with different geometries. On reduction with hydrogen the EPR signals disappear, possibly forming EPR-silent Ni(II), and subsequently a new spectrum (Ni-C) appears. The Ni-C signal has been variously assigned to Ni(I) or to Ni(III) (76); it correlates with hydrogenase activity and disappears upon further reaction with hydrogen, leading to assignment of the Ni-C state as the active form of the enzyme. Electron spin echo spectroscopy suggests a nitrogen donor is present (77), although EPR studies using ¹⁴N indicated no detectible hyperfine splittings. Experiments with ³³S showed interaction in the oxidized and H₂-reduced forms; comparison of the spectrum with those of nickel peptide complexes gave closest correspondence for peptides with one sulfur donor and tetragonal geometry. In some nickel hydrogenases there is evidence of significant interaction between the nickel and an iron-sulfur cluster but in *D. gigas* this is relatively weak.

EXAFS studies on the oxidized state of *D. gigas* hydrogenase are consistent with 2-3 sulfur atoms at 2.21 Å and 2-4 at 2.28 Å (78); for the *Methanobacterium thermoautotrophicum* enzyme, the spectrum was interpreted as due to 2.9 sulfur atoms at 2.25 Å (79). There is some uncertainty in the number of donors and as to the possible presence of

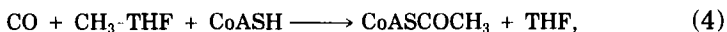
lighter donors; this was ascribed to a lack of suitable Ni(I) and Ni(III) model compounds with sulfur ligation. Recently Maroney and co-workers (80) reported K-edge XANES data for 44 Ni(II) and Ni(III) complexes of varied ligation and geometry, revealing useful relationships between donor sets and spectral features. This information was used to interpret the XANES data for *Thiocapsa roseopersicina* hydrogenase in the Ni-C form. The spectrum best matches a distorted trigonal bipyramidal geometry with one or two thiolate ligands, the remaining donors being O or N (or H). Comparison of XANES and XPS spectroscopies for enzyme and models suggests that sulfur donors are significantly involved in the redox processes at the nickel site. The XANES spectrum of this enzyme is different from that of *D. gigas* and consistent with the latter having more sulfur donors with pseudo-octahedral or five-coordinate geometry.

The apparent disagreement between the EXAFS and the ^{33}S EPR data is intriguing. Interpretation of the unusual spectroscopic properties of the two sulfur donors in the type 1 copper centers (Section IVB) demonstrates that the precise geometry of metal-sulfur bonding may influence the observed spectroscopic properties (including XANES) in ways difficult to predict in the absence of crystallographic data or extensive data from structurally characterized model complexes covering a range of unusual geometries. The mechanism of the reaction is postulated to involve interaction of Ni(II) with H_2 , involving heterolytic cleavage of the hydrogen and forming a nickel hydride (79), chemistry not normally seen in classical nickel coordination complexes. The inactive, fully oxidized Ni(III) state, with its stability and EPR signature, and the less stable Ni-C form are attractive targets for model studies.

Nickel is also found in a number of bacterial carbon monoxide dehydrogenases or CODHs (81). These are all involved in C_1 chemistry, they catalyze the oxidation of carbon monoxide to carbon dioxide:



Often, the same enzyme also acts as an acetyl coenzyme-A synthase; carbon monoxide, a methyl group, and coenzyme-A are bound at the active site and the condensation reaction to form acetyl coenzyme-A is catalyzed (81),



where THF is tetrahydrofolate and CoA is coenzyme A. This reaction is likely to involve a migratory ligand insertion and is an important

part of the process by which acetogenic bacteria fix carbon dioxide to form acetate. The most studied example of the bifunctional enzyme is that from *Clostridium thermoaceticum*, an $\alpha_3\beta_3$ protein containing approximately 2 Ni, 10–13 Fe, 14 acid-labile sulfurs, and 1–3 zinc atoms per $\alpha\beta$ dimer. It is assumed, in the absence of contrary evidence, that the nickel sites are equivalent, although the subunits are not identical.

Again, the iron–sulfur clusters mask the UV–visible spectrum of the nickel site and, in both the reduced and the oxidized forms of the protein, the nickel is EPR silent. When CO is bound to the oxidized enzyme, however, a distinctive Ni EPR is observed below ca. 150 K. Studies with labeled ^{61}Ni , ^{13}CO , and ^{57}Fe are interpreted in terms of an $S = \frac{1}{2}$ system involving Ni(III), CO, and at least three iron atoms, leading to the suggestion that the nickel atom is bound to carbon monoxide and linked to (or part of) an iron–sulfur cluster (81, 82). Recent FTIR studies imply that CO binds as a terminal ligand to nickel (83) and, therefore, the link between the nickel ion and the Fe–S cluster must be via some other, as yet unidentified, group. Iron EXAFS data are consistent with the presence of [4Fe–4S] clusters. Nickel EXAFS have been measured for both the CO-bound (84) and the oxidized (85) forms of the protein. Both sets of data imply some sulfur ligation to the nickel but do not permit discrimination between S_4 and $S_2(\text{N/O})_2$. There is no convincing evidence for an Ni–Fe interaction and, although this does not mean that such an interaction is not present, it seems to argue against a short Ni–Fe distance such as the 2.7 Å expected for a NiFe_3S_4 cluster. On the other hand, the Mössbauer spectra of two synthetic NiFe_3S_4 clusters show marked similarities to spectra of the oxidized and reduced forms of CODH from *C. thermoaceticum* (86, 87). To complicate matters further, Lindahl and co-workers (87) have deduced that current preparations of CODH may not be spectroscopically homogeneous, which could give rise to spurious and nonreproducible results. XANES studies of the reduced, oxidized, and CO-bound forms (85) suggest that the redox process involves the nickel atom and also that the geometry about the nickel is most likely to be distorted square planar or square pyramidal. Possible models for the Ni–Fe–S assembly are considered in Section VC.

A large number of Ni(III) complexes have been investigated in the last two decades and the chemistry of both macrocyclic and nonmacrocyclic systems has been reviewed (2, 3, 88). Most of this work has concentrated on ligands containing oxygen and nitrogen donors but recently interest in thioether complexes has increased (44, 46). Classical Ni(III) complexes have reduction potentials for the $\text{Ni}^{\text{III/II}}$ couple in the range

+500 to +1500 mV vs SCE (114); for the nickel hydrogenases this couple is in the range -390 to -640 mV. Recently $[\text{Ni}(\text{L14})]^{2-}$ (89) and $[\text{Ni}(\text{L15})]^{2-}$ (90) (Fig. 15) have been demonstrated to have $\text{Ni}^{\text{III/II}}$ couples of -760 and -735 mV, respectively (in DMF vs SCE). The common factor between these apparently very different complexes is that both thiolates and deprotonated oximes are electron rich and polarizable ligands.

Busch and co-workers (2, 91) first attempted to correlate data for the oxidation and reduction of an extensive series of $\text{Ni}(\text{II})$ tetraamine macrocyclic complexes. The data have since been extended to other macrocyclic systems and have been reviewed a number of times (3, 88). The most striking feature of the tetraamine series is the very large range spanned by the reduction potentials; ca. 2 V for both $\text{Ni}^{\text{III/II}}$ and $\text{Ni}^{\text{II/I}}$ couples (2), generally measured in acetonitrile solution, for which the geometries are assumed to be tetragonally distorted pseudo-octahedral. Within related series of ligands, changes in macrocyclic structure result in shifts of $E_{1/2}$ that are broadly additive and predictable (2, 91). For example, a change from a 14-membered to a 15-membered ring raises $E_{1/2}$ for $\text{Ni}^{\text{III/II}}$ by 225 mV, in line with the differences in ionic radii for the two states; charge delocalization stabilizes $\text{Ni}(\text{III})$, changing $E_{1/2}$ by -430 mV. Two extreme illustrations are $[\text{Ni}(\text{L16})]^{3+/2+}$ and $[\text{Ni}(\text{L17})]^{3+/2+}$ (Fig. 16), which have $E_{1/2}$ values of -0.5 and +1.3 V, respectively (vs Ag/AgNO_3 in acetonitrile). Fabbri (92) has pointed out that the magnitude of $E_{1/2}$ depends directly on the energy of the orbital to which the electron is added and can therefore be correlated with the ligand field. Many macrocyclic $\text{Ni}(\text{III})$ complexes are stable for long periods in dry air and a remarkable stable tetrahedral $\text{Ni}(\text{I})$ catenate has been reported by Sauvage *et al.* (93). Although these

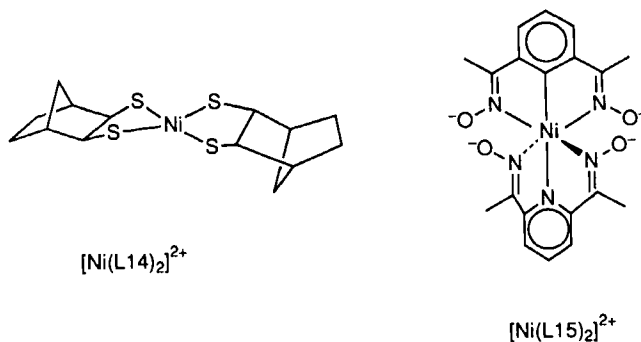


FIG. 15. Two nickel complexes with very negative redox potentials for the $\text{Ni}^{\text{III/II}}$ couple.

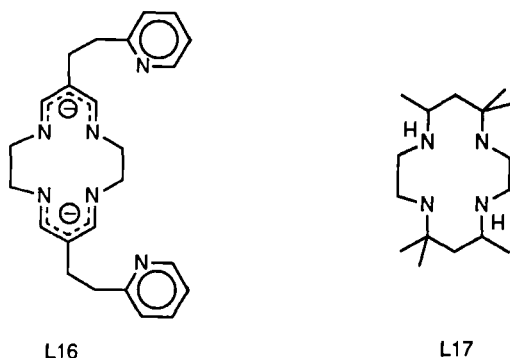
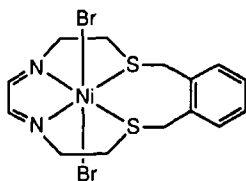
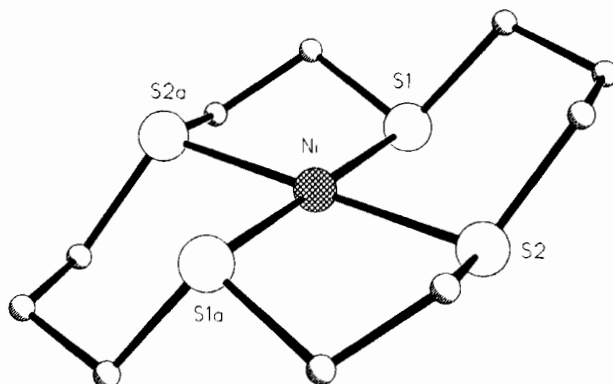


FIG. 16. Ligands L16 and L17.

complexes cannot be regarded as accurate structural models for nickel metalloenzymes, they illustrate the very large effects that can be induced by relatively small changes in ligation. By extending understanding of the chemistry of Ni(I) and Ni(III), they provide a basis for understanding the metalloenzyme chemistry.

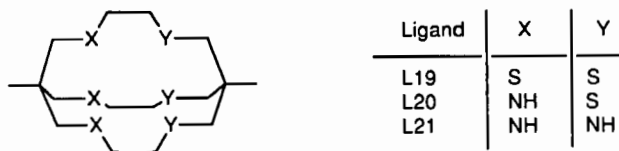
Since the structural data on the nickel enzymes postdate most of the studies on the redox chemistry of nickel complexes, there have been few attempts to synthesize specific macrocyclic model complexes for hydrogenase or CODH. The structural requirements for such a model currently appear less stringent than those for type 1 copper; between two and six sulfur donors in tetragonal-based geometry (except possibly for *T. roseopersicina*). Many nickel macrocyclic complexes meeting these criteria have been synthesized, starting with $[\text{Ni}(\text{L18})(\text{Br})_2]$ (Fig. 17), characterized by Thomson and Busch in 1964 (94). The $[\text{14}] \text{aneS}_x\text{N}_{(4-x)}$ series (Fig. 9) affords complexes of appropriate ligation and geometry (Fig. 18), whereas the many studies on the redox properties of nickel complexes (2, 3, 88, 91) provide the information needed to tune the reduction potentials of such systems. The rather low stability of thioether systems compared with their amine analogs (95) might be offset by binding the nickel atom within a suitable cryptand. Sarge-

FIG. 17. The complex $[\text{Ni}(\text{L18})(\text{Br})_2]$.

FIG. 18. The structure of $[\text{Ni}([14]\text{aneS}_4)]^{2+}$.

son and co-workers (96) have reported the synthesis of the hexathioether cage L19, which, along with L20 and L21 (97), make up a set of three-dimensional analogs to the $[14]\text{aneS}_x\text{N}_{(4-x)}$ series (Fig. 19). The cages do not have a vacant coordination site for substrate bonding but their nickel complexes would nonetheless be interesting speculative models for the biological nickel sites.

A number of macrocyclic complexes undergo reactions related to the nickel hydrogenases and CODH; these systems act as basic functional models for the behavior of the enzymes. Electrolytic reduction of H^+ to H_2 is catalyzed by $[\text{Ni}(\text{L1})]^{2+}$ (98). Upon reduction in DMF the first electron is added to the ligand, forming $[\text{Ni}(\text{L1}^{\cdot-})]^+$ (at -0.68 V vs Ag/AgCl) and this is subsequently further reduced (at -1.25 V) to the Ni(I) complex $[\text{Ni}(\text{L1}^{\cdot-})]$. In aqueous solution at pH 2, H_2 is released at a potential of -1.1 V at a carbon electrode. The potential implies that the initial catalyst is the Ni(II) complex of the ligand anion radical $[\text{Ni}(\text{L1}^{\cdot-})]^+$. The reduction of H^+ to H_2 proceeds with high efficiency and, perhaps surprisingly, no hydrogenation of the ligand imine bonds is observed. Studies in both DMF and aqueous solution led to the proposal of the mechanism shown in Fig. 20, involving a Ni(III) hydride species, as proposed for the hydrogenase cycle.

FIG. 19. Some $\text{S}_x\text{N}_{(6-x)}$ cryptands.

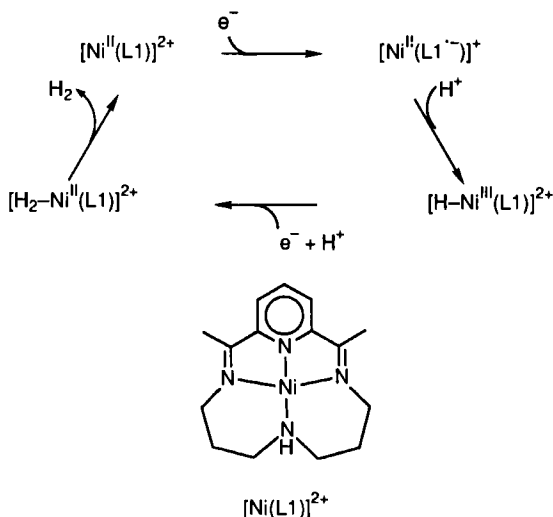


FIG. 20. Mechanism for the electroreduction of H^+ by $[\text{Ni}(\text{L1})]^{2+}$.

A number of nickel tetraaza macrocyclic complexes have been used in the electrocatalytic reduction of carbon dioxide to carbon monoxide (99); most are rather unspecific and produce H_2 in addition to CO. Sauvage and co-workers (100, 101) have demonstrated that $[\text{Ni}([14]\text{aneN}_4)]^{2+}$ and the related complex $[\text{Ni}_2(\text{bis}[14]\text{aneN}_4)]^{2+}$, adsorbed on a mercury electrode, are extremely efficient and specific catalysts for the electroreduction of CO_2 to CO in water, so that these complexes may be considered functional models for the action of carbon monoxide dehydrogenases. In the absence of the catalyst, potentials of the order of 2 V vs NHE are required for appreciable CO_2 reduction at metal cathodes, but in the presence of the nickel complexes the reaction proceeds at potentials of -0.9 V. At -1.0 V in water the reaction is quantitative, no H_2 is detected, and no decomposition of the catalyst occurs. Spectroscopic data suggest the presence of a $[\text{Ni}[14]\text{aneN}_4]\text{CO}]^+$ adduct as an intermediate in the reaction, and the mechanism shown in Fig. 21 was proposed. An identical scheme can be written for the bis[14]aneN₄ complex. The particular efficiency of these systems, compared with that of partially methylated rings (99), in catalyzing the reaction has been ascribed to their marked kinetic inertness. In addition, there may also be an interaction between bound CO_2 and one amine proton, stabilizing the initial Ni— CO_2 complex (Fig. 21).

Ni(I) alkyl chemistry, which may have some relevance to the acetyl coenzyme A synthase mechanism, has also been observed in nickel

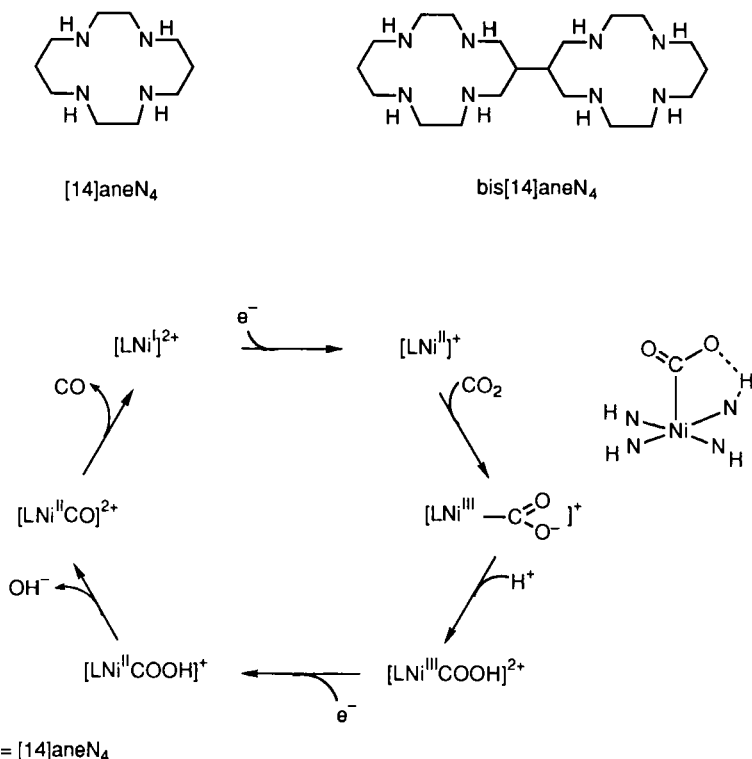


FIG. 21. Mechanism for the electroreduction of CO₂ by [Ni([14]aneN₄)]²⁺.

tetraaza systems (102). Reaction of excess CH₃I with [Ni(Me₄[14]aneN₄)]⁺ results in formation of CH₄. The reaction is thought to proceed via transfer of an electron from Ni(I) to CH₃I, followed by capture of the resulting ·CH₃ radical by a second Ni(I) complex:



The modeling process for nickel enzymes is still in the early “speculative” phase; however, these functional models illustrate that the chemistry performed by the enzymes is accessible by relatively simple synthetic complexes.

IV. Dinuclear Sites

Modeling dinuclear sites involves some extra variables in addition to the factors of ligation and geometry. The most important of these is the metal-metal distance because this in turn controls the introduction of bridging groups and the interaction between the metal ions. A related problem involves restricting the complex to a dinuclear structure and preventing formation of larger assemblies.

Two main strategies are apparent. The first strategy is to design dinucleating ligands in which the metal ions are held in proximity to one another and the metal-metal distance is fixed (or a variable within a fixed range). The second is to use mononucleating ligands that constrain the coordination geometry of the metal (for example by capping one face of the coordination polyhedron). Mononuclear units may then be bridged by suitable ligands in self-assembly reactions.

A. DIZINC ENZYMES

Two zinc enzymes with dinuclear active sites have been characterized, promoting interest in dinuclear zinc model systems. Phospholipase C from *Bacillus cereus* (103) contains three zinc atoms per subunit. An X-ray crystal structure determination at good resolution (1.5 Å) revealed that two of these constitute a dinuclear site with a Zn—Zn distance of 3.3 Å. The metal atoms are symmetrically bridged by an aspartate residue and by OH[−] or H₂O. Each zinc atom has approximate trigonal bipyramidal geometry with the ligation shown in Fig. 22. The third zinc atom is quite close to the bridged pair.

The structure of bovine lens leucine aminopeptidase (104) has also been determined by X-ray crystallography but in this case the resolu-

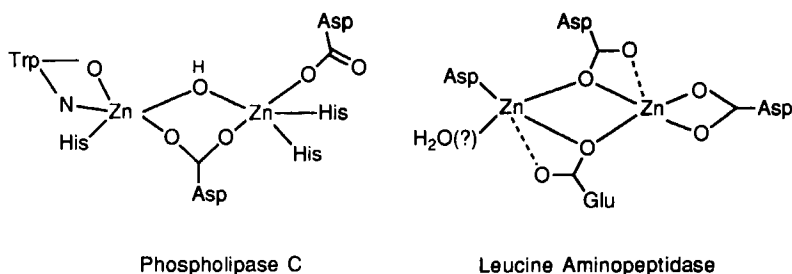


FIG. 22. The active site structure of phospholipase C and a proposed structure for the leucine aminopeptidase site.

tion is too low (2.7 Å) to reveal the details of the active site geometry. The zinc atoms are linked by aspartate and glutamate residues and the intermetallic distance is surprisingly short at 2.88 Å. In the bridged dinuclear iron and manganese analogs (Sections IVF and IVG), metal-metal distances are controlled by (and to a large degree diagnostic for) the number and nature of the bridging species. They are largely

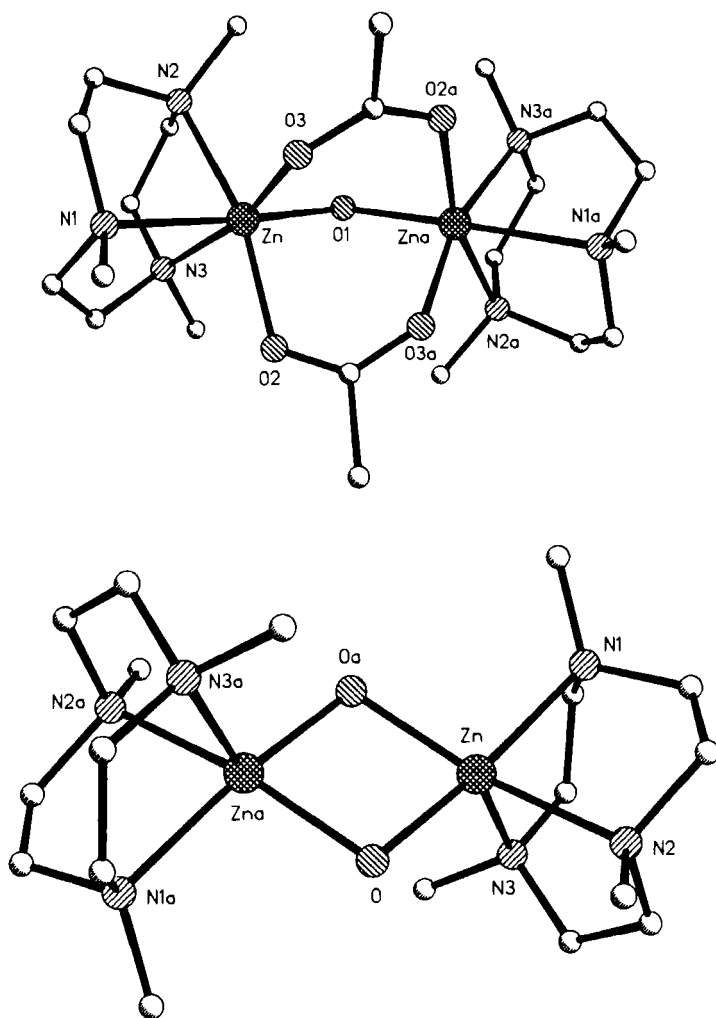


FIG. 23. The structures of $[(\text{Me}_3[9]\text{aneN}_3)\text{Zn}(\text{OH})]_2^{2+}$ (bottom) and $[(\text{Me}_3[9]\text{aneN}_3)\text{Zn}_2(\text{OH})(\text{CH}_3\text{COO})_2]^+$ (top).

independent of the identity of the metal ion. This consideration led Wieghardt *et al.* (105) to propose that the aminopeptidase site must involve two single atom bridges, possibly as shown in Fig. 22. Zinc complexes of $\text{Me}_3[9]\text{aneN}_3$ have been prepared (105) and support this assignment.

The structures of two dimeric complexes have been obtained. The centrosymmetric cation of $[(\text{Me}_3[9]\text{aneN}_3)\text{Zn}(\mu\text{-OH})_2](\text{ClO}_4)_2$ has a Zn—Zn separation of 3.024 Å; this distance and the geometry of the bridge unit are typical of the $\text{M}_2(\mu\text{-OH})_2$ core. The geometry at each zinc is approximately square pyramidal, the apical donor being N3 of the macrocycle (Fig. 23). In the presence of acetate ions, the triply bridged complex $[(\text{Me}_3[9]\text{aneN}_3)\text{Zn}(\mu\text{-OH})(\mu\text{-CH}_3\text{CO}_2)_2\text{Zn}(\text{Me}_3[9]\text{aneN}_3)]\text{ClO}_4 \cdot \text{H}_2\text{O}$ was obtained. The structure of the cation is shown in Fig. 23. The metal—metal distance is 3.31 Å, again in the range typical for such a unit and consistent with other bridged zinc systems (105).

The phenol substituted [9]aneN3 derivative $\text{H}_2\text{L22}$ (Fig. 24) also forms a dinuclear zinc complex ion with the formula $[\text{Zn}_2(\text{HL22})_2(\text{OH})]^+$, in which one phenol from each ligand is deprotonated. The two zinc atoms are linked by one μ -hydroxo bridge supported by two hydrogen bonds between the phenol on one macrocycle and the phenolate of the second. The Zn—Zn distance is 3.55 Å (106).

Derivatives of $[12]\text{aneN}_3$ have also been used in the synthesis of dinuclear zinc systems. The pendant imidazole ligand L8 (Fig. 6) forms five-coordinate species such as the structurally characterized $[\text{Zn}(\text{L8})\text{Cl}]^+$ (107). The imidazole pendant has the potential to act as a bridging group if deprotonated. Mixed ligand complexes containing $[(12]\text{aneN}_3)\text{M}_2(\text{L8})]^{3+}$ (where $\text{M} = \text{Zn}$ or Cu) have been isolated and characterized by microanalysis and spectroscopy; they have properties consistent with the presence of an imidazolate bridge but neither complex yielded crystals suitable for crystallography. Both complexes are

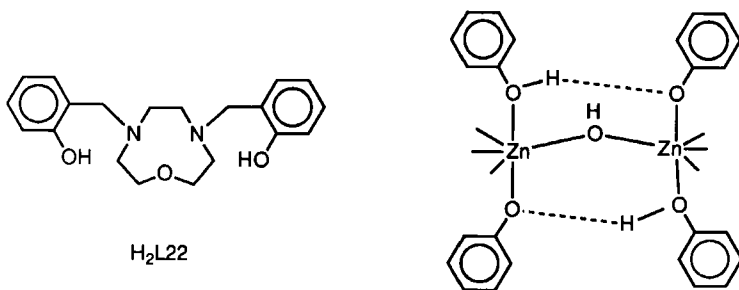


FIG. 24. The bridging structure in $[\text{Zn}_2(\text{HL22})_2(\text{OH})]^+$.

very sensitive to water but the dicopper complex shows some potential as a model for superoxide dismutase (Section IVC).

B. UREASE

Urease, the first nickel metalloenzyme to be discovered (108), catalyzes the hydrolysis of urea in bacteria, plants, and some invertebrates (71, 109):



In subsequent steps the initial carbamate product is further hydrolyzed to bicarbonate. Jack bean urease is a hexamer containing two nickel ions per monomeric subunit. It is unusually difficult to remove the metal atoms from the protein, requiring low pH and resulting in irreversible inactivation of the enzyme. There are indications that one nickel ion is more tightly bound than the other and, therefore, that the two sites are inequivalent.

Urease has an effective magnetic moment of 3.04 BM per nickel, consistent with approximately octahedral geometry. There is weak antiferromagnetic coupling between the metal ions ($J = -6.6 \text{ cm}^{-1}$), although about 22% of the nickel appears to be noninteracting (110). EXAFS and XANES data, necessarily averaged over both sites, suggest that the coordination spheres consist of five to six N/O donors at 2.06 Å in pseudo-octahedral geometry. The electronic spectrum of the enzyme has not been fully investigated but is also consistent with octahedral geometry, showing bands at 407, 745, and 1060 nm. Addition of the inhibitor 2-mercaptoethanol results in the appearance of $\text{S} \rightarrow \text{Ni}$ charge transfer transitions, implying that the sulfur binds to at least one nickel atom (110, 111).

Addition of 2-mercaptoethanol also results in apparent diamagnetism (110). Since there is no evidence for sufficient geometrical change to generate a low-spin nickel ion, the most likely interpretation is that the nickel centers are very strongly coupled, probably via a sulfur bridge. EXAFS data for the 2-mercaptoethanol adduct are consistent with a $(\text{N/O})_5\text{S}$, approximately octahedral coordination sphere, requiring either that one sulfur donor bridge the nickel ions or that two 2-mercapthethanol ligands bind, one to each metal ion (112). No metal-metal distance has been reported. Reaction of urease with aceto-hydroxamic acid (a strong inhibitor) reduces the antiferromagnetic coupling (110), possibly by removing a bridging donor.

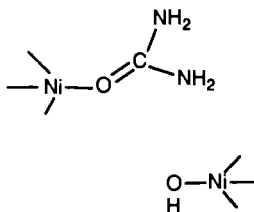


FIG. 25. A possible structure for the urease active site.

It has been proposed (109) that one nickel atom acts as a Lewis base, binding and activating urea, whereas the second generates a Ni—OH nucleophile (Fig. 25). Such a scheme has obvious parallels with the zinc metalloenzymes discussed in Sections IIIA and IVA and raises the question of why nickel should be used in this particular hydrolytic enzyme instead of zinc. The recent evidence of antiferromagnetic coupling implies the two nickel ions are likely to be bridged and the studies with inhibitors suggest that urea may also bind as a bridging ligand.

The number of reported dinuclear nickel(II) complexes is surprisingly small and, although a number of dinuclear complexes with macrocyclic ligands have been reported (113–117), few have been structurally characterized. These fall into two groups, those involving dinucleating macrocycles and those using the smaller [9]aneN₃ systems.

Dinucleating macrocycles such as L23 and L24 (Fig. 26) provide two transition metal coordination sites and impose di- μ -phenoxo bridging. Nickel(II) ions are coordinated by two imine nitrogen donors and the two bridging phenoxides in an essentially planar array and pseudo-

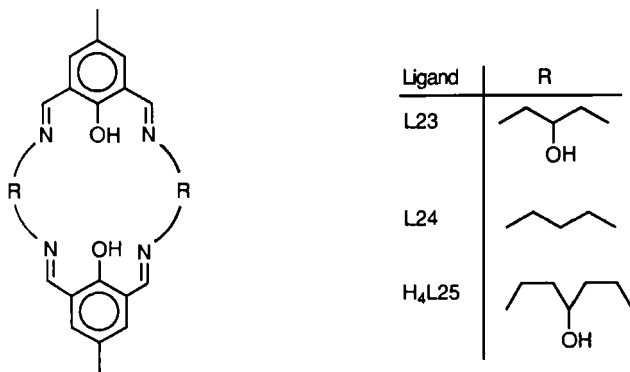


FIG. 26. Some macrocycles incorporating phenol donors.

octahedral coordination is completed by counter ions or solvent molecules. X-ray crystal structures of $[\text{Ni}_2(\text{L23})(\text{Cl})_2(\text{H}_2\text{O})]\cdot 2\text{H}_2\text{O}$ (Fig. 27) (113) and of $[\text{Ni}_2(\text{L24})(\text{CH}_3\text{OH})_2(\text{ClO}_4)_2]\cdot 2\text{NHET}_3\text{ClO}_4$ (114) have been reported. Both are centrosymmetric with the expected approximately octahedral geometry and have Ni—Ni distances of 3.10 and 3.135 Å, respectively. All the dinuclear Ni(II) complexes of this class show anti-ferromagnetic coupling via the phenoxo bridges. When coupling constants have been reported (113, 117) they are in the range -23 to -27 cm^{-1} , with the interesting exception of $[\text{Ni}_2(\text{L23})(\text{CH}_3\text{COO})_2]\cdot \text{H}_2\text{O}$, where J is approximately -3 cm^{-1} . The crystal structure of this acetate complex has not yet been reported but spectral data suggest that the acetate group may be bridging. In solution the axial ligands can generally be displaced by solvent or by stronger donors, but no studies on thiolate or urea binding have been published. Cyclic voltammograms of $[\text{Ni}_2(\text{L23})]^{3+}$ in DMF solution show two oxidation peaks, $E_{\text{pa}} = -1.23\text{ V}$ and -1.06 V (vs SCE), interpreted as oxidation to Ni(III)Ni(II) and to Ni(III)Ni(III), respectively. The corresponding reduction steps are closely spaced and appear as a single peak with $E_{\text{pc}} = -1.32\text{ V}$. The electronic spectra of the complexes are compatible with approximately octahedral geometry.

The X-ray crystal structure of $[\text{Ni}_2(\mu\text{-OH})(\mu\text{-CH}_3\text{COO})_2(\text{Me}_3[9]\text{aneN}_3)_2]\text{ClO}_4\cdot \text{H}_2\text{O}$ (115) has been reported and is quite similar to

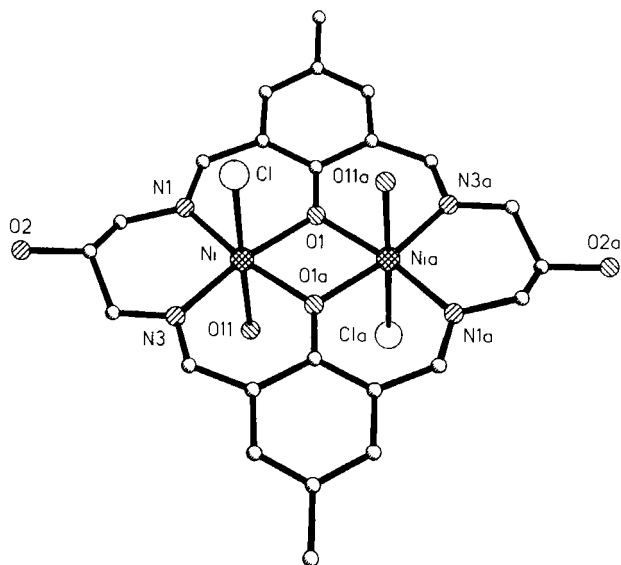


FIG. 27. The structure of $[\text{Ni}_2(\text{L23})(\text{Cl})_2(\text{H}_2\text{O})_2]$.

the much more extensively studied iron and manganese equivalents (Sections IVF and IVG). The Ni—Ni distance in the hydroxy bridged complex is 3.400 Å with the antiferromagnetic coupling constant $J = -4.5 \text{ cm}^{-1}$; in the related aquo bridged case (118) the Ni—Ni distance is 3.56 Å and the coupling appears to be reduced. Again, the electronic spectra are as expected for octahedral geometry and there is no evidence of significant decomposition to monomer in solution. Cyclic voltammetry for the μ -hydroxo complex shows irreversible reduction at -0.85 V (vs Ag/AgCl in ethanol). There are two oxidation peaks; the second (at ca. $+1.04 \text{ V}$ vs Fc/Fc $^+$) is irreversible and the first is quasi-reversible at fast scan speeds ($E^0 = -0.38 \text{ V}$ vs Fc/Fc $^+$).

Both these systems match the basic ligation and geometrical features of urease. Both appear to show some changes in coupling with ligation and some possibility of binding or displacing ligands. They represent early speculative models for the metalloprotein. As with the mononuclear nickel enzymes, the available data on the urease active site have recently increased substantially and have reached the point at which more meaningful model studies could be undertaken.

C. SUPEROXIDE DISMUTASE

The active site of bovine superoxide dismutase (119) is shown in Fig. 28. It contains one copper ion and one zinc ion bridged by a deprotonated histidine residue. The geometry at the zinc is approximately tetrahedral, whereas that at copper approaches square planar. The metalloenzyme contains two such sites and is usually denoted $\text{Cu}_2\text{Zn}_2\text{SOD}$. Metal ion replacement experiments show that the zinc atom may be replaced by copper (or other metals) without loss of function, and the copper-substituted form ($\text{Cu}_2\text{Cu}_2\text{SOD}$) has been much studied as it provides some information not available from the native enzyme. The imidazolate bridge is rather unusual and is important in the suggested "ping-pong" mechanism of the enzyme (Fig. 28), which depends on imidazolate binding Cu(II) in preference to protons but protons in preference to Cu(I). The properties of the bridged site are conveniently monitored

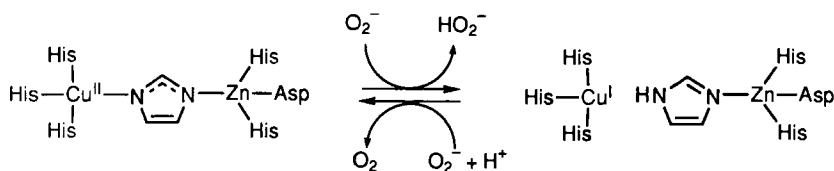


FIG. 28. The active site and reaction mechanism of superoxide dismutase.

by the extent of antiferromagnetic coupling in the $\text{Cu}_2\text{Cu}_2\text{SOD}$ derivative, where $J = -26 \text{ cm}^{-1}$.

The Cu-im-Cu bridged unit was an early target for model studies and a number of nonmacrocyclic systems were investigated (120). Some of these, notably complexes containing $[\text{Cu}_2(\text{L26})_2(\text{im})]^{3+}$ and $[\text{Cu}_2(\text{L27})(\text{im})]^{3+}$ (Fig. 29) show antiferromagnetic coupling constants ($J = 25.8$ and 26.9 cm^{-1} , respectively) and EPR spectra that are very similar to those of $\text{Cu}_2\text{Cu}_2\text{SOD}$. However, these models have limited stability in solution; the bridged complex $[\text{Cu}_2(\text{L26})_2(\text{im})]^{3+}$, for example, is the major species in solution only in the range $8.5 < \text{pH} < 9.5$ compared with $4.5 < \text{pH} < 11$ in $\text{Cu}_2\text{Cu}_2\text{SOD}$. A dramatic increase in solution stability was achieved using the macrocyclic ligands L28 and L29. The bridged complex $[\text{Cu}_2(\text{L28})(\text{im})]^{3+}$ (Fig. 30) is the major species in solution over the range $7 < \text{pH} < 11.5$, and the equivalent complex of L29 shows antiferromagnetic coupling ($J = -29.4 \text{ cm}^{-1}$) and EPR spectra comparable with those of the copper-substituted enzyme (120–122). The macrocyclic complexes will catalyze the disproportionation of superoxide ions but this in itself is not surprising as free Cu(II) ions will also promote the reaction.

The enhanced stability of the macrocyclic complexes over the closely related complex of L26 is partly a manifestation of the macrocyclic effect (3). There is also an effect peculiar to di- or polynucleating systems and related to the chelate effect; the two copper atoms are maintained in

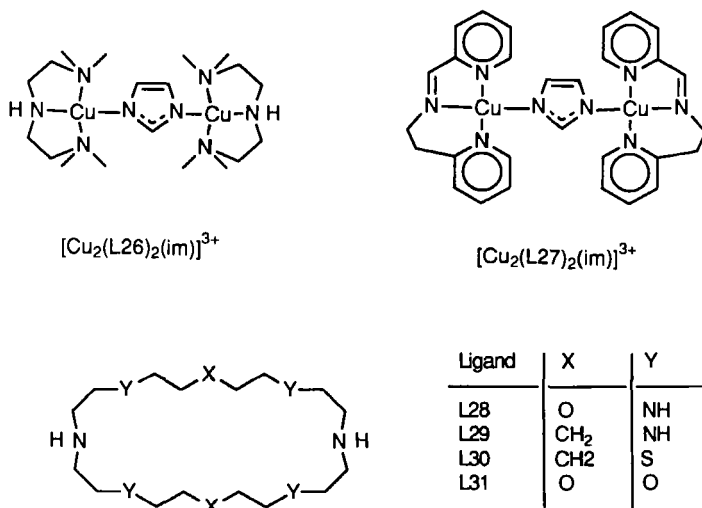


FIG. 29. Models for $\text{Cu}_2\text{Cu}_2\text{SOD}$.

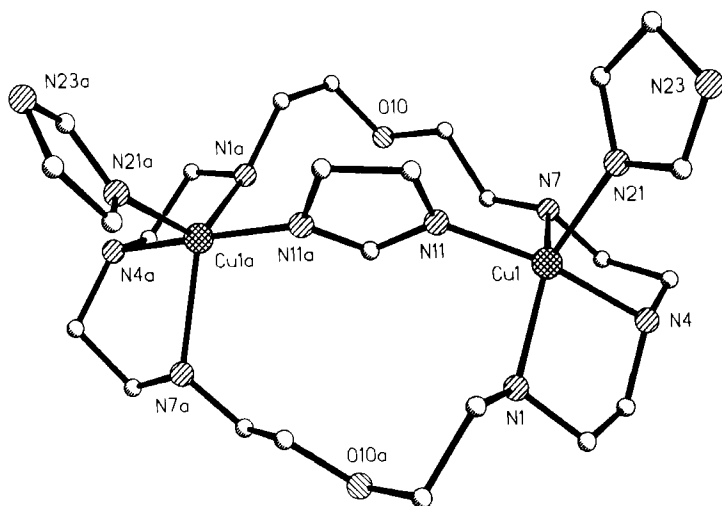
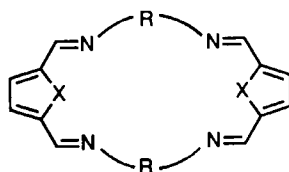
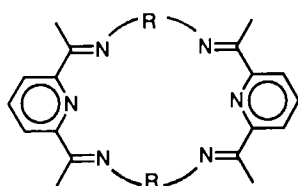


FIG. 30. The structure of $[\text{Cu}_2(\text{L28})(\text{im})_3]^{3+}$.



Ligand	R	Ligand	X	R
L32		L38	S	
H ₂ L33		L39	O	
L34		L40	O	
L35				
L36				
L37				

FIG. 31. Some dinucleating Schiff-base macrocycles.

close proximity to each other and, in the absence of other ligands, they are coordinatively unsaturated. Imidazole (or imidazolate) bonding to one copper ion results in a high local concentration of imidazole at the second copper atom. This promotes formation of the bridge and retards its dissociation. It was observed that an equimolar mixture of Cu^{2+} and L29 (which contains largely mononuclear $[\text{Cu}(\text{L29})]^{2+}$) will rearrange itself upon addition of 1 eq of imidazole to form $[\text{Cu}_2(\text{L29})(\text{im})]^{3+}$ in good yield (120, 122). It was suggested that such a rearrangement is equivalent to the migration of copper ions in zinc-depleted superoxide dismutase (designated $\text{Cu}_2\text{E}_2\text{SOD}$, where E implies an empty site); at $\text{pH} > 7$, copper ions migrate to form $\text{Cu}_2\text{Cu}_2\text{SOD}$ and $\text{E}_2\text{E}_2\text{SOD}$ (123).

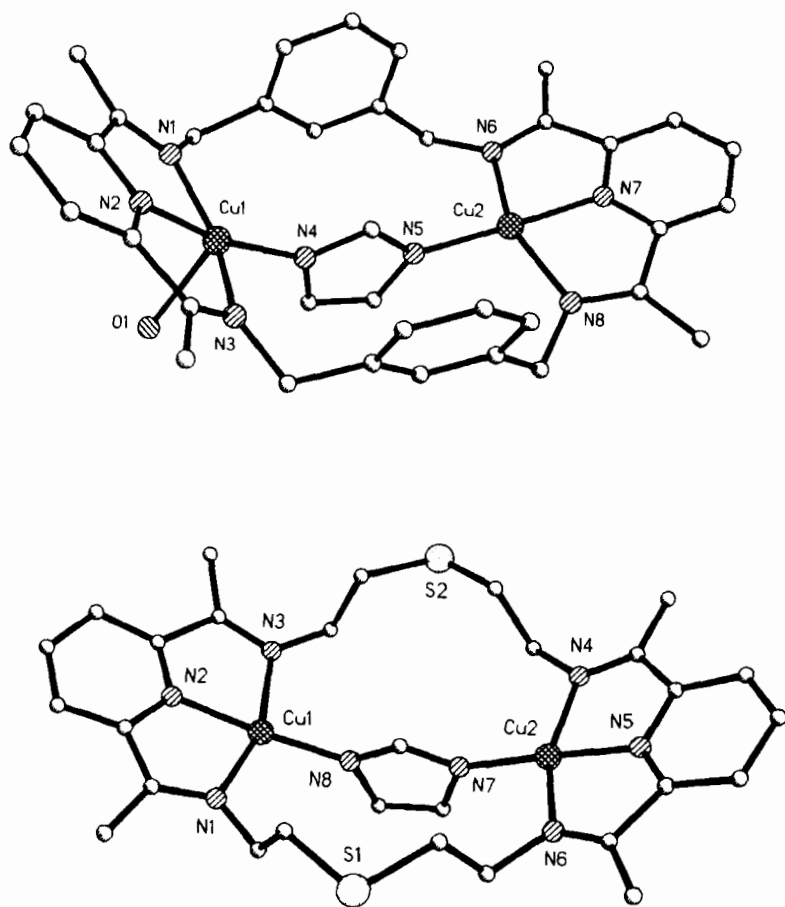


FIG. 32. The structures of $[\text{Cu}_2(\text{L37})(\text{im})(\text{H}_2\text{O})]^{3+}$ (top) and $[\text{Cu}_2(\text{L34})(\text{im})]^{3+}$ (bottom).

These reactions reflect both the stability of the Cu-im-Cu species and a good match between this unit and the host cavity (macrocycle or protein). A similar effect is probably responsible for the“(template)²⁺” (124) formation of $[\text{Cu}_2(\text{L37})(\text{im})]^{3+}$ (Figs. 31 and 32).

Following the above work a number of other macrocycles containing Cu-im-Cu units were characterized (124–127) and some of these are shown in Fig. 32. This activity was partly related to SOD investigations and partly resulted from the suggestion that the cytochrome *c* oxidase active site contained a Cu-im-Fe bridge. This site shows strong antiferromagnetic coupling and the fact that none of the imidazolate-bridged model complexes showed anything other than weak to moderate coupling (Table IV) contributed significantly to the eventual abandonment of this model.

As mentioned in Section IVA, mixed ligand complexes of formula $[(12]\text{aneN}_3)_2\text{M}_2(\text{L8})]^{3+}$ (where M is Zn or Cu) have been synthesized and characterized spectroscopically (107). The data are consistent with an imidazolate bridged structure as illustrated in Fig. 33. EPR spectroscopy on the dicopper(I) complex shows evidence of coupling; there is a weak $\Delta M = \pm 2$ transition at half field (ca. 1560 G compared with ca. 1540 G in $\text{Cu}_2\text{Cu}_2\text{SOD}$). Attempts to prepare heterodinuclear CuZn complexes as $\text{Cu}_2\text{Zn}_2\text{SOD}$ models have, so far, been unsuccessful. However, some heterodinuclear complexes of related ligands have been

TABLE IV
PROPERTIES OF SOME BRIDGED DICOPPER(II) COMPLEXES

Ligand	Bridge(s)	Cu—Cu (Å)	<i>J</i> (cm ⁻¹)	Reference
L34	Imidazolate	5.87	-21.2	125, 126
L36	Imidazolate	5.99	-21.0	126, 127
L36	1,3-Azide	6.02	Weak	144
L30	(1,3-Azide) ₂	5.14	Diamagnetic	138
Me ₃ [12]aneN ₃	(1,3-Azide) ₂	5.77	-331	145
Me ₃ [12]aneN ₃	(1,3-Azide) ₂	5.06	> -400	145
L30	(1,3-Azide) ₂	5.15	Diamagnetic	138
L31	(1,1-Azide) ₂	3.16	+50-90	140
L28	OH, ClO ₄	3.64	-496	137
L32	OH, H ₂ O	3.15	-32	146
L41	OH	3.38	-410	147
L38	(OEt) ₂	3.00	ca. -320	141
L42	OMe, OAc	3.10	-35.4	148
L23	(Phenoxide) ₂	3.09	-414	149
HL33	Alkoxide	3.64	-42	150

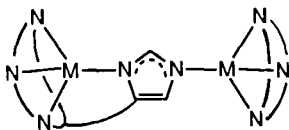


FIG. 33. Proposed structure of $[(12]aneN_3)M_2(L8)]^{3+}$.

prepared in good yield (128), suggesting that a Cu_2Zn_2SOD model may be accessible. Such a complex might usefully model the proposed role of the zinc ion in controlling the pK_a of the imidazole residue except that it is unlikely to have the solution stability of the macrocyclic systems.

D. DINUCLEAR COPPER SITES

Active sites containing two copper ions that are antiferromagnetically coupled in the oxidized state are often referred to as type 3 copper sites (129). It has recently become evident that these centers cannot all be considered alike and that in the blue copper oxidases the "type 3" sites are in fact part of a tricopper cluster; these will be considered in Section VA. The proteins containing dinuclear type 3 copper sites comprise hemocyanin and a number of oxygenase enzymes, of which the best known are tyrosinase and dopamine β -hydroxylase.

Hemocyanin is an oxygen carrier in molluscs and arthropods; it is capable of reversibly binding one dioxygen molecule per dicopper site. Spectroscopic studies on various forms of the protein (38, 130) established that the dioxygen is bound symmetrically to both copper ions as peroxide. In oxidized forms, the copper ions are in tetragonal geometry and each is bonded to two or three histidine groups (38). The $Cu_2^{II}O_2^{2-}$ unit shows intense ligand-to-metal charge transfer bands at 345 and 570 nm ($\epsilon = 20,000$ and $1000 M^{-1} cm^{-1}$) and a circular dichroism band at $485 cm^{-1}$. EXAFS spectra suggested a Cu—Cu distance of 3.55 Å for deoxyhemocyanin, 3.66 Å for the azidomet form, and 3.66 Å for oxyhemocyanin. Strong antiferromagnetic coupling is observed in oxyhemocyanin and other oxidized forms, leading to diamagnetism of the site. To mediate this coupling, a second "endogenous" bridge (in addition to peroxide) was suggested and bridging species such as serine (alkoxide), tyrosine (phenolate), or hydroxide were proposed. These data led to the proposal of the 1,2- μ -peroxo model (Fig. 34) for dioxygen binding in oxyhemocyanin.

X-ray crystal structures of deoxyhemocyanin show that each copper atom is coordinated only to three histidine groups (131, 132). The Cu—Cu distances and the geometry about the copper ions differ in the

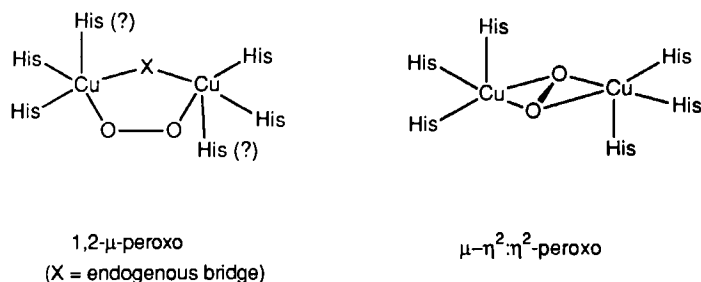


FIG. 34. Proposals for the active site structure of hemocyanin.

two structures determined (3.8 Å and pyramidal in one case (131) or 4.6 Å and trigonal planar in the other (132)). It is possible that these differences are related to the cooperativity of the hemocyanin molecule and the particular protein subunit investigated. In neither case is there any evidence of a bridging ligand.

The X-ray structure of oxyhemocyanin has been reported recently (132) and contains a μ - $\eta^2:\eta^2$ -peroxo bridge (Fig. 34). No endogenous bridge is present but the peroxide provides two one-atom links that can mediate antiferromagnetic coupling. The copper ions are 3.6 Å apart and each has tetragonal geometry. This structure was not unprecedented, Kitajima has characterized some model complexes containing dioxygen bound in this geometry (133) and, subsequently, Solomon predicted such a structure was likely for oxyhemocyanin (38). However, most model studies undertaken to date have been directed toward synthesis of a 1,2- μ -peroxo complex.

Model studies involving dinuclear copper sites have been reviewed many times (6, 120, 134–136); it is possible to discern a number of distinct phases as these studies progressed and the requirements for new model complexes became more sophisticated. The most significant contributions from macrocyclic chemistry toward understanding the type 3 copper proteins were in the earlier stages of the investigation and relate to the general chemistry of bridged bicopper complexes. Discovery of the type 3 copper site (along with the Cu—Zn and Cu—Fe active sites of superoxide dismutase and cytochrome *c* oxidase, respectively) led to general interest in exploring the chemistry of dinuclear copper systems. Several classes of dinucleating macrocyclic ligands that gave access to complexes with a wide range of properties were developed (6, 135, 137–139). Tuning these systems, by modification of the number and type of donors or size and rigidity of the ring, allowed variation of Cu—Cu distances, coordinative unsaturation, bridging,

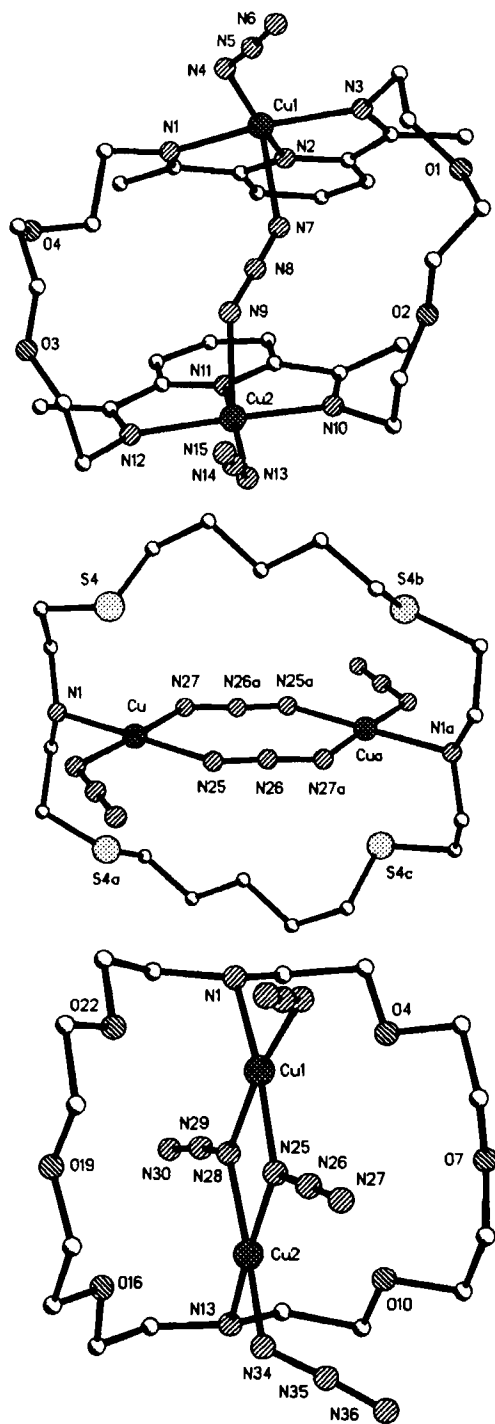
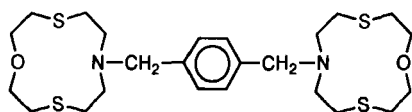


FIG. 35. Azide bridging modes in $[\text{Cu}_2(\text{L36})(\text{N}_3)_3]^+$ (top), $[\text{Cu}_2(\text{L30})(\text{N}_3)_4]$ (middle), and $[\text{Cu}_2(\text{L31})(\text{N}_3)_4]$ (bottom).

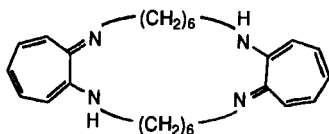
and redox properties. In flexible macrocycles such as L28 and related systems (137, 138, 140), the macrocycle defines the maximum Cu—Cu separation but additional bridging or nonbridging ligands are accommodated by adjustment of the macrocyclic conformation. As the ligand becomes less flexible, the geometry and Cu—Cu distances become more tightly controlled and the specificity toward binding guest molecules is increased (124, 141, 142).

Two sets of bridging species were of particular relevance to early studies on hemocyanin. The azide ion bridges the two copper ions in azidomethemocyanin and the resulting complex exhibits informative spectroscopy (143). The structure was thought (erroneously, as it now turns out (132)) to be similar to that of oxyhemocyanin and its extra stability made it an attractive target for model studies. A number of macrocyclic μ -azido-dicopper(II) complexes showing different coordination modes are illustrated in Fig. 35 and some of their properties are listed in Table IV (144–150); the ligands are shown in Figs. 30, 31, and 36. The azidomethemocyanin site is believed to contain a μ -1,3-azido bridge and this has been quite accurately modeled in nonmacrocyclic systems (134, 143) but not in macrocyclic complexes.

As stated above the diamagnetism of oxy- and azidomethemocyanin prompted suggestions of an additional “endogenous” bridge between the copper atoms that would mediate most of the coupling. Phenolate, alkoxide, and hydroxide were suggested as possible bridging species and a number of investigations on the geometry (especially the Cu—Cu distance) and magnetism of bridged dicopper(II) complexes were undertaken. Dinucleating macrocyclic ligands were especially useful for this work as they provided a means of maintaining two copper ions adjacent to each other while varying the Cu—Cu distances in a controlled manner. Examples of such complexes are shown in Table IV, along with Cu—Cu distances and antiferromagnetic coupling constants. The latter cover a wide range, reflecting considerable variation in geometry and macrocyclic donor type. These studies revealed that each of the candidates for “endogenous” ligand was capable of mediating strong antiferromagnetic coupling; however, X-ray studies of deoxy- and oxyhemocyanin



L41



L42

FIG. 36. Structures of some dinucleating ligands.

anin have revealed that, although there are two atoms bridging the copper ions, there is no endogenous bridge and the coupling is mediated by the (then unknown) $\mu\text{-}\eta^2\text{:}\eta^2\text{-peroxo}$ linkage. The considerable synthetic and theoretical effort expended on these systems has resulted in a much fuller understanding of, in particular, the factors influencing antiferromagnetic coupling in dicopper systems, a valuable spin-off from the modeling effort.

Clearly, the oxygen-carrying properties of hemocyanin were also an important target for model studies and the next obvious step was to investigate the interaction of Cu(I) model complexes with molecular oxygen (or Cu(II) models with superoxide or peroxide (151)). There are a number of reports in the literature concerning reactions between macrocyclic copper complexes and dioxygen to yield dioxygen (usually peroxo) adducts (147, 152–153c). Where dioxygen uptake by dicopper(I) complexes has been measured, it usually corresponds initially to a Cu:O₂ ratio of 1:2 but this first stage is followed by slower reaction involving further dioxygen uptake (153, 153c). The reaction, in solution or the solid state, is accompanied by a color change (generally to green) and this may be partially or largely reversed by heating and pumping (152) or by flushing the oxygenated solution with an inert gas (152, 153, 153b). This cycle can usually be repeated a number of times but is accompanied by gradual degradation of the complex. A $\mu\text{-peroxo}$ bridge seems likely to be present in most of these complexes (Fig. 37), and there is convincing spectroscopic evidence to support this in at least one case (153b). Bulkowski and co-workers have reported the X-ray crystal structure of $[\text{Cu}_2(\text{L43})\text{O}_2(\text{H}_2\text{O})_2]_2^{6+}$, which appears to show two $\mu\text{-peroxo}$ bridges linking the two dicopper macrocycles. However, the quality of the data is poor and the structural conclusions unreliable (153a).

Unstable dioxygen adducts may also be described more optimistically as complexes containing activated dioxygen. If no other suitable substrate is present, decomposition of the adduct occurs with oxidation of the ligand (153) but, if suitable substrates are added, catalytic oxidations may be observed. The dicopper(II) ions $[\text{Cu}_2(\text{L39})(\text{X})_2]^{2+}$ (where X represents a bridging hydroxo or alkoxo group) can be reduced upon heating in acetonitrile solutions. The products are the dicopper(I) complex $[\text{Cu}_2(\text{L39})(\text{CH}_3\text{CN})]^{2+}$ and oxidized X. If oxidizable substrates, such as thiols, catechols, and hydrogen peroxide, are added, these are oxidized in preference to X and several of these reactions have been shown to be catalytic in the presence of dioxygen. The catalytic cycle is thought to involve a 1,1- $\mu\text{-peroxo}$ adduct (141, 142, 154).

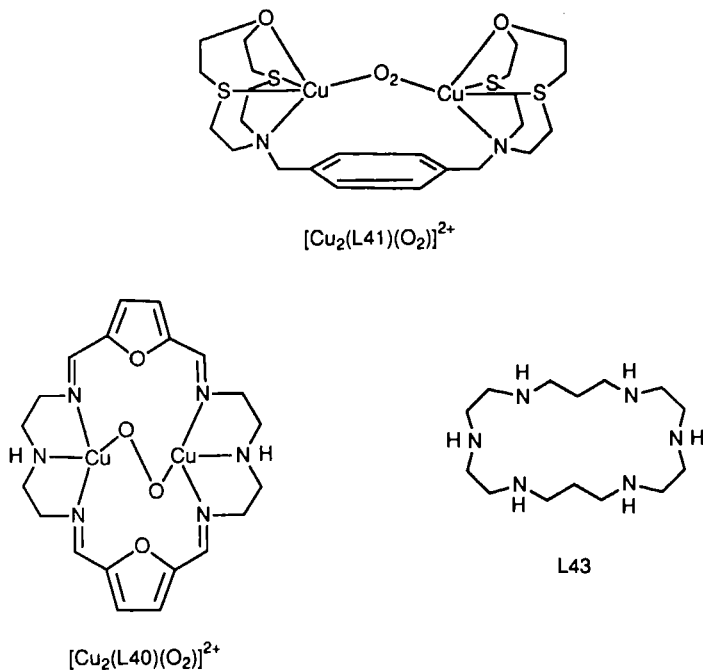


FIG. 37. Proposed structures for some μ -peroxo-dicopper complexes.

Stable and well-characterized dioxygen adducts have been prepared using nonmacrocyclic ligands (133, 134, 136, 155) but no macrocyclic compounds of similar stability have yet been reported. Interestingly, however, the ligands used by Kitajima and co-workers to prepare μ - η^2 : η^2 -peroxo complexes are sterically hindered derivatives of hydrotris(1-pyrazolyl)borate (133). In their iron and manganese chemistry (Sections IVF and IVG), these ligands show behavior very similar to that of [9]aneN₃ series so it may yet be possible to use suitably modified macrocyclic systems as useful oxyhemocyanin models.

E. MIXED-VALENCE DICOPPER

Mixed-valence dicopper complexes have been of some interest as models for the spectroscopically informative half-met hemocyanins (156, 157). These complexes are described as Class I if the unpaired electron is localized on one copper ion (i.e., $[\text{Cu(I)Cu(II)}]$) and Class III if it is fully delocalized (i.e., $[\text{Cu(1.5)Cu(1.5)}]$); intermediate situations

are assigned to Class II (156, 158, 159). Delocalization is indicated by the appearance of an intervalence transfer band in the electronic spectrum and by a characteristic seven-line EPR spectrum.

Mixed-valence copper species have recently been proposed for several multicopper enzymes; nitrous oxide reductase (160), the Cu_A site of cytochrome *c* oxidase (161), and cysteamine-treated tyrosinase (162). The Cu_A site of cytochrome *c* oxidase and site A (160) in nitrous oxide reductase both appear to act as electron-transfer centers. The two sites are spectroscopically very similar and each exhibits a seven-line EPR signal in the oxidized form (160, 161, 163). Although neither site has been shown unequivocally to be dinuclear, no convincing explanation for the EPR signal, other than the presence of a Class III $[\text{Cu}(1.5)\text{—Cu}(1.5)]$ center, has been forthcoming. The visible and MCD spectra of these sites have been interpreted (160, 164) as requiring some cysteine ligation to account for the high intensity and the presence of two bands of opposite sign in the MCD spectrum (473 and 678 nm), which have been assigned to Cu-Cys charge transfer.

The substrate-binding site in nitrous oxide reductase is a dinuclear copper unit that, in some states, also exists as a mixed-valence species (160); this center does not show a seven-line EPR spectrum and is similar to the (Class II) mixed-valence derivatives of hemocyanin (156).

The hexaimino cryptand L44 (Fig. 38) is close to the lower limit of cavity size for a dinucleating ligand. A dinuclear copper (I) complex of

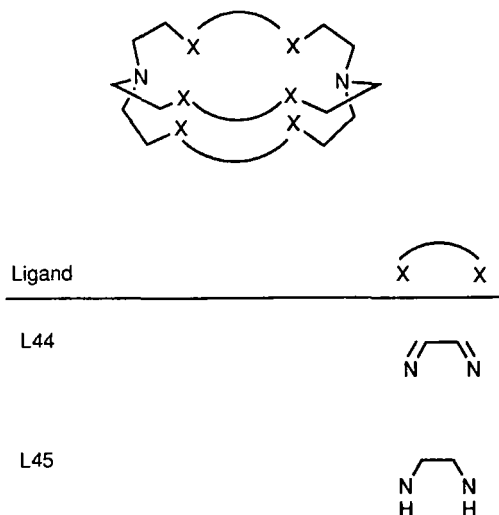


FIG. 38. Some small cryptands.

formula $[\text{Cu}_2(\text{L44})](\text{ClO}_4)_2$ results from transmetallation of mononuclear group II complexes with $\text{Cu}(\text{CH}_3\text{CN})_4\text{ClO}_4$, whereas treatment with formulae $[\text{Cu}_2(\text{HL44})]\text{X}_4$ or $[\text{Cu}_2(\text{L44})]\text{X}_3$, where $\text{X} = \text{CF}_3\text{SO}_3^-$, ClO_4^- , etc., and HL44 represents the protonated ligand (70, 165, 166). Instability in solution has prevented growth of crystals of the pure mixed-valence complex large enough for X-ray structure analysis. However, blue crystals of a dicopper(I) complex doped with approximately 30% of the mixed-valence form have been shown to be isomorphous with the brown dicopper(I) analog $[\text{Cu}_2(\text{L44})](\text{ClO}_4)_2$, so gross structural differences between the two are unlikely. The Cu—Cu distance (2.448 Å) in the dicopper(I) complex is at the short end of the literature range (70, 167). The geometry about each copper ion is approximately trigonal bipyramidal, with the axial direction lying along the Cu—Cu vector (Fig. 39).

Solutions of the mixed-valence complexes are blue-green ($\lambda_{\text{max}} = 756 \text{ nm}$, $\epsilon = 5000 \text{ M}^{-1} \text{ cm}^{-1}$, $\Delta\nu_{1/2} = 2500 \text{ cm}^{-1}$), with a shoulder on the low wavelength side (166). The solutions are not stable and the half-life for their decomposition is dependent on both pH and solvent. The solid complexes show Curie law magnetic behavior, and the magnetic moment for the complex (1.9 BM) is consistent with the presence

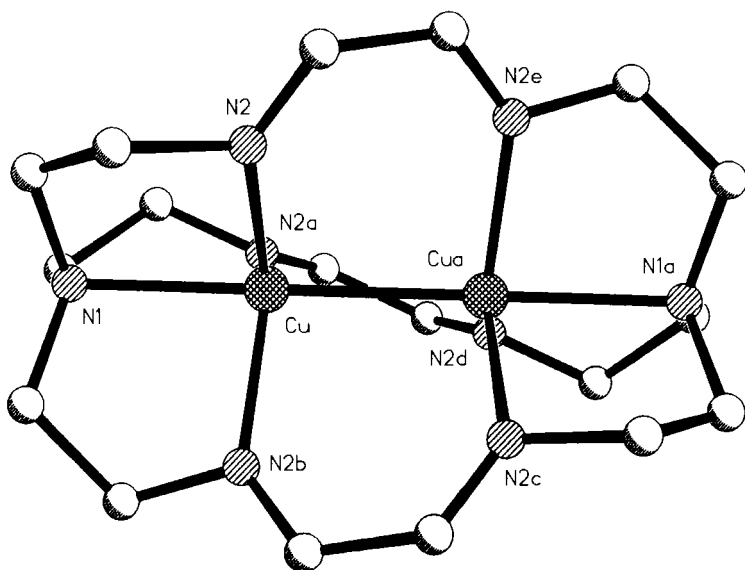


FIG. 39. The structure of $[\text{Cu}_2(\text{L44})]^{2+}$.

of one unpaired electron. Remarkably, the mixed-valence complexes show nearly isotropic, seven-line EPR spectra as fluid or frozen dmf solutions over the full temperature range from ambient temperature to 4 K. This signal is characteristic of a fully delocalized Class III mixed-valence system, $[\text{Cu}(1.5)\text{—Cu}(1.5)]$. Preliminary work (166) on simulating the EPR signal suggests that the exchange process is via overlap of the copper d_{z^2} orbitals (i.e., through a direct copper–copper “bond”) rather than via the diimine bridges of the ligand. This conclusion is supported by the report of a mixed-valence complex, with very similar properties, formed from the reduced cryptand L45 (166, 168).

Many Class II complexes are known for which the EPR signal shows localization occurring at low temperatures (169, 170) but only one (167) other synthetic example in which the seven-line signal is still evident at 77 K is known. Delocalization is most evident in systems in which the ligand imposes very similar geometry at both copper centers and the small, dinuclear cryptate achieves this very effectively. The properties observed are those of the encapsulated $[\text{Cu}(1.5)\text{—Cu}(1.5)]$ unit and are independent of the details of ligand structure.

As stated above, the electronic spectra of the Class III mixed-valence biological sites have been interpreted in terms of sulfur ligation. However, similar intense features are observed in the visible and MCD spectra of mixed-valence complexes of L44 and L45, which contain no sulfur donors. Further, the presence of essentially identical spectra for model complexes with imine donors and with amine donors suggests that the absorption is not due to charge transfer involving the donor atoms. These bands are therefore ascribed to electronic transitions within the $[\text{Cu}(1.5)\text{—Cu}(1.5)]$ unit and this may suggest an alternative explanation for the metalloprotein spectra.

F. OXO-BRIDGED DIIRON

The dinuclear iron proteins contain the Fe—O—Fe unit, supported by bridging carboxylate. Understanding of these systems has advanced rapidly and a number of reviews are available (171–175). There are four major classes: hemerythrins (oxygen transport and storage); ribonucleotide reductases (catalyze formation of deoxyribonucleotide phosphates in the first step of DNA synthesis); methane monooxygenases (catalyze the oxidation of methane to methanol, along with other oxygen atom insertions); and purple acid phosphatases (unknown physiological role, although they catalyze hydrolysis of phosphate esters at low pH).

Hemerythrin is the best studied example and high-resolution X-ray data are available for the deoxy (176), oxy (176), met (177), and azido-met (177) forms. Extensive spectroscopic studies have also been carried out on these forms and on the semi-met $\text{Fe}^{\text{III}}\text{Fe}^{\text{II}}$ form (178). The active site structure of hemerythrin is illustrated in Fig. 40. The two iron atoms are bridged by an oxygen donor (OH^- or O^{2-}) and by two carboxylates, one aspartate and one glutamate. The remaining protein donors are five histidine residues, three coordinated to one iron and two to the other. In the deoxy form one iron atom is five coordinate and this vacant site can be occupied by dioxygen in oxyhemerythrin or by other

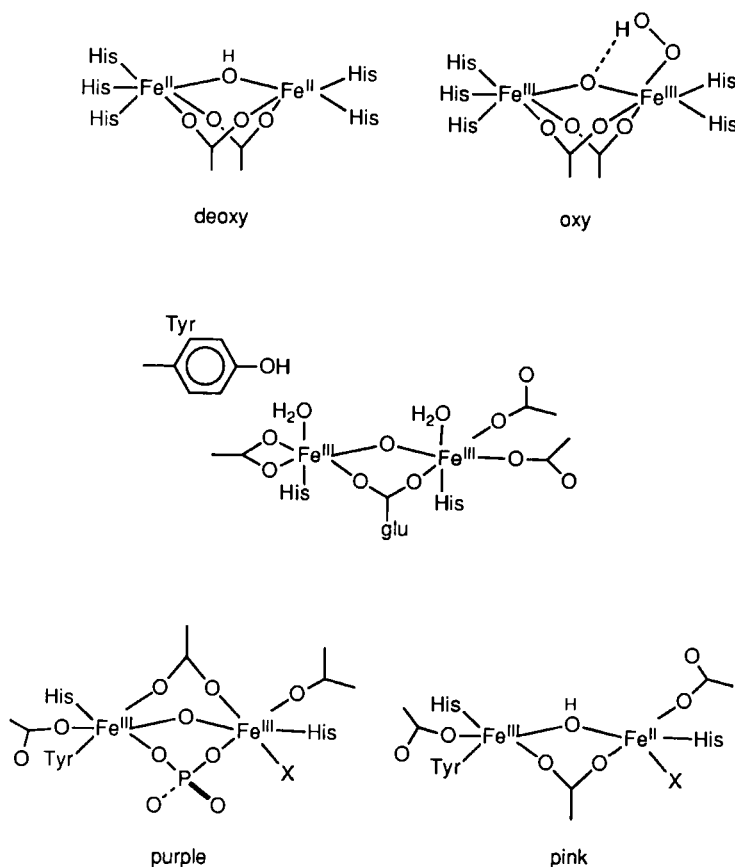
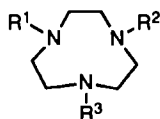


FIG. 40. The active sites of some μ -oxo-diiron proteins, hemerythrin (top), ribonucleotide reductase (middle), and purple acid phosphatase (bottom).

exogenous ligands in various met derivatives. Dioxygen binding is believed to involve abstraction of a proton from the μ -OH bridge of the deoxy protein to form a hydroperoxide that is stabilized by hydrogen bonding to the μ -oxo bridge ($\text{Fe}_2\text{O} \cdots \text{HO}-\text{O}$, 2.80 Å (176)).

X-ray data are also available for the met B2 form of ribonucleotide reductase at 2.2 Å resolution (179) and the diiron site is shown in Fig. 40. In the active form tyrosine 122 is present as a radical, approximately 5 Å from the nearer of the two iron atoms. The function of the iron center is to generate and stabilize this radical, and this requires interaction of dioxygen with the diiron(II) form of the protein (171). Near-IR circular dichroism spectroscopy (178) suggests that the diiron(II) form has vacant coordination sites at both iron atoms and it has been suggested that, in the peroxo intermediate (180), the iron atoms may be bridged by μ -1,1-hydroperoxide (178). The coordination environments around the iron atoms are nonidentical but both are pseudo-octahedral. There are more oxygen donors than those observed for hemerythrin and the μ -oxo bridge is supported by only one μ -carboxylate link. Structural proposals for the purple acid phosphatases and for methane monooxygenase are derived from comparison of their properties with those of hemerythrin and with model complexes and these will be discussed below.

In comparison with the previous section, it might be expected that dinucleating ligands would be important in the model chemistry of the dinuclear sites. Although it is true that many dinucleating systems have been investigated (172, 173), the most significant results have come from studies using small, mononucleating ligands, notably [9]aneN₃ (Fig. 41) and derivatives and the nonmacrocyclic hydrotris(1-pyrazolyl)borate systems.



Ligand	R ¹	R ²	R ³
[9]aneN ₃	H	H	H
Me ₃ [9]aneN ₃	CH ₃	CH ₃	CH ₃

FIG. 41. Ligands derived from [9]aneN₃.

A major factor in advancing understanding of the Fe—O—Fe proteins was the synthesis and characterization of series of model complexes that reproduce the structural and spectral features of the bridged unit. Although many μ -oxo diiron systems are known (173), examples of μ -oxo-di- μ -carboxylate systems have appeared only relatively recently. The simplest route to such complexes is to use a ligand able to cap one face of the octahedral coordination array, forcing facial geometry and leaving the other three sites free for bridging. The first ligands to be used for this purpose were the hydrotris(1-pyrazolyl)borate species, followed by [9]aneN₃ and derivatives (181, 182). Both sets of ligands bind facially to first-row transition metal ions and therefore tend to encourage octahedral coordination geometries. Many other systems have since been developed but, in general, the nature of the ligand has little effect on the structure or spectroscopy of the (μ -oxo)(bis- μ -carboxylato)diiron unit, provided it enforces the facial coordination geometry (173, 175, 183). This is an encouraging observation in terms of translation between model and protein data. Self-assembly in these systems demonstrates that the bridging features of these systems are not imposed by the proteins, except insofar as they set up the appropriate facial coordination.

Where protein structures are well established, the match with model complexes is good both structurally and spectroscopically, although the protein bridging units are less symmetrical (175). This agreement then provides a basis for predicting structures based on partial data, such as metal-metal distances from EXAFS or characteristic electronic spectra. Model systems for the Fe—O—Fe proteins have been comprehensively reviewed (173–175) and only the macrocyclic systems will be considered here.

The close correspondence between protein and model complexes is illustrated in Table V for deoxyhemerythrin and $[\text{Fe}_2^{\text{II}}(\text{OH})(\text{CH}_3\text{COO})_2(\text{Me}_3[9]\text{aneN}_3)_2]^+$ and for oxy- and metazidohemerythrin and $[\text{Fe}_2^{\text{III}}\text{O}(\text{CH}_3\text{COO})_2(\text{Me}_3[9]\text{aneN}_3)_2]^{2+}$. The match between models and metalloproteins is remarkably good, especially for the diiron(II) systems. This emphasizes that, to a first approximation, the dimensions and properties of the bridged unit are independent of the precise nature of the other donors. Mössbauer spectroscopy reveals the presence of two nonequivalent iron sites in the diiron(III) proteins, whereas the five-coordinate site in deoxyhemerythrin is evident from detailed spectroscopic studies (178).

The $[\text{Fe}_2^{\text{II}}(\text{OH})(\text{CH}_3\text{COO})_2(\text{Me}_3[9]\text{aneN}_3)_2]^+$ cation is shown in Fig. 42 (181) and is broadly similar to the oxidized form, $[\text{Fe}_2^{\text{III}}\text{O}(\text{CH}_3\text{COO})_2(\text{Me}_3[9]\text{aneN}_3)_2]^{2+}$. The Fe—O (bridge) distance is considerably

TABLE V

COMPARISON OF STRUCTURAL DATA FOR HEMERYTHRINS AND MODEL COMPLEXES (L = Me₃[9]aneN₃)

	Deoxyhemerythrin	[Fe ₂ ^{II} (OH)(OAc) ₂ (L) ₂] (ClO ₄) ₂ ·H ₂ O	Oxyhemerythrin	[Fe ₂ ^{III} O(OAc) ₂ (L) ₂] (ClO ₄) ₂ ·H ₂ O	Azidomethemerythrin
Fe—Fe (Å)					
X-ray	3.32	3.32	3.27	3.12	3.25
EXAFS	3.57		3.24		3.13
Fe—O (Å)					
X-ray	2.15, 1.88 ^{a,b}	1.99	1.88, 1.79 ^{a,b}	1.80	1.78
EXAFS	1.98		1.82		1.80
Fe—O—Fe (°)					
X-ray	111	113.2	125	119.7	134.5
EXAFS	128		128		127
<i>J</i> (cm ⁻¹)	-13	-13	-77	-115	-134
δ (mm sec ⁻¹)	1.14	1.16	0.51, 0.52 ^a	0.47	0.51, 0.51 ^a
ΔE_Q (mm sec ⁻¹)	2.76	2.83	1.96, 0.95 ^a	1.50	1.95, 1.47 ^a
Fe-oxo CT			360 (sh, 4300)		380 (sh 5500)
λ (nm) (ϵ (M ⁻¹ cm ⁻¹))			330 (6800)	345 (10,500)	326 (6800)
ν (Fe—O—Fe)			486, 753	537	507, 768
(R. Raman, cm ⁻¹)					
References	175, 176	181, 182	175, 176	181, 182	175

^a For two independent iron centers.^b The iron atom bonded to three histidine groups is listed first.

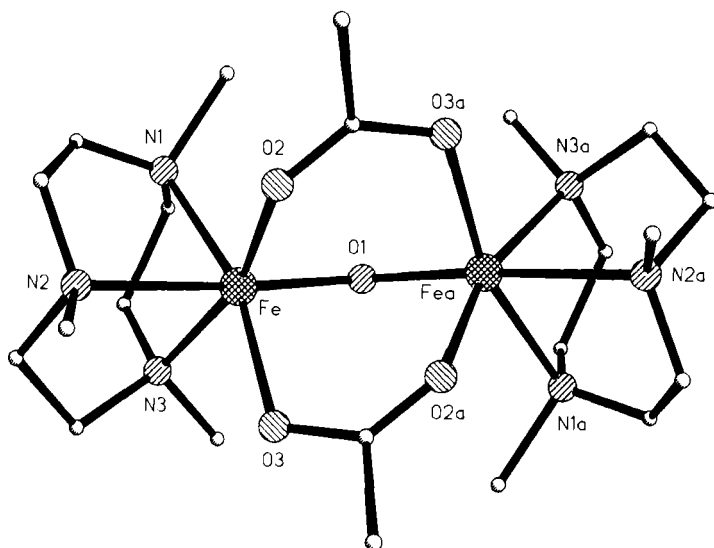


FIG. 42. The structure of $[\text{Fe}_2(\text{OH})(\text{CH}_3\text{COO})_2(\text{Me}_3[9]\text{aneN}_3)_2]^+$.

shorter in the μ -oxodiiron(III) complex and exercises a marked *trans* effect that is absent in the μ -hydroxo complex. Antiferromagnetic coupling is strong in the μ -oxo compounds and much weaker in μ -hydroxo species. Observations such as these from model complexes provide good evidence for the assignment of a μ -hydroxo bridge in deoxyhemerythrin and a μ -oxo link in oxyhemerythrin. They are also the basis for assigning an oxo-hydroperoxo hydrogen bond in oxyhemerythrin (strong coupling) rather than a hydroxo-peroxo interaction (weak coupling). Similarly, the properties of met B2 ribonucleotide reductase are consistent with a μ -oxo bridged structure (Fe—Fe, 3.19 Å (EXAFS), 3.3 Å (X-ray), $J = -108 \text{ cm}^{-1}$).

Methane monooxygenase is unique among the diiron metalloproteins in that the oxidized form shows no absorption bands corresponding to Fe—O—Fe charge transfer. These bands are observed in all μ -oxodiiron (III) model complexes, so that such a bridge in this protein is highly unlikely. Magnetic circular dichroism spectra of the reduced form (178) have been interpreted in terms of an open coordination site and weak ferromagnetic coupling and J is estimated at -32 cm^{-1} from EPR (184). The latter observation suggests that no μ -oxo bridge is present and alkoxide, hydroxide, or monodentate carboxylate bridges have been proposed (171, 178). EXAFS data lead to an iron—iron distance of 3.4

Å (184). The suggestion of an open coordination site is supported by a recent report of exogenous ligand binding to the diiron center (185).

The diiron(III) forms of the purple acid phosphatases are purple ($\lambda_{\max} = 550 \text{ nm}$, $\epsilon = 2000 \text{ M}^{-1} \text{ cm}^{-1}$ per Fe) and the active form is mixed valence $\text{Fe}^{\text{II}}\text{Fe}^{\text{III}}$ and pink ($\lambda_{\max} = 510 \text{ nm}$, $\epsilon = 2000 \text{ M}^{-1} \text{ cm}^{-1}$ per Fe); in both cases the color is attributed to coordination of tyrosine to $\text{Fe}(\text{III})$. The pink form is spectroscopically similar to semimethemerythrin, it shows weak antiferromagnetic coupling ($-J = 5\text{--}11 \text{ cm}^{-1}$) and has properties generally consistent with a μ -hydroxo bridge. EXAFS studies of the diiron(III) form and of the purple enzyme phosphate complex (the form usually isolated) show short Fe—Fe distances (3.0 and 3.2 Å, respectively), indicative of multiple bridging. Strong antiferromagnetic coupling (most recently measured as $J < -150 \text{ cm}^{-1}$ (186)) is consistent with a μ -oxo bridge. In the case of the phosphate adduct, direct bonding of phosphate to the iron center is also implied by the EXAFS data.

Wieghardt and co-workers (187) have displaced the acetate bridges from $[\text{Fe}_2^{\text{III}}\text{O}(\text{CH}_3\text{COO})_2(\text{Me}_3[9]\text{aneN}_3)_2]^{2+}$ by reaction with a phosphomonoester to form $[\text{Fe}_2^{\text{III}}\text{O}(\text{O}_3\text{P}(\text{OC}_6\text{H}_5)_2)(\text{Me}_3[9]\text{aneN}_3)_2]^{2+}$ and this has

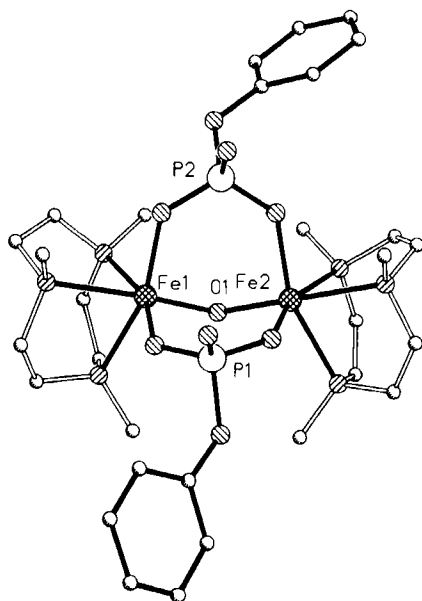


FIG. 43. The structure of $[\text{Fe}_2\text{O}(\text{O}_3\text{P}(\text{OC}_6\text{H}_5)_2)(\text{Me}_3[9]\text{aneN}_3)_2]^{2+}$.

been structurally characterized (Fig. 43). The larger bite of the bridging phosphate group, relative to acetate, increases the Fe—Fe distance to 3.198 Å and slightly lengthens the Fe—oxo bonds to 1.818 Å. The Fe—P distance (3.209 Å) is very similar to that reported from EXAFS study of the enzyme phosphate complex (3.1–3.2 Å) and suggests a similar bridging geometry in the protein. The antiferromagnetic coupling in the model ($J = -98 \text{ cm}^{-1}$) is somewhat lower than that in the enzyme and it has been suggested that the phosphatase site may have shorter Fe—oxo distances and hence stronger coupling (187) since only one bridge is phosphate. Removal of the μ -oxo bridge from the model complex by addition of a third phosphomonoester reduced the antiferromagnetic coupling constant to between -1 and -7.5 cm^{-1} .

Simple tridentate macrocycles and related tripodal ligands have proved to be extremely useful first-generation models for the diiron proteins. Second-generation models will have to address the question of nonequivalent iron sites. To date, only one such complex has been characterized (188).

G. OXO-BRIDGED DIMANGANESE

Several dinuclear manganese enzymes have been discovered; they are closely related to the diiron systems (indeed iron and manganese are sometimes interchangeable without loss of function) but are less well characterized (175, 189). Many synthetic dimanganese complexes have been synthesized, the most extensive series being complexes derived from [9]aneN₃ and related macrocycles and compiled by Wiegardt and others (189–200). The dimanganese units and some structural data are shown in Fig. 44.

As observed for the diiron complexes, the Mn—Mn distance and Mn—O—Mn geometry depend on the number and nature of the bridging groups; the oxidation level of the metal ions is less important (201). Strong antiferromagnetic coupling is found in Mn^{III}Mn^{IV} or Mn^{IV}Mn^{IV} complexes but Mn^{II}Mn^{II}, Mn^{II}Mn^{III}, or Mn^{III}Mn^{III} complexes show weak antiferromagnetic or ferromagnetic exchange. The di- μ -oxo-Mn^{III}Mn^{IV} complexes show distinctive 16-line EPR spectra at low temperatures; spectra for the other systems are less easily interpreted. The μ -oxo-bis(μ -carboxylato)dimanganese(III) unit is characterized by the appearance of two intense bands in the 400- to 600-nm region ($\epsilon > 600 \text{ M}^{-1} \text{ cm}^{-1}$) (189). Redox studies on the μ -oxo complexes show reversible behavior, with the Mn^{II}Mn^{II}, Mn^{II}Mn^{III}, Mn^{III}Mn^{III}, Mn^{III}Mn^{IV}, and Mn^{IV}Mn^{IV} complexes accessible without structural rearrangement. In the μ -hydroxo series, the same is true for the Mn^{II}Mn^{II}, Mn^{II}Mn^{III}, and

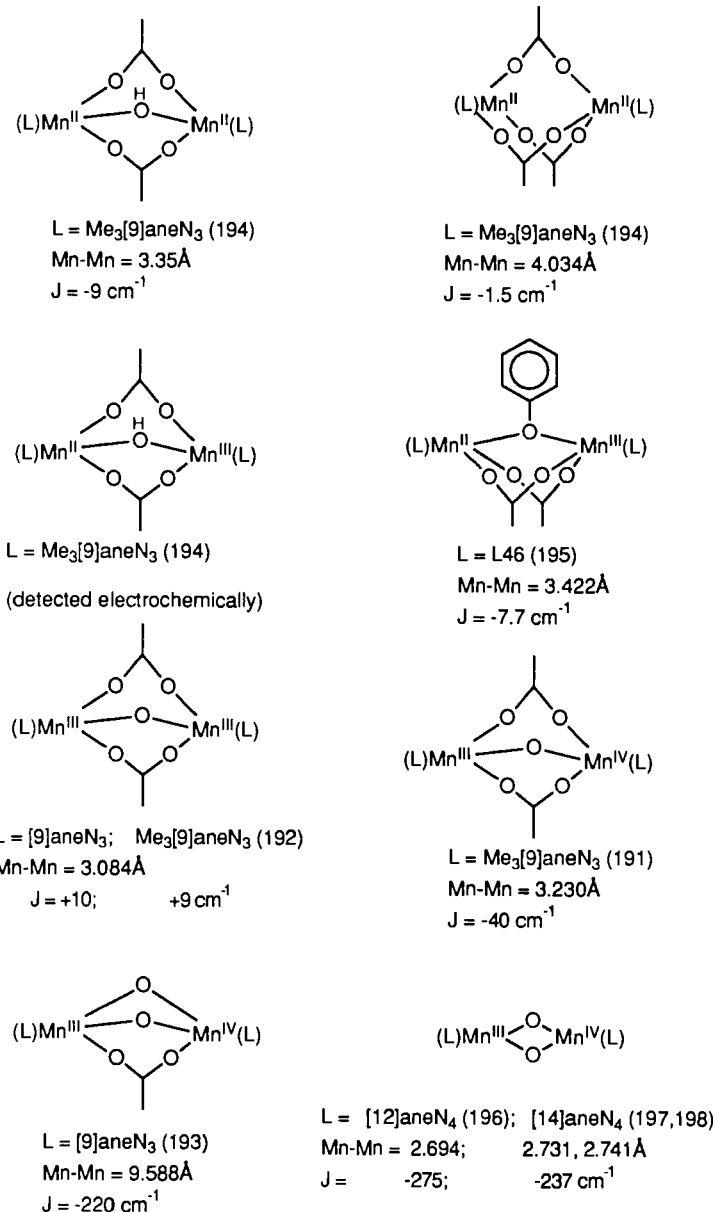


FIG. 44. Structural data for bridged dimanganese model complexes.

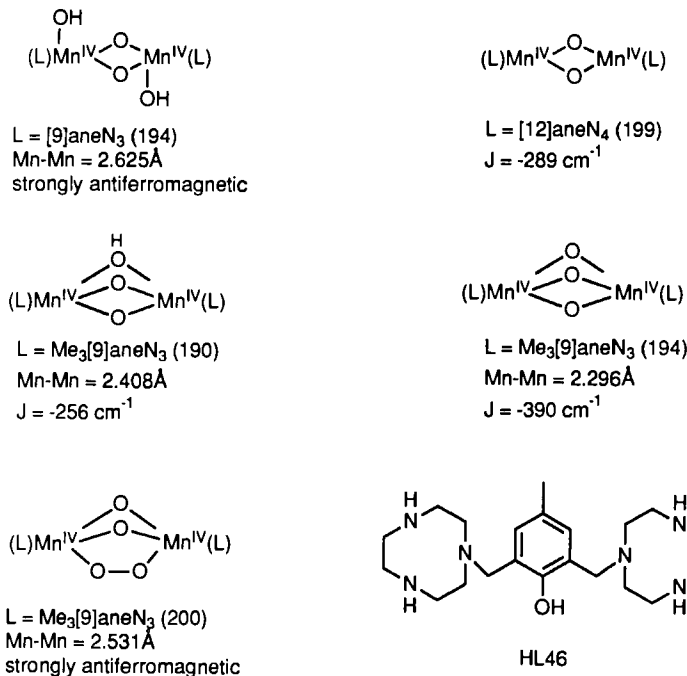


FIG. 44. (Continued)

Mn^{III}Mn^{III} complexes and the two series are linked by pH-dependent equilibria.

The electronic spectrum of the dimanganese(III) form of catalase from *Thermus thermophilus* shows an intense absorption at 450 nm with a shoulder at 500 nm. EPR studies show that Mn^{II}Mn^{II}, Mn^{II}Mn^{III}, and Mn^{III}Mn^{IV} forms are also accessible and the Mn^{III}Mn^{IV} protein exhibits a 16-line spectrum, characteristic of a μ -oxo bridged system (202). Comparison with the model complexes leads to prediction of μ -oxo-bis(μ -carboxylato)dimanganese(III) structure for the catalase. X-ray crystal data (203) have indicated an Mn—Mn distance of 3.6 ± 3 Å for the enzyme; this appears to be inconsistent with the above proposal but, as the X-ray data are at rather low (3 Å) resolution, this may be the least reliable piece of data.

The catalase (or pseudocatalase) from *Lactobacillus plantarum* is also believed to contain a dimanganese(III) site in the oxidized form. It can be reduced to dimanganese(II) or superoxidized to a Mn^{III}Mn^{IV} state. The last complex shows a 16-line EPR spectrum (189). The visible spectrum of the dimanganese(III) form shows a strong absorption at

470 nm with shoulders at 398 and 500 nm. As with *T. thermophilus*, these data lead to an assignment of a μ -oxo-bis(μ -carboxylato)dimanganese(III) center in the oxidized form. EXAFS studies (204) of the superoxidized enzyme indicate a Mn—Mn distance of 2.67 Å, suggesting a di- μ -oxo bridge. No Mn—Mn distance has been unambiguously identified in the reduced enzyme, suggesting that the distance is at least 3.3 Å and consistent with formation of a μ -hydroxo bridge. Ribonucleotide reductases from *Brevibacterium ammoniagenes* and *Micrococcus luteus* are also dimanganese enzymes (205). Once again, their electronic spectra (maxima at 455 and 485 nm) are indicative of μ -oxo-bis(μ -carboxylato)dimanganese(III) cores.

The dimanganese systems constitute one of the unusual cases in which the data for the relatively sophisticated model complexes contrast with the rather sparse information available for most of the enzyme active sites. The properties of the synthetic systems are being used in a predictive fashion to assign structures to the enzymes as spectroscopic data are obtained.

V. Polynuclear Active Sites

In principle, the parameters involved in designing model complexes for polynuclear sites are the same as those for dinuclear systems, although limiting the extent of aggregation can be a greater problem. Metal-metal interactions in polynuclear active sites can be very complicated and, therefore, good model systems are necessary for reliable interpretation of spectroscopic and magnetic data.

A. TRINUCLEAR COPPER

The multicopper oxidases, ascorbate oxidase, laccase, and ceruloplasmin, as discussed elsewhere in this volume, all reduce dioxygen to water and oxidize organic substrates. Early spectroscopic work suggested that the copper is present in three distinct sites, blue (type 1), normal (type 2), and coupled dinuclear (type 3). Recent spectroscopic investigations have concentrated on laccase (38, 206, 207) because it is one of the simpler enzymes, containing one of each type of copper site (and therefore four copper ions) per molecule. Good quality X-ray crystallographic data (1.9 Å resolution) have been obtained for the fully oxidized form of ascorbate oxidase from zucchini (208). Spectroscopic and crystallographic data showed that the type 2 and type 3 sites are not independent and are better considered together as a single trinuclear site (207, 208).

This tricopper cluster is the site of dioxygen binding and reduction of all three copper atoms is required in order for it to function (207).

The structure of the ascorbate oxidase tricopper site is illustrated in Fig. 45. The three copper atoms form an almost equilateral triangle of sides ca. 3.7 Å. The Cu1 and Cu2 atoms are bridged by OH⁻ or O²⁻ and make up the EPR-silent type 3 pair; each copper atom is coordinated to three histidine residues and the Cu—N(His) distances are all comparable and unexceptional. In contrast to the hemocyanin active site (Section IVD), the copper ions have approximately tetrahedral coordination geometry and are not in identical environments. The third copper ion is coordinated to two histidine residues and to either hydroxide or water. There is no evidence for a μ_3 -OH or μ_3 -O donor at the center of the cluster (and the Cu—Cu distances are too long to support such a bridge).

The spectroscopic evidence suggests that the trinuclear centers in ascorbate oxidase and laccase are essentially identical, although the azide binding geometry suggested (206) for laccase appears to be sterically prohibited in ascorbate oxidase (208). Solomon and co-workers have proposed (38, 209) that dioxygen binds as μ -1,1-hydroperoxidase, bridging Cu3 and one copper atom of the coupled site. Possible mechanisms for the reduction of dioxygen through to water have been proposed (208).

Quite a number of nonmacrocylic, triangular tricopper complexes have been synthesized and characterized (210), frequently showing interesting magnetochemistry. Almost invariably these complexes involve a bridging group, usually μ_3 -hydroxo, which is largely responsible for maintaining the structure. Discovery of the trinuclear site in the multicopper oxidases has extended interest in modifying these systems so that they model the structure, and ultimately the chemistry, of the metalloenzyme active sites.

The structure of the trinuclear complex $[\text{Cu}_3(\text{Me}_3[9]\text{aneN}_3)(\text{im})_3]^{3+}$ (where im is imidazolate) has recently been reported by Chaudhuri *et al.*

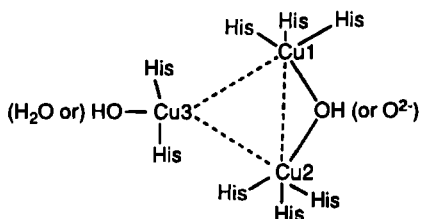


FIG. 45. The active site of ascorbate oxidase.

(211) and is illustrated in Fig. 46. Each copper atom has approximately square pyramidal geometry, the equatorial donors being two imidazole groups and two amine nitrogen donors from the macrocycle; the apical position is occupied by the third macrocyclic donor. Each pair of copper atoms is linked by a bridging imidazole group and it controls the Cu—Cu distance of 5.92 Å, considerably longer than that in the metalloenzyme sites. All the metal ions interact magnetically and, as a consequence, the molecule exhibits spin frustration. Like the ascorbate oxidase site, this complex has a triangular array of copper atoms without a central μ_3 bridge; however, unlike the protein case, the three copper sites are identical.

In principle, a suitably designed large macrocyclic ligand would define a cavity within which three copper atoms could be bound in a fixed geometrical relationship without requiring a μ_3 bridging unit. If the copper coordination sites are designed to be inequivalent, it should be possible to bridge only one pair of metal ions. Tricopper complexes of the large polyaza macrocycles [33]aneN₁₁ and [36]aneN₁₂ have been reported (212). In solution a number of species are present but clean solid products with formulae $\text{Cu}_3([\text{33}] \text{aneN}_{11})(\text{ClO}_4)_6 \cdot 2\text{H}_2\text{O}$ and $\text{Cu}_3([\text{36}] \text{aneN}_{12})(\text{ClO}_4)_6 \cdot 3\text{H}_2\text{O}$ have been isolated. X-ray structures have not been obtained for either complex but two possible structures are proposed, one of which is triangular (Fig. 47). This complex is related to $[\text{Cu}_3(\mu_3\text{-OH})_2([\text{27}] \text{aneN}_6\text{O}_3)]^{4+}$ (Fig. 48), which was published by Lehn and co-workers (213). Again, in this complex the copper environments are all identical; each is coordinated to two adjacent macrocyclic amine

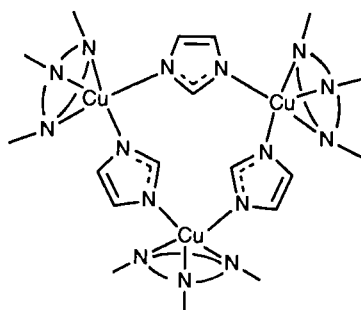


FIG. 46. The tricopper complex $[\text{Cu}_3(\text{Me}_3[9]\text{aneN}_3)_3(\text{im})_3]^{3+}$.

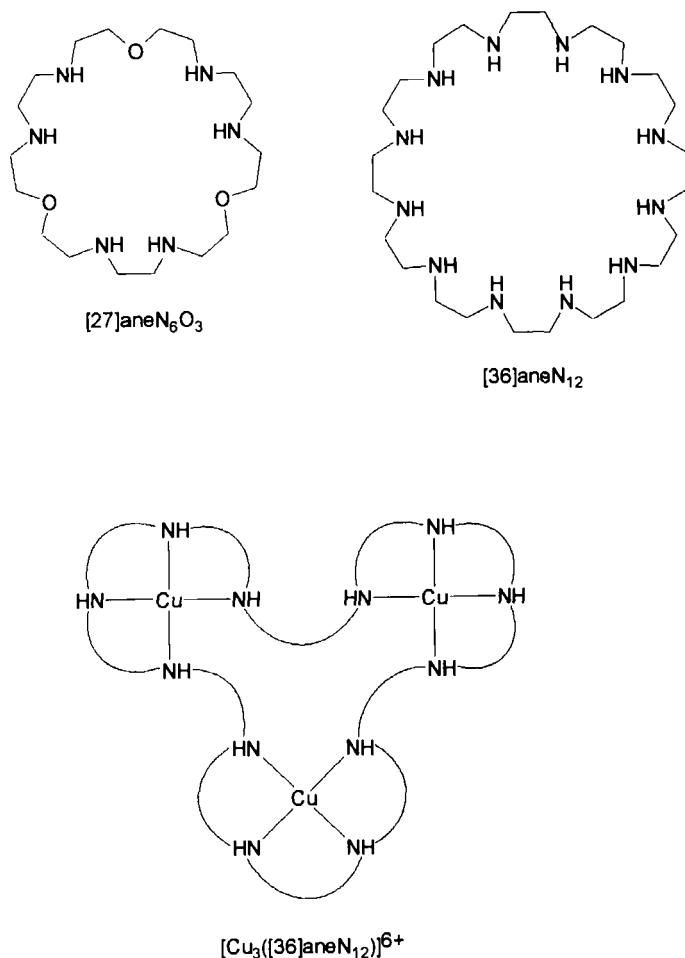


FIG. 47. Some large saturated macrocycles and the proposed structure of [Cu₃[36]aneN₁₂]⁶⁺.

nitrogen atoms and to two μ_3 -hydroxo donors in tetrahedrally distorted square-planar geometry. There are also weaker interactions with macrocyclic ether groups, resulting in somewhat distorted tetragonal geometry. The Cu—Cu distance is 2.808 Å, considerably shorter than the normal Cu—Cu distance in Cu₃(μ_3 -OH) units (3.2–3.3 Å) (210). The two μ_3 -hydroxo groups in the macrocyclic structure are also much farther out of the plane of the three copper atoms than is usually observed and are best described as capping the Cu₃ triangle. These differences demonstrate that the geometry of the complex is controlled largely by

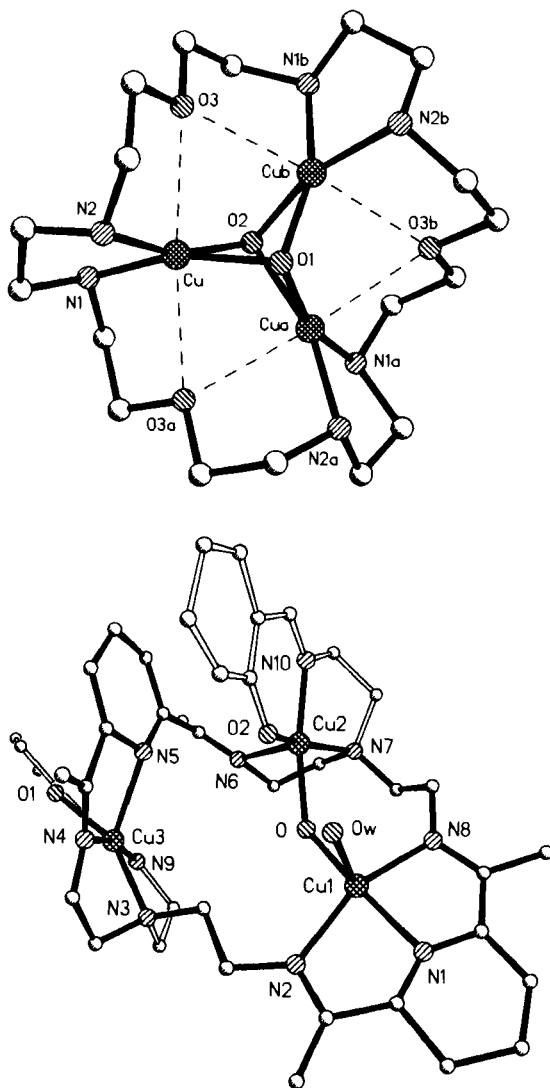


FIG. 48. The structures of the tricopper complexes $[\text{Cu}_3(\text{OH})_2([27]\text{aneN}_6\text{O}_3)]^{4+}$ (top) and $[\text{Cu}_3(\text{OH})(\text{L47})(\text{H}_2\text{O})]^{3+}$ (bottom).

the properties of the macrocycle and not by the steric preferences of the $\text{Cu}_3(\mu_3\text{-OH})$ unit. However, the symmetry of the copper sites is higher and the $\text{Cu}-\text{Cu}$ distance shorter than those in the copper oxidase sites.

Fenton and co-workers have designed ligands in which two pendant arms are added to a dinucleating macrocycle. These ligands, such as

L47 (Fig. 49), were expected to coordinate one copper ion in each pyridinediimine unit, whereas the pendant arms could coordinate a third metal atom in a different coordination site (214). The crystal structure of $[\text{Cu}_3(\text{OH})(\text{L47})(\text{H}_2\text{O})]^{3+}$ is shown in Fig. 48. The geometry of the cation is unexpectedly unsymmetrical; each copper has a unique donor set and approximately square pyramidal geometry. The major feature of the structure in relation to the copper oxidases is that there is a μ_2 -hydroxo bridge linking Cu1 and Cu2 but no direct bridge involving Cu3. The Cu1—Cu2 distance is 3.62 Å, as expected for a $\text{Cu}_2(\mu\text{-OH})$ unit; the distances to Cu3 are longer (4.9 and 5.9 Å for Cu1 and Cu2, respectively). The magnetic moment is 1.66 BM per copper, suggesting some antiferromagnetic coupling between Cu1 and Cu2; no EPR spectra have yet been reported. This complex mimics the broad features of the protein site, a bridged and antiferromagnetically coupled pair of copper ions with a third copper making up a triangular array. It represents a useful step forward in modeling the tricopper sites.

B. MANGANESE IN PHOTOSYSTEM II

Understanding of the tetramanganese oxygen-evolving complex (OEC) of photosystem II has developed rapidly, and relevant reviews have appeared (189, 215–218). The structure of the active site is, however, much less well defined than those of the multicopper oxidases (Section VA), or the iron–sulfur clusters (Section VC). No crystallographic data revealing the geometry of the manganese cluster are available and the spectroscopy is very complex, on occasions leading to apparently contradictory conclusions.

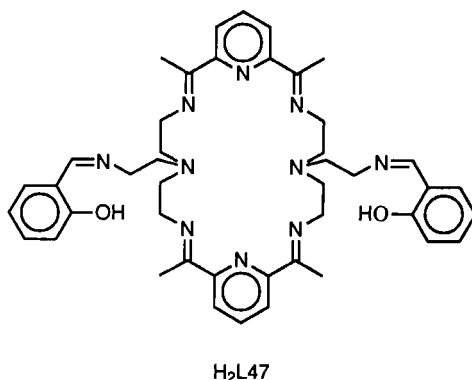


FIG. 49. The bibrachial ligand $\text{H}_2\text{L47}$.

Joliot and co-workers (219) observed that dark-adapted chloroplasts exposed to short flashes of light evolved oxygen periodically every fourth flash. Subsequently, Kok *et al.* (220) proposed that during the water-oxidation cycle, the manganese cluster cycles through five "S-states" (S_0 – S_4). A recent study has noted the same periodicity in the K-edge XANES spectra of the manganese cluster (221). As it progresses from S_0 to S_4 , the manganese cluster accumulates oxidizing equivalents. The S_4 state releases oxygen and is reduced to S_0 , which reoxidizes to S_1 in the dark. The oxidation levels of the manganese ions are not firmly established but are likely to be ca. Mn(III) for the early S states and ca. Mn(IV) for the later stages. The oxidation levels of the manganese atoms do not change in the $S_2 \rightarrow S_3$ step, implying the involvement of an organic radical; it is suggested that water binds at this stage in the cycle.

The S_2 state is EPR active, showing a multiline signal at ca. $g = 2.0$ (assigned to a multinuclear mixed-valence complex (215)) and a second signal at $g = 4.1$. Recent EPR studies of the S_1 state are inconclusive; Brudvig *et al.* report that the cluster is diamagnetic, whereas Klein and co-workers have detected a signal (222). The S_3 state shows an EPR signal assigned to an organic radical; again there is some controversy as to whether the radical is tyrosine (223) or histidine (224).

In the absence of crystallographic information X-ray absorption studies are of great importance in deriving structural parameters for the OEC. K-edge XANES and EPR data suggest that the four manganese atoms are present in a cluster that is not of high symmetry (225, 226). Two Mn–Mn distances have been identified, at 2.7 and 3.3 Å, with the former making the larger contribution (225–227). Studies with model complexes (189, 215, 217, 228–231) show that the 2.7 Å distance is consistent with a di- μ -oxo bridged system, whereas the 3.3 Å interaction is similar to that observed for a single μ -oxo or a μ -carboxylato- μ -oxo structure (Section IVG). The manganese atoms are ligated by O or N donors; the nitrogen level appears to be low, possibly involving histidine (231, 232a), whereas the most likely oxygen donors are oxo (or hydroxo) and protein carboxylate (216, 226). There is no EXAFS evidence for sulfur or chlorine in the coordination spheres, although an Mn–Cl bond cannot be categorically ruled out and chloride is required for the OEC to function (as are calcium ions). K-edge studies have led to proposals of various oxidation states for the S states (232); however, these data are not unambiguous. Promising results have been achieved for mixed-valence model complexes using L-edge absorption and this may prove more revealing than K-edge data (233). Cramer and co-workers (225) have shown angular variations in the XANES and

EXAFS spectra of oriented chloroplasts and have proposed structures consistent with geometrical analysis of the data (Fig. 50, top). Many mechanistic proposals for the water-oxidation process have been put forward (215, 229, 230, 234–237). Most recent schemes are built around tetramanganese clusters belonging to one or more of the “dimer-of-dimers,” “butterfly,” cubane, or adamantane structural classes (Fig. 50). However, X-ray absorption data suggest that the biosite is of lower symmetry than any of the structures shown (225, 226). This suggests, for instance, that a regular cubane structure is unlikely but a distorted geometry (such as that proposed by Cramer) is possible. Such irregular geometry is readily imposed within a protein but is difficult to reproduce in a synthetic model.

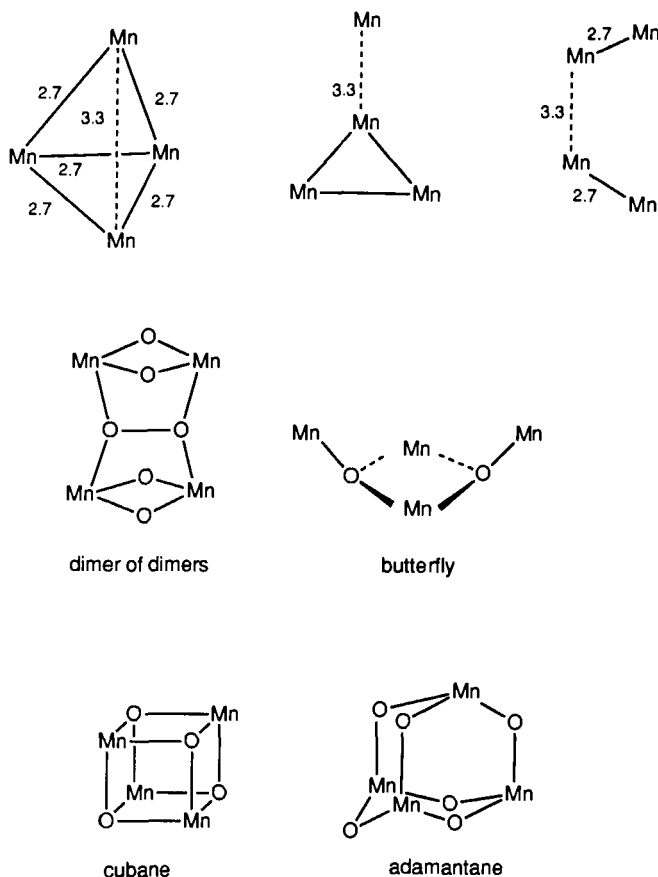


FIG. 50. Proposed active site structures for the OEC.

Advances in understanding the OEC active site and proposals as to its structure have driven a parallel expansion in the chemistry of polymanganese complexes with biologically relevant ligands. Examples of each structural class have been characterized and the field reviewed (189, 217, 229–231). Much excellent work has been carried out, notably by Christou and co-workers, on the polynuclear chemistry of manganese in the presence of carboxylate and hydroxide or oxo groups (frequently in combination with nitrogen donors). These complexes seem to have two drawbacks: the undefined nature of their composition in solution and a marked tendency to form large polymanganese aggregates (228, 231). Nevertheless, polymanganese structures have revealed much of the chemistry and structural preferences of manganese systems, providing the foundations for reasonable structural proposals in biological systems.

Macrocyclic ligands, by occupying coordination sites in fixed and predictable relationships to each other, reduce the tendency to form large structures; also their kinetic stabilities increase the likelihood that the complexes will remain intact in solution. Further, the geometric requirements of macrocyclic ligands can potentially be used to build in irregular or nonequivalent coordination sites.

Macrocyclic tetramanganese complexes illustrating all four structural types shown in Fig. 50 have been prepared and structurally characterized. Two examples of dimeric structures are shown in Fig. 51; these are generated from the dinucleating macrocycles H₂L33 (Fig. 31), which contains pendant alcohol groups, and L32, which contains no potentially bridging groups. The complex $[\text{Mn}_2^{\text{II}}(\text{HL33})(\text{Cl})_4]_2^{2+}$ contains two dinuclear manganese units linked by two chloride bridges and two hydrogen bonds (238). Within each macrocycle the manganese ions are bridged by two alkoxide donors and one chloride ion. This complex is of some interest for EXAFS studies due to the presence of the Mn—Cl bonds at a distance (2.5–2.6 Å) at which there is no overlapping Mn—Mn signal. One reason EXAFS studies have not been able to determine unambiguously if chloride is coordinated to manganese in the OEC is that any Mn—Cl signal would be at least partially obscured by the 2.7 Å Mn—Mn peak. Extracting information on a possible Mn—Cl interaction will require accurate data on the behavior of model complexes containing a similar bond. For example, the intensity of the Mn—Cl EXAFS signal for the chloride-bridged tetramanganese complex shows a strong temperature dependence, which may need to be included in the model (239).

Of more direct relevance to proposed mechanisms of water oxidation is the mixed-valence complex ion $[\text{Mn}^{\text{II}}\text{Mn}^{\text{III}}(\text{L32})(\text{O})(\text{OH})\text{DMF}]_2^{4+}$

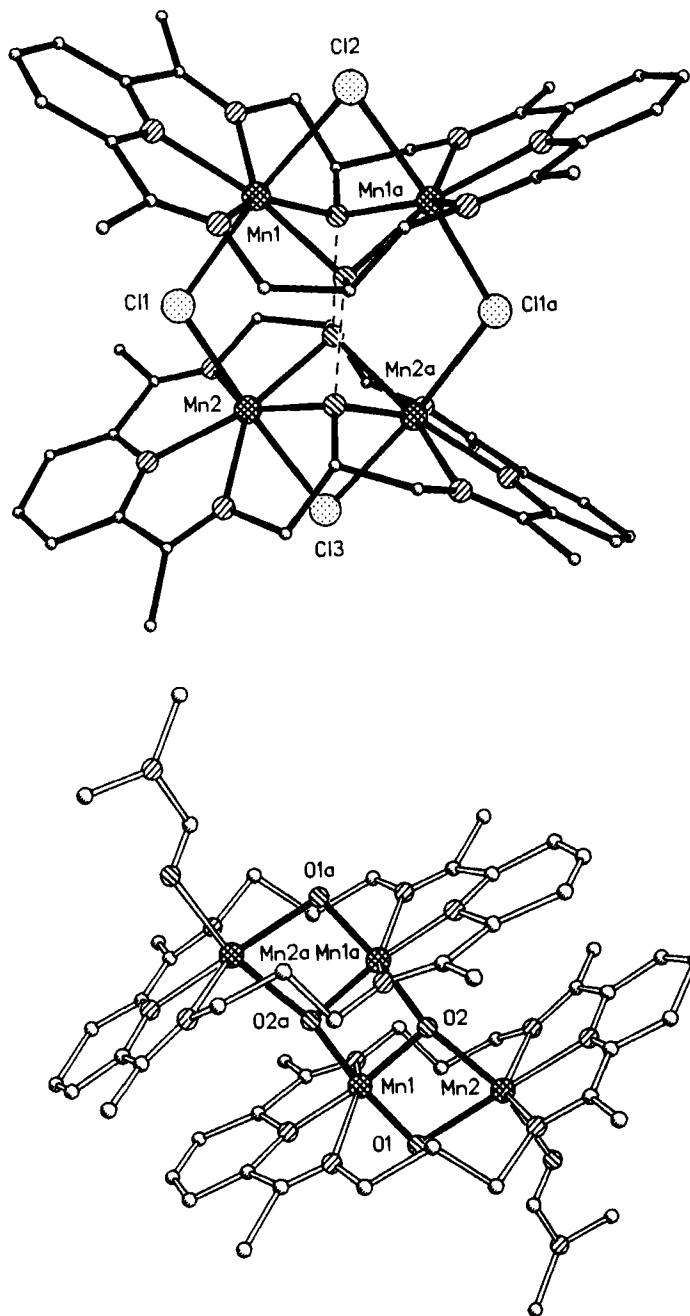


FIG. 51. The structures of $[\text{Mn}_2(\text{HL33})(\text{Cl})_4]_2^{2+}$ and $[\text{Mn}_2(\text{L32})(\text{O})(\text{OH})\text{DMF}]_2^{4+}$.

(240). In this case the two dimanganese units are bridged by two μ_3 -oxo donors so that the Mn(III) ions are linked by a di- μ -oxo bridge and are separated by 2.77 Å. The two manganese atoms within each macrocycle are also bridged by a μ_2 -hydroxo ligand and separated by 3.05 Å. Each manganese has irregular six-coordinate geometry, the coordination sphere of the Mn(II) ions being completed by a DMF molecule. The structure could equally be viewed as having somewhat distorted, planar butterfly geometries in which the μ_3 -oxo donors are T-shaped rather than trigonal. Such geometries have also been observed in nonmacrocyclic systems (231). This complex is related to those observed by Armstrong (236) and to the water oxidation intermediates proposed by Lippard (237) and Hoffman (235).

Figure 52 shows the structure of $[\text{Mn}_4^{\text{II}}(\text{HL33})(\text{L33})(\text{NCS})_4]^+$, which can also be viewed as either a dimer-of-dimers or a severely distorted butterfly. The links between the two macrocycles are two triply bridging alkoxide donors, one from each macrocycle. The "wings" of the butterfly have closed to bring the two outer manganese ions quite close to one another; an extension of this movement would result in formation of a cubane.

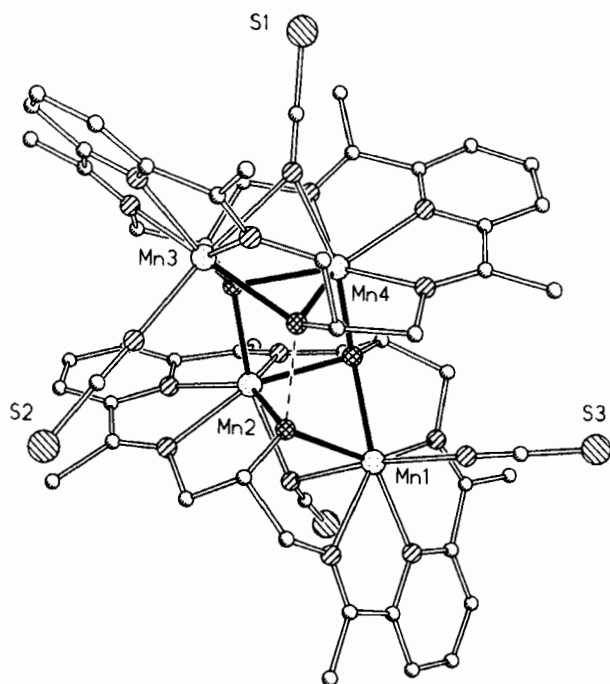


FIG. 52. The structure of $[\text{Mn}_4(\text{HL33})(\text{L33})(\text{NCS})_4]^+$.

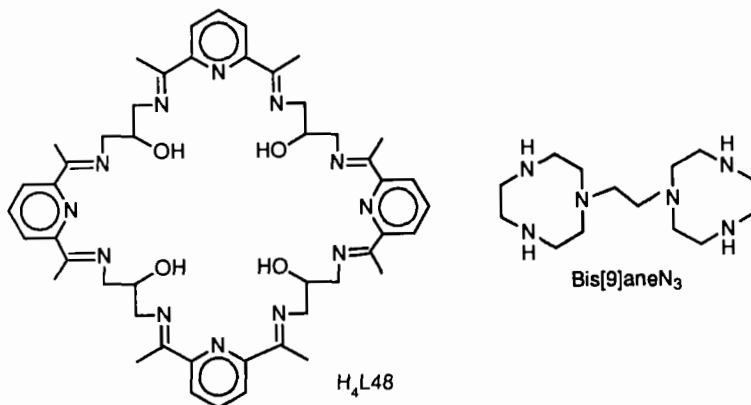


FIG. 53. Two ligands that can form tetramanganese complexes.

Discrete Mn_4O_4 cubanes are quite rare. Two examples with formula $[Mn_4^I(CO)_{12}X_4]$ ($X = F, OH$, or OR with $R = \text{alkyl}$) have been reported (241) and a number of Mn_4O_4 cubane units have been observed within larger polymanganese structures (224, 228). To date, the only discrete Mn_4O_4 cubanes reported with biologically relevant donor atoms are the macrocyclic complexes $[Mn_4^{II}(L48)(ClO_4)_4]$ (242) and $[Mn_2^{II}(L33)(CH_3COO)_2]^{2+}$ (243), which are shown in Fig. 54. In each structure the cubane core is made up of four similar seven-coordinate $Mn(II)$ ions and four μ_3 -alkoxide groups. Christou and co-workers have isolated

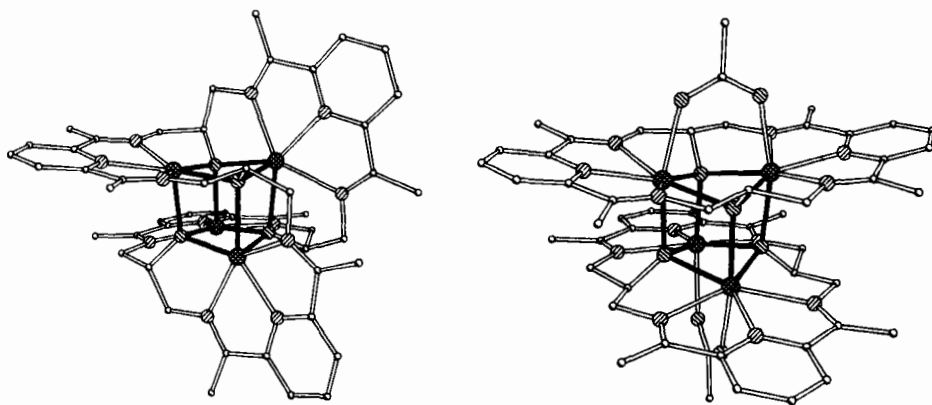


FIG. 54. The structures of $[Mn_4(L48)(ClO_4)_4]$ (left, perchlorate anions removed for clarity) and $[Mn_2(L33)(CH_3COO)_2]^{2+}$ (right).

higher-valent discrete $\text{Mn}_4\text{O}_3\text{Cl}$ cubanes and related their structure to the butterfly geometry (244, 245).

The proposal that a Mn_4O_6 adamantane structure may be involved in the OEC cycle originates from the characterization by Wieghardt and co-workers of $[\text{Mn}_4^{\text{IV}}\text{O}_6([\text{9}] \text{aneN}_3)_4]^{4+}$ (194). This cation (Fig. 55) contains four similar Mn(IV) ions, each facially coordinated by one [9]aneN₃ macrocycle and by three other μ_2 -oxo donors. Spectroscopic evidence suggests that $[\text{Mn}_4(\text{bis}[9] \text{aneN}_3)\text{O}_6](\text{ClO}_4)_4$ (Fig. 53) has the same adamantane structure (246).

Both the cubane and the adamantane structures can be described as containing tetrahedra of manganese ions. A third member of this class is the mixed-valence complex $[\text{Mn}_2^{\text{II}}\text{Mn}_2^{\text{III}}(\mu_4\text{-O})(\text{L25})(\text{CH}_3\text{COO})_3\text{Cl}(\text{MeOH})]$ (247). The central μ_4 -oxo donor is coordinated to all four manganese ions and has distorted tetrahedral geometry (Fig. 55). The manganese ions are also linked by three bridging acetate ligands and four μ_2 -alkoxide bridges. Each manganese has five oxygen donors in the coordination sphere and only one nitrogen.

With the exception of the Mn(IV) adamantane, all the macrocyclic complexes discussed above are at oxidation levels much below those likely to be present in functional OEC states. For this reason they are unlikely to mimic the spectroscopic properties of the active states unless they can be oxidized (an unfavorable process for seven-coordinate Mn(II) (248)). However, the variable and sometimes irregular geometries observed make these complexes valuable as calibrants for X-ray absorption studies (233, 239). The low symmetry observed in some of the macrocyclic tetramanganese structures and predicted for the OEC highlights that the differences among the four structural classes illustrated in Fig. 50 are not as great as it first appears and interconversions may be possible without major disruption of the coordination environment. The planar dimer-of-dimers structure, twisted or folded slightly, becomes a butterfly structure and if this is folded sufficiently a cubane results. The disposition of the Mn atoms in the cubane is identical to that in the adamantane structure.

In many (215, 229, 230, 234), but not all (235, 236, 237), of the reaction schemes proposed for the water oxidation process, the fully oxidized S_4 state is postulated to involve a μ -peroxodimanganese unit, generally as part of the tetranuclear cluster. The water oxidation process may then be viewed as occurring at an effectively dinuclear manganese center, with the other two manganese ions acting as electron sinks or electron transfer species. In this view the redox series of dinuclear manganese complexes characterized by Wieghardt and others (Section IVG) constitute a set of models covering each S state. The S_4 state is

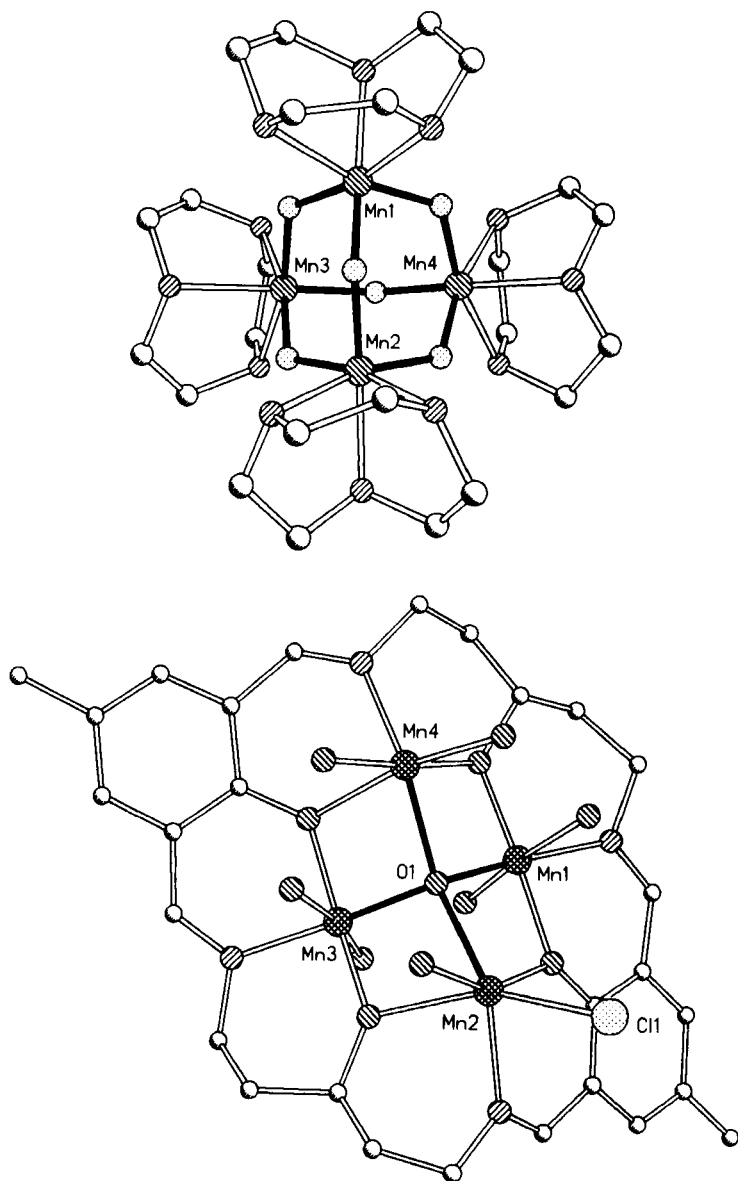


FIG. 55. The structures of $[\text{Mn}_4\text{O}_6([9]\text{aneN}_3)]^{4+}$ (top) and $[\text{Mn}_4\text{O}(\text{L25})(\text{CH}_3\text{COO})_3\text{Cl}(\text{MeOH})]$ (bottom, carbon atoms of the acetate groups and methanol molecule have been removed for clarity).

modeled by the dinuclear μ -peroxodimanganese(IV) species $[\text{Mn}_2^{\text{IV}}(\text{Me}_3[9]\text{aneN}_3)_2(\mu\text{-O}_2)(\mu\text{-OH})_2]^{2+}$. The structure of this cation is shown in Fig. 56 (200). The two Mn(IV) ions have pseudo-octahedral geometry with the $\text{Me}_3[9]\text{aneN}_3$ macrocycles coordinated in the expected facial manner. The complex is stable in acetonitrile solution for many hours but in aqueous solution at ambient temperatures dioxygen is released with disproportionation of the dimanganese complex. To date, the only other characterized example of a μ -peroxo dimanganese unit is in the trinuclear ion $[\text{Mn}_3(\text{dien})_3(\text{CH}_3\text{COO})_2(\mu\text{-O})(\mu\text{-O}_2)]^{3+}$ (249).

C. [4Fe-4S] CLUSTERS

The ligation and geometry of the [4Fe-4S] active sites in proteins, although unprecedented when first discovered, are very accurately duplicated by self-assembly reactions, yielding clusters of general formula $[\text{Fe}_4\text{S}_4(\text{SR})_4]^{n+}$ (250, 251). Not only geometry, but also Mössbauer spectra and the magnetochemistry of the protein sites are well reproduced by synthetic model complexes. However, reduction potentials, which are of prime importance to the electron-transfer function of most [4Fe-4S] sites, are more difficult to reproduce. A major reason for this is that the polarity of the active site environment makes an important contribution to the reduction potential. Reduction potentials of synthetic models are significantly lower than for metalloprotein sites with the same Mössbauer spectra, magnetic properties, etc. This difference is usually ascribed to the hydrophobic nature of the protein active site, a conjecture that is supported by experiments on the effects of denaturing the protein (250).

Such protein effects are often considered impossible to model, but Okuno and co-workers have reported remarkable results from wrap-

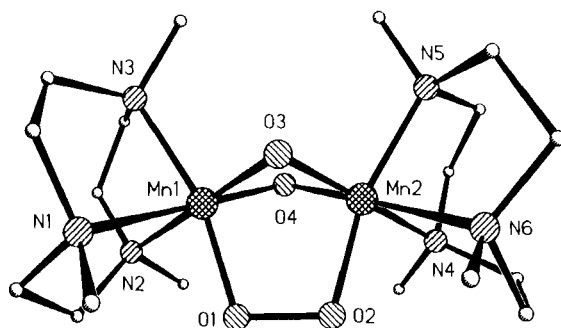


FIG. 56. The structure of $[\text{Mn}_2(\text{Me}_3[9]\text{aneN}_3)_2(\text{O}_2)(\text{OH})_2]^{2+}$.

ping [4Fe-4S] clusters inside a series of large macrocycles with pendant thiolate groups (252-255). The ligands and proposed complex structure are shown in Fig. 57. The complexes were obtained in very good yield and characterized by microanalysis, UV-visible, NMR, and Mössbauer spectroscopy (253, 255). As yet no crystals suitable for X-ray diffraction work have been obtained, so there is no direct evidence that discrete 1:1 macrocycle:cluster complexes are formed (this lack of structural

Ligand L	X and X'	R	$E_{1/2}$ for $[\text{Fe}_4\text{S}_4\text{L}]^n$ (V)			Ref
			-1/-2	-2/-3	-3/-4	
L49	$(\text{CH}_2)_8$		-0.36	-0.85	-1.64	254
L50	$(\text{CH}_2)_8$		-0.35	-1.12	-1.86	254
L51	$(\text{CH}_2)_8$		+0.25	-1.13		254
L52	$(\text{CH}_2)_6$		+0.24	-1.25		252
L53	$(\text{CH}_2)_7$		+0.24	-1.29		252
L54	$(\text{CH}_2)_9$		+0.26	-1.25		252
L55	$(\text{CH}_2)_{10}$		+0.25	-1.30		252
		$[\text{Fe}_4\text{S}_4(\text{SPh})_4]^{n-}$		-0.92	-1.70	
		$[\text{Fe}_4\text{S}_4(\text{SCH}_2\text{Ph})_4]^{n-}$	-1.14			
		$[\text{Fe}_4\text{S}_4(\text{SBu}^t)_4]^{n-}$	-1.11	-1.4		

$[\text{Fe}_4\text{S}_4\text{L}]^n$

Ligand L

FIG. 57. Properties of [4Fe-4S] clusters encapsulated by large macrocycles.

data may often be the price of good modeling of protein effects). The half-wave potentials for the $-1/-2$ and $-2/-3$ couples of $[\text{Fe}_4(\text{S}_4(\text{SBu}^t)_4)]^{n-}$ are -0.11 and -1.40 V, respectively (vs SCE in dmsO at pH 7). The macrocyclic complexes all show significant increases in $E_{1/2}$, to ca. 0.25 V for the $-1/-2$ couple and to ca. -1.29 for the $-2/-3$ couple (Fig. 57). The values for the $-1/-2$ couple are approaching those of the high potential $[\text{4Fe-4S}]$ clusters ($+0.35$ V), and this represents an important advance in modeling these systems. The half-wave potentials are not sensitive to changes in the macrocyclic ring size, suggesting that the fit is less important in this regard than the hydrophobic nature of the environment.

The stability of the encapsulated clusters toward reaction with molecular oxygen is increased by binding to the macrocycle. In contrast to the electrochemical properties, this stabilization is dependent on macrocyclic ring size. The stability order is $\text{L51} > \text{L54} > \text{L53} > \text{L52} > \text{L55} > [\text{Fe}_4\text{S}_4(\text{SBu}^t)_4]^{2-}$, which can be attributed to the macrocyclic effect. The CPK model studies suggest that L51 will give the best fit for the $[\text{4Fe-4S}]$ core, although there may also be some effects due to accessibility of the cluster. In an extension of this work (256), several of the complexes have been shown to catalyze the electrochemical reduction of CO_2 more efficiently than free $[\text{Fe}_4\text{S}_4(\text{RS})_4]^{2-}$ clusters.

Model complexes with simple thiolate ligands have higher symmetry than the metalloprotein sites as, in the latter case, the protein environment about each iron atom is different. Often such differences are of little significance, but in a number of cases they give rise to distinctly different properties for one (or more) of the iron atoms. These clusters are termed "subsite differentiated" and have been recently reviewed by Holm *et al.* (251).

Perhaps the best characterized example of a subsite differentiated $[\text{4Fe-4S}]$ protein is aconitase, which catalyzes the citrate-isocitrate isomerization in the citric acid cycle (257). Aconitase isolated aerobically is inactive and contains a $[\text{3Fe-4S}]$ cluster. Activity is restored by incubation with Fe^{2+} and this also reconstitutes the $[\text{4Fe-4S}]$ cluster. Oxidation of the core results in loss of the fourth iron atom, regenerating the $[\text{3Fe-4S}]$ form. Mössbauer studies have demonstrated that only one of the four iron sites is exchanged (258). X-ray studies on both $[\text{3Fe-4S}]$ and $[\text{4Fe-4S}]$ forms of pig heart aconitase (258a) showed that insertion of iron into $[\text{3Fe-4S}]$ occurs isomorphously. The positions of the common atoms in the two forms of the core agree to within 0.1 Å, supporting the view of the $[\text{3Fe-4S}]$ cluster as an "iron-voided" cubane. A similar result was obtained for the seven iron ferredoxin from *Azo-*

bacter vinelandii; the bond lengths and angles of the [3Fe–4S] cluster are very similar to those of the [4Fe–4S] core (259, 260). Interconversion of [3Fe–4S] and [4Fe–4S] cores has also been observed in *D. gigas* ferredoxin (261), although there are indications that this reaction is less site specific than is the case for aconitase. In aconitase the subsite-differentiated iron atom is not coordinated to cysteine. The current view of the enzyme mechanism (257) is that the substrate citrate binds at this site as a bidentate ligand (Fig. 58).

The macrocycle H_3L50 reacts with the synthetic cluster $(Bu_4N)_2[Fe_4S_4(SET)_4]$ to displace three ethanethiolate groups and quantitatively form $(Bu_4N)_2[Fe_4S_4(L50)(SET)]$ (262). The product was characterized by NMR as having the cluster bound to the macrocycle *via* three Fe–S bonds. The quantitative nature of the reaction is presumably a consequence of the good match between the dimensions and geometry of host and guest and those of the macrocyclic effect. The resulting cluster is “subsite differentiated,” with one iron in an environment different from that of the other three. The remaining ethanethiolate group can be replaced by chloride and this in turn can be substituted by a range of other ligands (including [9]aneN₃) without displacing L50 from the complex. The macrocyclic ligand reduces the redox potentials of the cluster by 0.10–0.15 V. Similar results have been obtained (251, 263, 264) using cavitand trithiolate hosts and the crystal structures of some of these have been obtained (Fig. 59). In this case, the stability of the complexes can be ascribed to the semirigid cavitand nature of the ligand, i.e., to multiple juxtapositional fixedness (265). Both the L50 and the nonmacrocyclic ligand are equally effective in inducing the desired differentiation between iron atoms and are useful

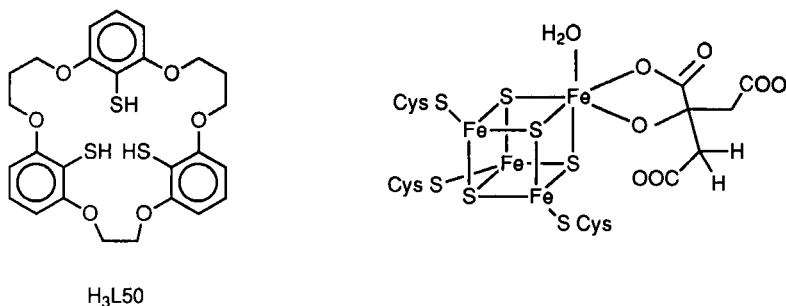


FIG. 58. A macrocyclic host for [4Fe–4S] clusters (left) and the active site of aconitase (right).

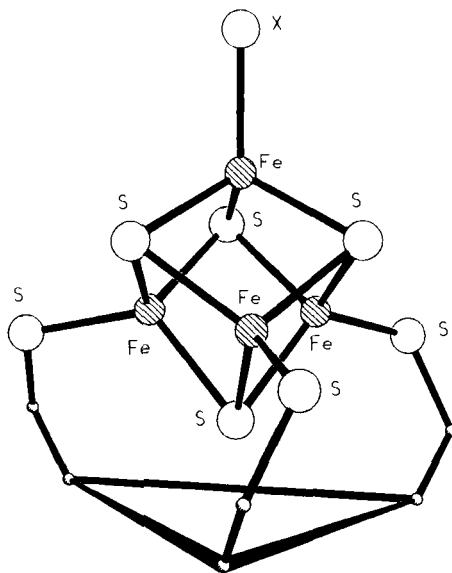


FIG. 59. A schematic representation of $[(L50)([4Fe-4S])X]$.

models for the $Fe_4S_4(S-Cys)_3$ site in acotinase. They are also promising starting points for investigating binding of physiologically relevant ligands at the unique iron site and the stabilization of the voided cubanes (251).

As discussed in Section IIIC, it has been suggested that the nickel site in carbon monoxide dehydrogenases is associated with an iron-sulfur cluster (266). Possible geometries include a mixed-metal cubane, $[Ni-3Fe-4S]$ and a sulfur-bridged assembly (Fig. 60). A synthetic $[Ni-3Fe-4S]$ cluster has been characterized and its Mössbauer properties are very similar to those of CODH from *C. thermoaceticum* (86).

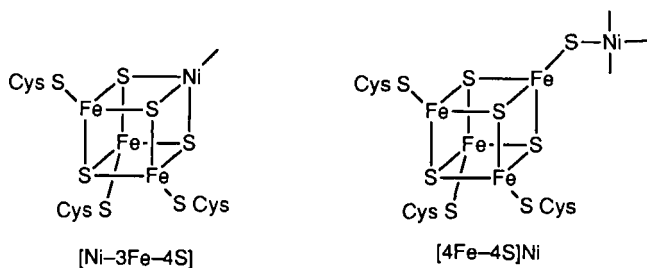


FIG. 60. The proposed active site structures for the $Ni-Fe-S$ cluster in CODH.

The subsite differentiated synthetic clusters provide a good basis for further investigation of both possible structures for the CODH enzyme.

VI. Conclusion

Ligands designed to model bioinorganic active sites are usually required to define the spatial relationships between metals and donors (or other metals) and to promote or impose nonclassical geometries or donor sets on the metal ion. One way in which these requirements may be addressed is through the use of suitably designed macrocyclic ligands. The preceding sections illustrate the use of macrocyclic complexes at all stages of the modeling process, from speculative, through corroborative (or noncorroborative), to functional analogs.

REFERENCES

1. Goedken, V. L., in "Coordination Chemistry of Macrocyclic Compounds" (G. A. Melson, ed.), p. 603. Plenum, New York, 1979.
2. Busch, D. H., *Acc. Chem. Res.* **11**, 393 (1978).
3. Lindoy, L. F., "The Chemistry of Macrocyclic Ligand Complexes." Cambridge Univ. Press, Cambridge, UK, 1989.
4. Ibers, J. A., and Holm, R. H., *Science* **209**, 223 (1980).
5. Hill, H. A. O., *Chem. Br.* **12**, 119 (1976).
6. Fenton, D. E., *Pure Appl. Chem.* **61**, 903 (1989).
7. Cram, D. J., *Angew. Chem., Int. Ed. Engl.* **27**, 1009 (1988); Lehn, J.-M., *Pure Appl. Chem.* **52**, 2441 (1980).
8. Williams, R. J. P., *J. Chem. Soc., Dalton Trans.*, p. 539 (1991).
9. Silverman, D. N., and Lindsog, S., *Acc. Chem. Res.* **21**, 30 (1988).
10. Kannan, K. K., Notstrand, B., Fridborg, K., Lövgren, S., Ohlsson, A., and Petef, M., *Proc. Natl. Acad. Sci. U.S.A.* **72**, 51 (1975).
11. Liljas, A., Kannan, K. K., Bergsten, P. C., Fridborg, K., Strandberg, B., Carlbom, U., Järup, L., Lörgren, S., and Petef, M., *Nature (London)* **235**, 131 (1972).
12. Pocker, Y., and Stone, J. T., *J. Am. Chem. Soc.* **87**, 5497 (1965).
13. Hughes, M. N., *Compr. Coord. Chem.* **7**, 541-754, and references therein (1987).
14. Pocker, Y., and Stone, J. T., *Biochemistry* **6**, 668 (1967).
15. Pesando, J. M., *Biochemistry* **14**, 681 (1975).
16. Merz, K. M., Hoffman, R., and Dewar, M. J. S., *J. Am. Chem. Soc.* **111**, 5636 (1989).
17. Lindsog, S., and Coleman, J. E., *Proc. Natl. Acad. Sci. U.S.A.* **70**, 2505 (1973).
18. Bertini, I., Luchinat, C., and Monnanni, R., *J. Chem. Educ.* **62**, 924 (1985).
19. Christianson, D. W., and Lipscomb, W. N., *Acc. Chem. Res.* **22**, 62 (1989).
20. Chin, J., *Acc. Chem. Res.* **24**, 145 (1991).
21. Suh, J., *Acc. Chem. Res.* **25**, 273 (1992).
22. Bertini, I., and Luchinat, C., *Acc. Chem. Res.* **16**, 272 (1983).
23. Woolley, P., *Nature (London)* **258**, 677 (1975).

24. Kimura, E., and Koike, T., *Comments Inorg. Chem.* **11**, 285 (1991); Kimura, E., Shiota, T., Kioke, T., Shiro, M., and Kodama, M., *J. Am. Chem. Soc.* **112**, 5805 (1990).
25. Gellman, S. H., Petter, R., and Breslow, R., *J. Am. Chem. Soc.* **108**, 2388 (1986).
26. Koike, T., and Kimura, E., *J. Am. Chem. Soc.* **113**, 8935 (1991).
27. Pocker, Y., and Stone, J. T., *Biochemistry* **7**, 2936 (1968).
28. Kimura, E., Koike, T., and Toriumi, K., *Inorg. Chem.* **27**, 3687 (1988).
29. Koike, T., Kimura, E., Nakamura, I., Hashimoto, Y., and Shiro, M., *J. Am. Chem. Soc.* **114**, 7338 (1992).
30. Alcock, N. W., Benniston, A. C., Moore, P., Pike, G. A., and Rawle, S. C., *J. Chem. Soc., Chem. Commun.*, p. 706 (1991).
31. Rawle, S. C., Clarke, A. J., Moore, P., and Alcock, N. W., *J. Chem. Soc., Dalton Trans.*, p. 2755 (1992).
32. Clewley, R. G., Slebocka-Tilk, H., and Brown, R. S., *Inorg. Chim. Acta* **157**, 233 (1989).
33. Sykes, A. G., *Adv. Inorg. Chem.* **36**, 377 (1991).
34. Guss, J. M., Harrowell, P. R., Murata, M., Norris, V. A., and Freeman, H. C., *J. Mol. Biol.* **192**, 361 (1986); Guss, J. M., and Freeman, H. C., *ibid.* **169**, 521 (1983); Colman, P. M., Freeman, H. C., Guss, J. M., Murata, M., Norris, V. A., Ramshaw, J. A. M., and Ventakappa, M. P., *Nature (London)* **272**, 319 (1978).
35. Baker, E. N., *J. Mol. Biol.* **203**, 1071 (1988); Norris, G. E., Anderson, B. F., and Baker, E. N., *J. Am. Chem. Soc.* **108**, 2784 (1986).
36. Guss, J. M., Merritt, E. A., Phizackerley, R. P., Hedman, B., Murata, M., Hodgson, K. O., and Freeman, H. C., *Science* **241**, 806 (1988).
37. Adman, E. T., Turley, S., Branson, R., Petratos, K., Banner, D., Tsernoglou, D., Beppu, T., and Watanabe, H., *J. Biol. Chem.* **264**, 87 (1989).
38. Solomon, E. I., Baldwin, M. J., and Lowery, M. D., *Chem. Rev.* **92**, 521 (1992).
39. Thomann, H., Bernardo, M., Baldwin, M. J., Lowery, M. D., and Solomon, E. I., *J. Am. Chem. Soc.* **113**, 5911 (1991).
40. Lowery, M. D., and Solomon, E. I., *Inorg. Chim. Acta* **198-200**, 233 (1992).
41. Rorabacher, D. B., Martin, M. J., Koenigbauer, M. J., Malik, M., Schroeder, R. R., Endicott, J. F., and Ochrymowycz, L. A., in "Copper Coordination Chemistry: Biochemical and Inorganic Perspectives" (K. D. Karlin and J. Zubieta, eds.), p. 167. Adenine Press, New York, 1983.
42. Endicott, J. F., and Durham, B., in "Coordination Chemistry of Macrocyclic Compounds" (G. A. Melson, ed.), p. 393. Plenum, New York, 1979.
43. Reid, G., and Schröder, M., *Chem. Soc. Rev.* **19**, 239 (1990).
44. Blake, A. J., and Schröder, M., *Adv. Inorg. Chem.* **35**, 1 (1990).
45. Cooper, S. R., *Acc. Chem. Res.* **21**, 141 (1988).
46. Cooper, S. R., and Rawle, S. C., *Struct. Bonding (Berlin)* **72**, 1 (1990).
47. Addison, A. W., *Inorg. Chim. Acta* **162**, 217 (1989).
48. Sakaguchi, U., and Addison, A. W., *J. Chem. Soc., Dalton Trans.*, p. 600 (1979).
49. Westerby, B. C., Juntunen, K. L., Leggett, G. H., Pett, V. B., Koenigbauer, M. J., Purgett, M. D., Taschner, M. J., Ochrymowycz, L. A., and Rorabacher, D. B., *Inorg. Chem.* **30**, 2109 (1991).
50. Bernardo, M. M., Heeg, M. J., Schroeder, R. R., Ochrymowycz, L. A., and Rorabacher, D. B., *Inorg. Chem.* **31**, 191 (1992).
51. Diaddario, L. L., Jr., Dockal, E. R., Glick, M. D., Ochrymowycz, L. A., and Rorabacher, D. B., *Inorg. Chem.* **24**, 356 (1985).
52. Micheloni, M., Paoletti, P., Siegfried-Hertli, L., and Kaden, T. A., *J. Chem. Soc., Dalton Trans.*, p. 1169 (1985).

53. Balakrishnan, K. P., Kaden, T. A., Siegfried, L., and Zuberh  ler, A. D., *Helv. Chim. Acta* **67**, 1060 (1984); Siegfried, L., and Kaden, T. A., *ibid.*, p. 29.
54. Atkinson, N., Blake, A. J., Drew, M. G. B., Forsyth, G., Lavery, A. J., Reid, G., and Schr  der, M., *J. Chem. Soc., Chem. Commun.*, p. 985 (1989).
55. Goodwin, J. A., Stanbury, D. M., Wilson, L. J., Eigenbrot, C. W., and Scheidt, W. R., *J. Am. Chem. Soc.* **109**, 2979 (1987).
56. Bernardo, M. M., Robandt, P. V., Schroeder, R. R., and Rorabacher, D. B., *J. Am. Chem. Soc.* **111**, 1224 (1989).
57. Martin, M. J., Endicott, J. F., Ochrymowycz, L. A., and Rorabacher, D. B., *Inorg. Chem.* **26**, 3012 (1987).
58. Bernardo, M. M., Schroeder, R. R., and Rorabacher, D. B., *Inorg. Chem.* **30**, 1241 (1991).
59. Brunschwig, B. S., and Sutin, N., *J. Am. Chem. Soc.* **111**, 7454 (1989); Hoffman, B. M., and Ratner, M. A., *ibid.* **109**, 6237 (1987).
60. Patrick, G., and Hancock, R. D., *Inorg. Chem.* **30**, 1419 (1991).
61. Wainwright, K. P., *Inorg. Chem.* **19**, 1396 (1989).
62. Wainwright, K. P., and Ramasubbu, A., *J. Chem. Soc., Chem. Commun.*, p. 277 (1982).
63. Hancock, R. D., Dobson, S. M., Evers, A., Wade, P. W., Ngwenya, M. P., Boeyens, J. C. A., and Wainwright, K. P., *J. Am. Chem. Soc.* **110**, 2788 (1988).
64. Wainwright, K. P., Patalinghug, W., Skelton, B. W., White, A. H., and Healy, P. C., *J. Chem. Soc., Dalton Trans.*, p. 2301 (1988).
65. Martin, J. W. L., Organ, G. J., Wainwright, K. P., Weerasuria, K. D. V., Willis, A. C., and Wild, S. B., *Inorg. Chem.* **26**, 2963 (1987).
66. Timmons, J. H., Martin, J. W. L., Martell, A. E., Rudolf, P. R., and Clearfield, A., *Inorg. Chem.* **27**, 1638 (1988); Timmons, J. H., Rudolf, P., Marbell, A. E., Martin, J. W. L., and Clearfield, A., *ibid.* **19**, 2331 (1980).
67. Hay, R. W., Govan, N., and Pujari, M. P., *J. Chem. Soc., Dalton Trans.*, p. 963 (1987).
68. Drew, M. G. B., Cairns, C., McFall, S. G., and Nelson, S. M., *J. Chem. Soc., Dalton Trans.*, p. 2020 (1980).
69. Drew, M. G. B., Cairns, C., Nelson, S. M., and Nelson, J., *J. Chem. Soc., Dalton Trans.*, p. 942 (1981).
70. Harding, C., McKee, V., and Nelson, J., *J. Am. Chem. Soc.* **113**, 9684 (1991).
71. Cammack, R., *Adv. Inorg. Chem.* **32**, 297 (1988).
72. Wackett, I. P., Honek, J. F., Begley, T. P., Shames, S. L., Niederhoffer, E. C., Hausinger, R. P., Orme-Johnson, W. H., and Walsh, C. T., in "The Bioinorganic Chemistry of Nickel" (J. R. Lancaster, Jr., ed.), p. 249, VCH Verlagsges., Weinheim, 1988; Pfaltz, A., *ibid.*, p. 275.
73. Cammack, R., Fernandez, V. M., and Schneider, K., in "The Bioinorganic Chemistry of Nickel" (J. R. Lancaster, Jr., ed.), p. 167. VCH Verlagsges., Weinheim, 1988; Moura, J. J. G., Teixeira, M., Moura, I., and LeGall, J., *ibid.*, p. 191.
74. Eidsness, M. K., Scott, R. A., Prickril, B. C., DerVartanian, D. V., LeGall, J., Moura, I., Moura, J. J. G., and Peck, H. D., Jr., *Proc. Natl. Acad. Sci. U.S.A.* **86**, 147 (1989).
75. He, S. H., Teixeira, M., Le Gall, J., Patil, D. S., Moura, I., Moura, J. J. G., DerVartanian, D. V., Huynh, B. H., and Peck, H. D., Jr., *J. Biol. Chem.* **264**, 2678 (1989).
76. Eidsness, M. K., Sullivan, R. J., and Scott, R. A., in "The Bioinorganic Chemistry of Nickel" (J. R. Lancaster, Jr., ed.), p. 73. VCH Verlagsges., Weinheim, 1988.
77. Fan, C., Teixeira, M., Moura, J., Moura, I., Huyuti, B.-H., Le Gall, J., Peck, H. D., Jr., and Hoffman, B. M., *J. Am. Chem. Soc.* **113**, 20 (1991).

78. Scott, R. A., Wallin, S. A., Czechowski, M., DerVartanian, D. V., LeGall, J., Peck, H. D., Jr., and Moura, I., *J. Am. Chem. Soc.* **106**, 6864 (1984).
79. Lindahl, P. A., Kojima, N., Hausinger, R. P., Fox, J. A., Teo, B. K., Walsh, C. T., and Orme-Johnson, W. H., *J. Am. Chem. Soc.* **106**, 3062 (1984).
80. Colpas, G. J., Maroney, M. J., Bagyinka, C., Kumar, M., Willis, W. S., Suib, S. L., Baidya, N., and Mascharak, P. K., *Inorg. Chem.* **30**, 920 (1991).
81. Ragsdale, S. W., Wood, H. G., Morton, T. A., Ljungdahl, L. G., and DerVartanian, D. V., in "The Bioinorganic Chemistry of Nickel" (J. R. Lancaster, ed.), p. 331. VCH, Weinheim, 1988; Diekert, G., *ibid.*, p. 229.
82. Stephens, P. J., McKenna, M.-C., Ensign, S. A., Bonam, D., and Ludden, P. W., *J. Biol. Chem.* **264**, 16347 (1989).
83. Kumar, M., and Ragsdale, S. W., *J. Am. Chem. Soc.* **114**, 8713 (1992).
84. Bastian, N. R., Diekert, G., Niederhoffer, E. C., Teo, B.-K., Walsh, C. T., and Orme-Johnson, W. H., *J. Am. Chem. Soc.* **110**, 5581 (1988).
85. Cramer, S. P., Eidsness, M. K., Pan, W.-H., Morton, T. A., Ragsdale, S. W., DerVartanian, D. V., Ljungdahl, L. G., and Scott, R. A., *Inorg. Chem.* **26**, 2477 (1987).
86. Ciurli, S., Yu, S., Holm, R. H., Srivastava, K. K. P., and Münck, E., *J. Am. Chem. Soc.* **112**, 8169 (1990).
87. Lindahl, P. A., Ragsdale, S. W., and Münck, E., *J. Biol. Chem.* **265**, 3880 (1990).
88. Lappin, A. G., and McAuley, A., *Adv. Inorg. Chem.* **32**, 241 (1988); Fabbriizzi, L., *Comments Inorg. Chem.* **4**, 33 (1985); Haines, R. I., and McAuley, A., *Coord. Chem. Rev.* **39**, 77 (1981); Nag, K., and Chakravorty, A., *ibid.* **33**, 87 (1980).
89. Fox, S., Wang, Y., Silver, A., and Millar, M., *J. Am. Chem. Soc.* **112**, 3219 (1990).
90. Krüger, H.-J., and Holm, R. H., *J. Am. Chem. Soc.* **112**, 2955 (1990); Baucom, E. I., and Drago, R. S., *ibid.* **93**, 6469 (1971).
91. Lovecchio, F. V., Gore, E. S., and Busch, D. H., *J. Am. Chem. Soc.* **96**, 3109 (1974).
92. Fabbriizzi, L., *Inorg. Chim. Acta* **36**, L391 (1979).
93. Dietrich-Buchecker, C. O., Kern, J.-M., and Sauvage, J.-P., *J. Chem. Soc., Chem. Commun.*, p. 760 (1985).
94. Thomson, M. C., and Busch, D. A., *J. Am. Chem. Soc.* **86**, 3651 (1964).
95. Sokol, L. S. W. L., Ochrymowycz, L. A., and Rorabacher, D. B., *Inorg. Chem.* **25**, 2576 (1985).
96. Osvath, P., Sargeson, A. M., Skelton, B. W., and White, A. H., *J. Chem. Soc., Chem. Commun.*, p. 1036 (1991).
97. Sargeson, A. M., *Pure Appl. Chem.* **58**, 1511 (1986).
98. Efros, L. L., Thorp, H. H., Brudvig, G. W., and Crabtree, R. H., *Inorg. Chem.* **31**, 1722 (1992); Karn, J. L., and Busch, D. H., *Nature (London)* **211**, 160 (1966).
99. Fisher, B., and Eisenberg, R., *J. Am. Chem. Soc.* **102**, 7361 (1980).
100. Collin, J.-P., Jouaiti, A., and Sauvage, J.-P., *Inorg. Chem.* **27**, 1986 (1988).
101. Beley, M., Collin, J.-P., Ruppert, R., and Sauvage, J.-P., *J. Am. Chem. Soc.* **108**, 7461 (1986); Beley, M., Collin, J.-P., Ruppert, R., and Sauvage, J.-P., *J. Chem. Soc., Chem. Commun.*, p. 1315 (1984).
102. Bakac, A., and Espenson, J. H., *J. Am. Chem. Soc.* **108**, 713 (1986).
103. Hough, E., Hansen, L. K., Birknes, B., Jynge, K., Hansen, S., Hordvik, A., Little, C., Dodson, E., and Derewenda, Z., *Nature (London)* **338**, 357 (1989).
104. Burley, S. K., David, P. R., Taylor, A., and Lipscomb, W. N., *Proc. Natl. Acad. Sci. U.S.A.* **87**, 6878 (1990).
105. Chaudhuri, P., Stockheim, C., Weighardt, K., Deck, W., Gregorzik, R., Vahrenkamp, H., Nuber, B., and Weiss, J., *Inorg. Chem.* **31**, 1451 (1992).

106. Flassbeck, C., Weighardt, K., Bill, E., Butzlaff, C., Trautwein, A. X., Nuber, B., and Weiss, J., *Inorg. Chem.* **31**, 21 (1991).
107. Kimura, E., Kurogi, Y., Shionya, M., and Shiro, M., *Inorg. Chem.* **30**, 4524 (1991).
108. Dixon, N. E., Gazzola, C., Walters, J. J., Blakeley, R. L., and Zerner, B., *J. Am. Chem. Soc.* **97**, 4130 (1975); Dixon, N. E., Gazzola, C., Blakeley, R. L., and Zerner, B., *ibid.*, p. 4131.
109. Andrews, R. K., Blakeley, R. L., and Zerner, B., in "The Bioinorganic Chemistry of Nickel" (J. R. Lancaster, Jr., ed.), p. 141. VCH Verlagsges., Weinheim, 1988.
110. Clark, P. A., and Wilcox, D. E., *Inorg. Chem.* **28**, 1326 (1989).
111. Andrews, R. K., Blakeley, R. L., and Zerner, B., *Adv. Inorg. Biochem.* **6**, 225 (1984).
112. Clark, P. A., Wilcox, D. E., and Scott, R. A., *Inorg. Chem.* **29**, 579 (1990).
113. Downard, A. J., McKee, V., and Tandon, S. S., *Inorg. Chim. Acta* **173**, 181 (1990).
114. Das, R., and Nag, K., *Inorg. Chem.* **30**, 2831 (1991); Nanda, K. K., Das, R., Newlands, M. J., Hynes, R., Gabe, E. J., and Nag, K., *J. Chem. Soc., Dalton Trans.*, p. 897 (1992).
115. Chaudhuri, P., Küppers, H.-J., Wieghardt, K., Gehring, S., Haase, W., Nuber, B., and Weiss, J., *J. Chem. Soc., Dalton Trans.*, p. 1367 (1988).
116. Pilkington, N. H., and Robson, R., *Aust. J. Chem.* **23**, 2225 (1970); Okawa, H., and Kida, S., *Bull. Chem. Soc. Jpn.* **45**, 1759 (1972).
117. Spiro, C. L., Lambert, S. L., Smith, T. J., Duesler, E. N., Gagné, R. R., and Hendrickson, D. N., *Inorg. Chem.* **30**, 2831 (1991).
118. Ahlgren, M., Turpeineu, U., and Härmäläinen, R., *Acta Chem. Scand., Ser. A* **A32**, 189 (1978).
119. Bertini, I., Bianci, L., Piccioli, M., and Luchinati, C., *Coord. Chem. Rev.* **100**, 67 (1990); Valentine, J. S., and Mota de Freitas, D., *J. Chem. Educ.* **62**, 990 (1985); Fee, J. E., in "Metal Ions in Biological Systems" (H. Sigel, ed.) Vol. 13. Dekker, New York, 1981; Richardson, J. S., Thomas, K. A., Rubin, B. H., and Richardson, D. C., *Proc. Natl. Acad. Sci. U.S.A.* **72**, 1349 (1975).
120. Strothkamp, K. G., and Lippard, S. J., *Acc. Chem. Res.* **15**, 318 (1982).
121. Coughlin, P. K., Dewan, J. C., Lippard, S. J., Watanabe, E.-I., and Lehn, J. M., *J. Am. Chem. Soc.* **101**, 265 (1979).
122. Coughlin, P. K., Lippard, S. J., Martin, A. E., and Bulkowski, J. E., *J. Am. Chem. Soc.* **102**, 7617 (1980).
123. Valentine, J. S., Pantoliano, M. W., McDonnell, P. J., Burger, A. J., and Lippard, S. J., *Proc. Natl. Acad. Sci. U.S.A.* **76**, 4245 (1979).
124. Salata, C. A., Youinou, M.-T., and Burrows, C. J., *Inorg. Chem.* **30**, 3454 (1991); Salata, C. A., Youinou, M. T., and Burrows, C. J., *J. Am. Chem. Soc.* **111**, 9278 (1989).
125. Drew, M. G. B., Cairns, C., Lavery, A., and Nelson, S. M., *J. Chem. Soc., Chem. Commun.*, p. 1122 (1980).
126. Drew, M. G. B., Nelson, S. M., and Reedjik, J., *Inorg. Chim. Acta* **64**, L189 (1982).
127. Drew, M. G. B., McCann, M., and Nelson, S. M., *J. Chem. Soc., Dalton Trans.*, p. 1868 (1981).
128. Hotzelmann, R., Wieghardt, K., Flörke, U., and Haupt, H.-J., *Angew. Chem., Int. Ed. Engl.* **29**, 645 (1990).
129. Freiden, E., in "Metal Ions in Biological Systems" (H. Sigel, ed.), Vol. 13, p. 1. Dekker, New York, 1981.
130. Solomon, E. I., Penfield, K. W., and Wilcox, D. E., *Struct. Bonding (Berlin)* **53**, 1 (1983); Himmelwright, R. S., Eickman, N. C., and Solomon, E. I., *J. Am. Chem. Soc.* **101**, 1576 (1979).
131. Linzen, B., Soeter, N. M., Riggs, A. F., Schneider, H.-J., Schatrau, W., Moore, M. D.,

- Yokota, E., Behrens, P. Q., Nakashima, H., Takagi, T., Nemoto, T., Vereijken, J. M., Bak, H. J., Beintema, J. J., Volbeda, A., Gaykema, W. P. J., and Hol, W. G. J., *Science* **229**, 519 (1985); Gaykema, W. P. J., Hol, W. G. J., Vereijken, J. M., Soeter, N. M., Bak, H. J., and Beintema, J. J., *Nature (London)* **309**, 23 (1984).
132. Magnus, K., and Ton-That, H., *J. Inorg. Biochem.* **47**, 20 (1992).
133. Kitajima, N., Fujisawa, K., Fujimoto, C., Moro-oka, Y., Hashimoto, S., Kitagawa, T., Toriumi, K., Tatsumi, K., and Nakamura, A., *J. Am. Chem. Soc.* **114**, 1277 (1992); Kitajima, N., Koda, T., Hashimoto, S., Kitagawa, T., and Moro-oka, Y., *ibid.* **113**, 5664 (1991); Kitajima, N., *Adv. Inorg. Chem.* **39**, 1-77 (1992).
134. Sorrell, T. N., *Tetrahedron* **45**, 3 (1989).
135. Nelson, S. M., in "Copper Coordination Chemistry: Biochemical and Inorganic Perspectives" (K. D. Karlin and J. Zubieta, eds.), p. 331. Adenine Press, New York, 1983.
136. Tyeklár, Z., and Karlin, K. D., *Acc. Chem. Res.* **22**, 241 (1989); Karlin, K. D., and Gultneh, Y., *Prog. Inorg. Chem.* **35**, 219 (1987); Karlin, K. D., Cruse, R. W., Gultneh, Y., Hayes, J. C., McKown, J. W., and Zubieta, J., in "Biological and Inorganic Copper Chemistry" (K. D. Karlin and J. Zubieta, eds.), p. 101. Adenine Press, New York, 1985; Gultneh, Y., and Karlin, K. D., *J. Chem. Educ.* **62**, 983 (1985).
137. Coughlin, P. K., and Lippard, S. J., *J. Am. Chem. Soc.* **106**, 2328 (1984).
138. Agnus, Y., Louis, R., Gisselbrecht, J.-P., and Weiss, R., *J. Am. Chem. Soc.* **106**, 93 (1984); Agnus, Y. L., in "Copper Coordination Chemistry: Biochemical and Inorganic Perspectives" (K. D. Karlin and J. Zubieta, eds.), p. 371. Adenine Press, New York, 1983; Agnus, Y., Louis, R., and Weiss, R., *J. Am. Chem. Soc.* **101**, 3381 (1979).
139. Villacorta, G. M., and Lippard, S. J., *Pure Appl. Chem.* **58**, 1477 (1986).
140. Comarand, J., Plumier, P., Lehn, J.-M., Agnus, Y., Louis, R., Weiss, R., Kahn, O., and Morgenstern-Badarau, I., *J. Am. Chem. Soc.* **104**, 6330 (1982).
141. Nelson, S. M., Esho, F., Lavery, A., and Drew, M. G. B., *J. Am. Chem. Soc.* **105**, 5693 (1983).
142. Drew, M. G. B., Yates, P. C., Trocha-Grimshaw, J., Lavery, A., McKillop, K. D., Nelson, S. M., and Nelson, J., *J. Chem. Soc., Dalton Trans.*, p. 347 (1988).
143. Pate, J., Ross, P. K., Thamann, J. J., Reed, C. A., Karlin, K. D., Sorrell, T. N., and Solomon, E. I., *J. Am. Chem. Soc.* **111**, 5198 (1989).
144. Drew, M. G. B., McCann, M., and Nelson, S. M., *J. Chem. Soc., Chem. Commun.*, p. 481 (1979).
145. Chaudhuri, P., Oder, K., Wieghardt, K., Nuber, B., and Weiss, J., *Inorg. Chem.* **25**, 2818 (1986).
146. Drew, M. G. B., Nelson, J., Esho, F., McKee, V., and Nelson, S. M., *J. Chem. Soc., Dalton Trans.*, p. 1837 (1982).
147. Burk, P. L., Osborn, J. A., Youinou, M.-T., Agnus, Y., Louis, R., and Weiss, R., *J. Am. Chem. Soc.* **103**, 1274 (1981).
148. Davis, W. M., and Lippard, S. J., *Inorg. Chem.* **24**, 3688 (1985).
149. Tandon, S. S., Thompson, L. K., Bridson, J. N., McKee, V., and Downard, A. J., *Inorg. Chem.* **31**, 4635 (1992).
150. Bailey, N. A., Fenton, D. E., Moody, R., Rodriguez de Barbarin, C. O., Sciambarella, N. I., Latour, J. M., Limosin, D., and McKee, V., *J. Chem. Soc., Dalton Trans.*, p. 2519 (1987); McKee, V., and Smith, J., *J. Chem. Soc., Chem. Commun.*, p. 1465 (1983).
151. Nappa, M., Valentine, J. S., Miksztal, A. R., Schugar, H. J., and Isied, S. S., *J. Am. Chem. Soc.* **101**, 7744 (1979).

152. Bulkowski, J. E., Burk, P. L., Ludmann, M.-F., and Osborn, J. A., *J. Chem. Soc., Chem. Commun.*, p. 498 (1977).
153. Burnett, M. G., McKee, V., Nelson, S. M., and Drew, M. G. B., *J. Chem. Soc., Chem. Commun.*, p. 829 (1980).
- 153a. Bulkowski, J. E., and Summers, W. E., III, in "Biological and Inorganic Copper Chemistry" (K. D. Karlin and J. Zubieta, eds.), p. 445. Adenine Press, New York, 1985.
- 153b. Asato, E., Hashimoto, S., Matsumoto, N., and Kida, S., *J. Chem. Soc., Dalton Trans.*, p. 1741 (1990).
- 153c. Ngwenya, M. P., Chen, D., Martell, A. E., and Reibenspies, J., *Inorg. Chem.* **30**, 2732 (1991).
154. Nelson, S. M., Trocha-Grimshaw, J., Lavery, A., McKillop, K. P., and Drew, M. G. B., in "Biological and Inorganic Copper Chemistry" (K. D. Karlin and J. Zubieta, eds.), p. 27. Adenine Press, New York, 1985.
155. Sanyal, I., Mahroof-Tahir, M., Nasir, M. S., Ghosh, P., Cohen, B. I., Gultneh, Y., Cruse, R. W., Farooq, A., Karlin, K. D., Liu, S., and Zubieta, J., *Inorg. Chem.* **31**, 4322 (1992); Mahroof-Tahir, M., Murthy, N. N., Karlin, K. D., Blackburn, N. J., Shaikh, S. N., and Zubieta, J., *ibid.* p. 3001; Paul, P. P., Tyklar, Z., Jacobson, R. R., and Karlin, K. D., *J. Am. Chem. Soc.* **113**, 5322 (1991); Karlin, K. D., Wei, N., Jung, B., Kaderli, S., and Zuberbühler, A. D., *ibid.*, p. 5868; Sanyal, I., Strange, R. W., Blackburn, N. J., and Karlin, K. D., *ibid.*, p. 4692; Karlin, K. D., Tyeklár, Z., Farooq, A., Jacobson, R. R., Sinn, E., Lee, D. W., Bradshaw, J. E., and Wilson, L. J., *Inorg. Chim. Acta* **182**, 1 (1991); Blackburn, N. J., Strange, R. W., Cruse, R. W., and Karlin, K. D., *J. Am. Chem. Soc.* **109**, 1235 (1987).
156. Westmoreland, T. D., Wilcox, D. E., Baldwin, M. J., Mims, W. B., and Solomon, E. I., *J. Am. Chem. Soc.* **111**, 6106 (1989).
157. Himmelwright, R. S., Eickman, N. C., and Solomon, E. I., *J. Am. Chem. Soc.* **101**, 1576 (1979).
158. Hush, N. S., *Prog. Inorg. Chem.* **8**, 391 (1967).
159. Robin, M. B., and Day, P., *Adv. Inorg. Chem. Radiochem.* **10**, 247 (1967).
160. Farrar, J. A., Thomson, A. J., Cheesman, M. R., Dooley, D. M., and Zumft, W. G., *FEBS Lett.* **294**, 11 (1991).
161. Francisz, W., Scholes, C. P., Hyde, J. S., Wei, Y.-H., King, T. S., Shaw, R. W., and Beinert, H., *J. Biol. Chem.* **254**, 7482 (1979).
162. Aasa, R., Deinum, J., Lerch, K., and Reinhammar, B., *Biochim. Biophys. Acta* **535**, 287 (1978).
163. Kroneck, P. M. H., Antholine, W. A., Reister, J., and Zumft, W. G., *FEBS Lett.* **242**, 70 (1988).
164. Thomson, A. J., Greenwood, C., Peterson, J., and Barrett, C. P., *J. Inorg. Biochem.* **28**, 195 (1986).
165. Hunter, J., Nelson, J., Harding, C., McCann, M., and McKee, V., *J. Chem. Soc., Chem. Commun.*, p. 1148 (1990).
166. Nelson, J., personal communication (1992).
167. Gatteschi, D., Mealli, C., and Sacconi, L., *Inorg. Chem.* **15**, 2774 (1976).
168. Barr, M. E., and Smith, P. H., *Copper Coord. Chem. Bioinorg. Perspect. Symp.*, Baltimore, MD, 1992, Poster 52 (1992); Barr, M. E., personal communication (1992).
169. Gagné, R. R., Koval, C. A., Smith, T. J., and Cimolino, M. C., *J. Am. Chem. Soc.* **101**, 4571 (1979).
170. Hendrickson, D. N., Long, R. C., Hwang, Y. T., and Chang, H. R., in "Biological

- and Inorganic Copper Chemistry" (K. D. Karlin and J. Zubieta, eds.), p. 223. Adenine Press, New York, 1985; Long, R. C., and Hendrickson, D. N., *J. Am. Chem. Soc.* **105**, 1513 (1983).
171. Wilkins, R. G., *Chem. Soc. Rev.*, p. 171 (1992); Vincent, J. B., Olivier-Lilley, G. L., and Averill, B. A., *Chem. Rev.* **90**, 1447 (1990); Klotz, I. M., and Kurtz, D. M., Jr., *Acc. Chem. Res.* **17**, 16 (1984).
172. Que, L., Jr., and Scarrow, R. C., *ACS Symp. Ser.* **372**, 152 (1988).
173. Kurtz, D. M., Jr., *Chem. Rev.* **90**, 585 (1990).
174. Lippard, S. J., *Angew. Chem., Int. Ed. Engl.* **27**, 344 (1988).
175. Que, L., and True, A. E., *Prog. Inorg. Chem.* **38**, 97 (1990).
176. Holmes, M. A., LeTrong, I., Turley, S., Siekev, L. C., and Stenkamp, R. D., *J. Mol. Biol.* **218**, 583 (1991); Stenkamp, R. E., Sieker, L. C., Jensen, L. H., McCallum, J. D., and Sanders-Loehr, J., *Proc. Natl. Acad. Sci. U.S.A.* **82**, 713 (1985).
177. Holmes, M. A., and Stenkamp, R. E., *J. Mol. Biol.* **220**, 723 (1991).
178. Solomon, E. I., and Zhang, Y., *Acc. Chem. Res.* **25**, 343 (1992); Reem, R. C., McCormick, J. M., Richardson, D. E., Devlin, F. J., Stephens, P. J., Musselman, R. L., and Solomon, E. I., *J. Am. Chem. Soc.* **111**, 4689 (1989); Reem, R. C., and Solomon, E. I., *ibid.* **109**, 1216 (1987).
179. Nordlund, P., Sjöberg, B.-M., and Eklund, H., *Nature (London)* **345**, 593 (1990).
180. Bollinger, J. M., Edmondson, D. E., Huynh, B. H., Filley, J., Norton, J., and Stubbe, J., *Science* **253**, 292 (1991).
181. Hartman, J. R., Rardin, R. L., Chaudhuri, P., Pohl, K., Wieghardt, K., Nuber, B., Weiss, J., Papaefthymiou, G. C., Frankel, R. B., and Lippard, S. J., *J. Am. Chem. Soc.* **109**, 7387 (1987).
182. Wieghardt, K., Pohl, K., and Ventur, D., *Angew. Chem., Int. Ed. Engl.* **24**, 392, 778 (1985).
183. Feng, X., Bott, S. G., and Lippard, S. J., *J. Am. Chem. Soc.* **111**, 8046 (1989).
184. De Witt, J. G., Bentsen, J. G., Rosenzweig, A. C., Hedman, B., Green, J., Pilkington, S., Papaefthymiou, G. C., Dalton, H., Hodgson, K. O., and Lippard, S. J., *J. Am. Chem. Soc.* **113**, 9219 (1991).
185. Andersson, K. K., Elgren, T. E., Que, L., Jr., and Lipscomb, J. D., *J. Am. Chem. Soc.* **114**, 8711 (1992).
186. Averill, B. A., Davis, J. C., Burman, S., Zirino, T., Sanders-Loehr, J., Loehr, T. M., Sage, J. T., and Debrunner, P. G., *J. Am. Chem. Soc.* **109**, 3760 (1987).
187. Drüeke, S., Wieghardt, K., Nuber, B., Weiss, J., Fleischhauer, H.-P., Gehring, S., and Haase, W., *J. Am. Chem. Soc.* **111**, 8622 (1989).
188. Tolman, W. B., Bino, A., and Lippard, S. J., *J. Am. Chem. Soc.* **111**, 8522 (1989).
189. Wieghardt, K., *Angew. Chem., Int. Ed. Engl.* **28**, 1153 (1989).
190. Niemann, A., Bossek, U., Wieghardt, K., Butzlaff, C., Trautwein, A. X., and Nuber, B., *Angew. Chem., Int. Ed. Engl.* **31**, 311 (1992).
191. Wieghardt, K., Bossek, U., Bonvoisin, J., Beauvillain, P., Girerd, J.-J., Nuber, B., Weiss, J., and Heinze, J., *Angew. Chem., Int. Ed. Engl.* **25**, 1030 (1986).
192. Wieghardt, K., Bossek, U., Ventur, D., and Weiss, J., *J. Chem. Soc., Chem. Commun.*, p. 347 (1985).
193. Wieghardt, K., Bossek, U., Zsolnai, L., Huttner, G., Blondin, G., Girerd, J.-J., and Babonneau, F., *J. Chem. Soc., Chem. Commun.*, p. 651 (1987).
194. Wieghardt, K., Bossek, U., Nuber, B., Weiss, J., Bonvoisin, J., Corbella, M., Vitols, S. E., and Girerd, J. J., *J. Am. Chem. Soc.* **110**, 7398 (1988); Wieghardt, K., Bossek, U., and Gebert, W., *Angew. Chem., Int. Ed., Engl.* **22**, 328 (1983).

195. Chang, H.-R., Dirdl, H. K., Nilges, M. J., Zhang, X., Potenza, J. A., Schugar, H. J., Hendrickson, D. N., and Isied, S. S., *J. Am. Chem. Soc.* **110**, 625 (1988).
196. Hagen, K. S., Westmoreland, T. D., Scott, M. J., and Armstrong, W. H., *J. Am. Chem. Soc.* **111**, 1907 (1989).
197. Goodson, P. A., Hodgson, D. J., and Michelsen, K., *Inorg. Chim. Acta* **172**, 49 (1990).
198. Brewer, K. S., Calvin, M., Lumpkin, R. S. Otvos, J. W., and Spreer, L. O., *Inorg. Chem.* **28**, 4446 (1989).
199. Goodson, P. A., Hodgson, D. J., Glerup, J., Michelsen, K., and Weihe, H., *Inorg. Chim. Acta* **197**, 141 (1992).
200. Bossek, U., Weyhermüller, T., Wieghardt, K., Nuber, B., and Weiss, J., *J. Am. Chem. Soc.* **112**, 6387 (1990).
201. Larson, E., Lah, M. S., Li, X., Bonadies, J. A., and Pecararo, V. L., *Inorg. Chem.* **31**, 373 (1992).
202. Khangulov, S. V., Barynin, V. V., Voevodskaya, N. V., and Grebenko, A. I., *Biochim. Biophys. Acta* **1020**, 305 (1990).
203. Barynin, V. V., Vagin, A. A., Melik-Adamyan, V. R., Grebenko, A. I., Khangulov, S. V., Popov, A. N., Andreanova, M. E., and Vainstein, B. K., *Dokl. Acad. Sci. USSR* **288**, 877 (1986).
204. Waldo, G. S., Yu, S., and Penner-Hahn, J. E., *J. Am. Chem. Soc.* **114**, 5869 (1992).
205. Willing, A., Follmann, H., and Auling, G., *Eur. J. Biochem.* **170**, 603 (1988); Schimpff-Weiland, G., Follmann, H., and Auling, G., *Biochem. Biophys. Res. Commun.* **102**, 1276 (1981).
206. Cole, J. L., Clark, P. A., and Solomon, E. I., *J. Am. Chem. Soc.* **112**, 9534 (1990).
207. Allendorf, M. D., Spira, D. J., and Solomon, E. I., *Proc. Natl. Acad. Sci. U.S.A.* **82**, 3063 (1985); Spira-Solomon, D. J., Allendorf, M. D., and Solomon, E. I., *J. Am. Chem. Soc.* **108**, 5318 (1986).
208. Messerschmidt, A., Ladenstein, R., Hubev, R., Bolognesi, M., Avigliano, L., Petruzzelli, R., Rossi, A., and Finazzi-Agò, A., *J. Mol. Biol.* **224**, 179 (1992); Messerschmidt, A., Rossi, A., Ladenstein, R., Huber, R., Bolognesi, M., Gatti, G., Marchesini, A., Petruzzelli, R., and Finazzi-Agrò, A., *ibid.* **206**, 513 (1989).
209. Cole, J. L., Ballou, D. P., and Solomon, E. I., *J. Am. Chem. Soc.* **113**, 8544 (1991).
210. See, for example, Meenkumari, S., and Chakravorty, A. R., *J. Chem. Soc., Dalton Trans.*, p. 2749 (1992); Angaroni, M., Ardizzola, G. A., Beringhell, T., La Monica, G., Gatteschi, D., Masciocchi, N., and Moret, M., *ibid.*, p. 3305 (1990); Karlin, K., Gan, Q., Farooq, A., Liu, S., and Zubietta, J., *Inorg. Chim. Acta* **165**, 37 (1989); Kwiatowski, M., Kwiatowski, E., Olechnowicz, A., Ho, D. M., and Deutch, E., *ibid.* **150**, 65 (1988); Huisbergen, F. B., ten Hoedt, R. W. M., Verschoor, G. C., Reedijk, J., and Spek, A. L., *J. Chem. Soc., Dalton Trans.*, p. 539 (1983); Datta, D., and Chakravorty, A., *Inorg. Chem.* **22**, 1611 (1983); Butcher, R. J., O'Connor, C. J., and Sinn, E., *ibid.* **20**, 537 (1981); Baral, S., and Chakravorty, A., *Inorg. Chim. Acta* **39**, 1 (1980); Ross, P. F., Murmann, R. K., and Schlemper, E. O., *Acta Crystallogr., Sect. B: Struct. Crystallogr. Cryst. Chem.* **B30**, 1120 (1974); Beckett, R., and Hoskins, B. F., *J. Chem. Soc., Dalton Trans.*, p. 291 (1972).
211. Chaudhuri, P., Karpenstein, I., Winter, M., Butzlaff, C., Bill, E., Trautwein, A. X., Flörke, U., and Haupt, H.-J., *J. Chem. Soc., Chem. Commun.*, p. 321 (1992).
212. Bencini, A., Bianchi, A., Garcia-España, E., Micheloni, M., and Paoletti, P., *Inorg. Chem.* **27**, 176 (1988).
213. Comarmond, J., Dietrich, B., Lehn, J.-M., and Louis, R., *J. Chem. Soc., Chem. Commun.*, p. 74 (1985).

214. Adams, H., Bailey, N. A., Dwyer, M. J. S., Fenton, D. E., Hellier, P. C., and Hempstead, P. D., *J. Chem. Soc., Chem. Commun.*, p. 1297 (1991).
215. Brudvig, G. W., Thorp, H. H., and Crabtree, R. H., *Acc. Chem. Res.* **24**, 311 (1991); Govindjee and Coleman, W. J., *Sci. Am.*, p. 42 (1990); Babcock, G. T., Barry, B. A., Debus, R. J., Hoganson, C. W., Atamain, M., McIntosh, L., Sithole, I., and Yocum, C. F., *Biochemistry* **28**, 9557 (1989); Brudvig, G. W., *ACS Symp. Ser.* **372**, 221 (1988); G. Renger, *Angew. Chem., Int. Ed. Engl.* **26**, 643 (1987); Dismukes, G. C., *Photochem., Photobiol.* **43**, 99 (1986).
216. Dismukes, G. C., *Chem. Scr.* **28A**, 99 (1988).
217. Christou, G., *Acc. Chem. Res.* **22**, 328 (1989); Vincent, J. B., and Christou, G., *Adv. Inorg. Chem.* **33**, 197 (1989); Christou, G., and Vincent, J. B., *ACS Symp. Ser.* **372**, 239 (1988).
218. Babcock, G. T., Barry, B. A., Debus, R. J., Hoganson, C. W., Atamian, M., McIntosh, L., Sithole, I., and Yocum, C. F., *Biochemistry* **28**, 9557 (1989); Brudvig, G. W., *ACS Symp. Ser.* **372**, 221 (1988); Renger, G., *Angew. Chem., Int. Ed. Engl.* **26**, 643 (1987); Dismukes, G. C., *Photochem. Photobiol.* **44**, 99 (1986).
219. Joliot, P., Joliot, A., Bouges, B., and Barbieri, G., *Photochem. Photobiol.* **14**, 287 (1971); Joliot, P., Barbier, G., and Chabaud, R., *ibid.* **10**, 309 (1969).
220. Kok, B., Forbush, B., and McGloin, M., *Photochem. Photobiol.* **11**, 309 (1970).
221. Ono, T., Noguchi, T., Inoue, Y., Kusunoki, M., Matsushita, T., and Oyanagi, H., *Science* **258**, 1335 (1992).
222. Dexheimer, S. L., and Klein, M. P., *J. Am. Chem. Soc.* **114**, 2821 (1992); Koulouligiotis, D., Hirsch, D. J., and Brudvig, G. W., *ibid.*, p. 8322.
223. Hallahan, B. J., Nugent, J. H. A., Warden, J. T., and Evans, C. W., *Biochemistry* **31**, 4562 (1992).
224. Boussac, A., and Rutherford, A. W., *Biochemistry* **31**, 7441 (1992); Boussac, A., Zimmerman, J.-L., Rutherford, A. W., and Lavergne, J., *Nature (London)* **347**, 303 (1990).
225. George, G. N., Prince, R. C., and Cramer, S. P., *Science* **243**, 789 (1989).
226. Penner-Hahn, J. E., Fronko, R. M., Pecoraro, V. L., Yocum, C. F., Betts, S. D., and Bowlby, N. R., *J. Am. Chem. Soc.* **112**, 2549 (1990).
227. Guiles, R. D., Zimmerman, J. L., McDermott, A. E., Yachandra, V. K., Cole, J. L., Dexheimer, S. L., Britt, R. D., Wieghardt, K., Bossek, U., Sauer, K., and Klein, M. P., *Biochemistry* **29**, 471 (1990); Kim, D. H., Britt, R. D., Klein, M. P., and Saver, K., *J. Am. Chem. Soc.* **112**, 9389 (1990); Yachandra, V. K., Guiles, R. D., Saver, K., and Klein, M. P., *Biochim. Biophys. Acta* **850**, 333 (1986).
228. See, for example, Wang, S., Tsai, H.-L., Streib, W. E., Christou, G., and Hendrickson, D. N., *J. Chem. Soc., Chem. Commun.*, p. 677 (1992); Schake, A. R., Tsai, H.-L., de Vries, N., Webb, R. J., Folting, K., Hendrickson, D. N., and Christou, G., *ibid.*, p. 181 (1992); Wang, S., Huffman, J. C., Folting, K., Streib, W. E., Lobkovsky, E. B., and Christou, G., *Angew. Chem., Int. Ed. Engl.* **30**, 1672 (1991); Bhula, R., and Weatherburn, D. C., *ibid.*, p. 668; Perlepes, S. P., Huffman, J. C., and Christou, G., *J. Chem. Soc., Chem. Commun.*, p. 1657 (1991); Hagan, K. S., Armstrong, W. H., and Olmstead, M. M., *J. Am. Chem. Soc.* **111**, 774 (1989); Schake, A. R., Vincent, J. B., Li, Q., Boyd, P. D. W., Folting, K., Huffman, J. C., Hendrickson, D. N., and Christou, G., *Inorg. Chem.* **28**, 1915 (1989); Boyd, P. D. W., Li, Q., Vincent, J. B., Folting, K., Chang, H.-R., Streib, W. E., Huffman, J. C., Christou, G., and Hendrickson, D. N., *J. Am. Chem. Soc.* **110**, 8537 (1988); Luneau, D., Savariault, J.-M., and Tuchagues, J.-P., *Inorg. Chem.* **27**, 3912 (1988); Christmas, C., Vincent, J. B., Chang, H.-R., Huffman, J. C., Christou, G., and Hendrickson, D. N., *J. Am. Chem.*

- Soc. **110**, 823 (1988); Christmas, C., Vincent, J. B., Huffman, J. C., Christou, G., Chang, H.-R., and Hendrickson, D. N., *Angew. Chem., Int. Ed. Engl.* **26**, 915 (1987); Baikie, A. R. E., Howes, A. J., Hursthouse, M. B., Quick, A. B., and Thornton, P., *J. Chem. Soc., Chem. Commun.*, p. 1587 (1986); Lis, T., *Acta Crystallogr., Sect. B: Struct. Crystallogr. Cryst. Chem.* **B36**, 2042 (1980).
229. Pecoraro, V. L., *Photochem. Photobiol.* **48**, 249 (1988).
230. Vincent, J. B., and Christou, G., *Adv. Inorg. Chem.* **33**, 197 (1989); Christou, G., and Vincent, J. B., *ACS Symp. Ser.* **372**, 239 (1988).
231. Christou, G., *Acc. Chem. Res.* **22**, 328 (1989).
232. Andreasson, L.-E., *Biochim. Biophys. Acta* **973**, 465 (1989).
- 232a. Ono, T., and Inoue, Y., *Biochemistry* **30**, 6183 (1990); Tamura, M., Ikeuchi, M., and Inoue, Y., *Biochim. Biophys. Acta* **973**, 281 (1989).
233. Cramer, S. P., deGroot, F. M. F., Ma, Y., Chen, C. T., Sette, F., Kipke, C. A., Eichhorn, D. M., Chan, M. K., Armstrong, W. H., Libby, E., Christou, G., Brooker, S., McKee, V., Mullins, O. C., and Fuggle, J. C., *J. Am. Chem. Soc.* **113**, 7937 (1991).
234. Volkov, A. G., *Bioelectrochem. Bioenerg.* **275**, 3 (1989).
235. Prosperio, D. M., Huffman, R., and Dismukes, G. C., *J. Am. Chem. Soc.* **114**, 4374 (1992).
236. Chan, M. K., and Armstrong, W. H., *J. Am. Chem. Soc.* **113**, 5055 (1991).
237. Micklitz, W., Bott, S. G., Bentsen, J. G., and Lippard, S. J., *J. Am. Chem. Soc.* **111**, 372 (1989).
238. Brooker, S., and McKee, V., *J. Chem. Soc., Chem. Commun.*, p. 619 (1989).
239. Brooker, S., Cramer, S. P., and McKee, V., unpublished work.
240. Brooker, S., Ph.D. Thesis, University of Canterbury (1989).
241. Horn, E., Snow, M. R., and Zeleny, P. C., *Aust. J. Chem.* **33**, 1659 (1980); Heberhold, M., Suss, G., Ellerman, J., and Gabelein, H., *Chem. Ber.* **11**, 2719 (1979); Clark, M. D., Copp, S. B., Subramanian, S., and Zaworotko, M. J., *Supramol. Chem.* **1**, 7 (1992).
242. Brooker, S., McKee, V., Shepard, W. B., and Pannell, L. K., *J. Chem. Soc., Dalton Trans.*, p. 2555 (1987); McKee, V., and Shepard, W. B., *J. Chem. Soc., Chem. Commun.*, p. 158 (1985).
243. Brooker, S., McKee, V., and Metcalfe, J. E., in preparation.
244. Wang, S., Folting, K., Streib, W. E., Schmitt, E. A., McCusker, J. K., Hendrickson, D. N., and Christou, G., *Angew. Chem., Int. Ed. Engl.* **30**, 305 (1991).
245. Hendrickson, D. N., Christou, G., Schmitt, E. A., Libby, E., Bashkin, J. S., Wang, S., Tsai, H.-L., Vincent, J. B., Boyd, P. D. W., Huffman, J. C., Folting, K., Li, Q., and Streib, W. E., *J. Am. Chem. Soc.* **114**, 2455 (1992); Li, Q., Vincent, J. B., Libby, E., Chang, H.-R., Huffman, J. C., Boyd, P. D. W., Christou, G., and Hendrickson, D. N., *Angew. Chem., Int. Ed. Engl.* **27**, 1731 (1988).
246. Wieghardt, K., Tolksdorf, I., and Herrmann, W., *Inorg. Chem.* **24**, 1230 (1985).
247. McKee, V., and Tandon, S. S., *J. Chem. Soc., Chem. Commun.*, p. 1335 (1988).
248. Brooker, S., and McKee, V., *J. Chem. Soc., Dalton Trans.*, p. 2397 (1990).
249. Bhula, R., Gainsford, G. J., and Weatherburn, D., *J. Am. Chem. Soc.* **110**, 7550 (1988).
250. Berg, J. M., and Holm, R. H., *Met. Ions Biol.* **4**, 1 (1982); Holm, R. H., *Acc. Chem. Res.* **10**, 427 (1977).
251. Holm, R. H., Ciurli, S., and Weigel, J. A., *Prog. Inorg. Chem.* **38**, 1 (1990).
252. Tomohiro, T., Uoto, K., and Okuno, H., *J. Chem. Soc., Dalton Trans.*, p. 2459 (1990).
253. Okuno, Y., Uoto, K., Sasaki, Y., Yonemitsu, O., and Tomohiro, T., *J. Chem. Soc., Chem. Commun.*, p. 874 (1987).

254. Okuno, Y., Uoto, K., Yonemitsu, O., and Tomohiro, T., *J. Chem. Soc., Chem. Commun.*, p. 1018 (1987).
255. Okuno, Y., Uoto, K., Tomohiro, T., and Youinou, M.-T., *J. Chem. Soc., Dalton Trans.*, p. 3375 (1990).
256. Tomohiro, T., Uoto, K., and Okuno, H., *J. Chem. Soc., Chem. Commun.*, p. 194 (1990).
257. Kennedy, M. C., and Stout, C. D., *Adv. Inorg. Chem.* **38**, 323 (1992); Emptage, M. H., *ACS Symp. Ser.* **392**, 343 (1988).
258. Kent, T. A., Dreyer, J.-L., Kennedy, M. C., Huyuh, B. H., Emptage, M. H., Beinert, H., and Münck, E., *Proc. Natl. Acad. Sci. U.S.A.* **79**, 1096 (1982).
- 258a. Robbins, A. H., and Stout, C. D., *Proc. Natl. Acad. Sci. U.S.A.* **86**, 3639 (1989).
259. Stout, C. D., *J. Mol. Biol.* **205**, 545 (1989).
260. Kissinger, C. R., Adman, E. T., Sieker, L. C., and Jensen, L. H., *J. Am. Chem. Soc.* **110**, 8721 (1988).
261. Moura, J. J. G., Moura, I., Kent, T. A., Lipscomb, J. D., Huynh, B. H., LeGass, J., Xavier, A. V., and Munck, E., *J. Biol. Chem.* **257**, 6259 (1982).
262. Whitener, M. A., Peng, G., and Holm, R. H., *Inorg. Chem.* **30**, 2411 (1991).
263. Stack, T. D. P., Weigel, J. A., and Holm, R. H., *Inorg. Chem.* **29**, 3745 (1990); Stack, T. D. P., and Holm, R. H., *J. Am. Chem. Soc.* **110**, 2484 (1988).
264. Wiegel, J. A., Srivastava, K. K. P., Day, E. P., Münck, E., and Holm, R. H., *J. Am. Chem. Soc.* **112**, 8015 (1990).
265. Busch, D. H., Farmery, K., Goedken, V., Katovic, V., Melnyk, A. C., Sperati, C. R., and Tokel, N., *Adv. Chem. Ser.* **100**, 44 (1971).
266. Starropoulos, P., Muettterties, M. C., Carrié, M., and Holm, R. H., *J. Am. Chem. Soc.* **113**, 8485 (1991).